Molecular Rod Rotors and Their Solid State Internal Dynamics

Dissertation

zur

Erlangung der naturwissenschaftlichen Doktorwürde

(Dr. sc. nat.)

vorgelegt

der

Mathematisch-naturwissenschaftlichen Fakultät

der

Universität Zürich

von

Fitore Kasumaj

von Zürich, ZH

Promotionskomitee:

Prof. Dr. Jay S. Siegel (Vorsitz)

Prof. Dr. Kim K. Baldridge

Prof. Dr. Hans-Beat Bürgi

Prof. Dr. Reto Dorta

Zürich, 2011

The following paper was accepted as a dissertation by the University of Zurich's Faculty of Science in spring semester 2011

Doctorate Committee:

Prof. Dr. Jay S, Siegel (Chair, dissertation supervisor)

Prof. Dr. Kim K. Baldridge

Prof. Dr. Hans-Beat Bürgi

Prof. Dr. Reto Dorta

ABSTRACT OF THE DISSERTATION

Molecular Rod Rotors and Their Solid State Internal Dynamics

by

Fitore Kasumaj

University of Zurich, 2010

Prof. Dr. Jay S. Siegel, Chair

This dissertation describes the synthesis and characterization of a new class of Brownian molecular rod rotors and is divided into three parts: 1.) A short historical review is given, starting from the observation of the Brownian motion and followed by a "gedankenexperiment " of Einstein and Smoluchowski, who dreamed about being able to harvest the Brownian motion in order to build molecular machines. This overview is followed by a discussion of Brownian molecular rotors in nature and in chemistry, including examples and their rotation barriers. 2.) In the second part physical methods for dynamic studies are presented and discussed, the focus lies on solid state dynamic studies. In the last part variable temperature NMR studies are explained. 3.) The third main part of this thesis focuses on molecular rod rotors. It starts with a history of trioxatricornan syntheses and a description of its physical properties. This introduction is then followed by the description of my own work: First the synthesis of different molecular rod ro-

tors with trioxatricornan caps is described and discussed, then physical properties of a selected system are described and finally dynamic studies are presented.

Molecular rod rotors consist of three distinct parts: The stator, the axle and the rotator. Our design is based on a new class of stators, namely trioxatricornan, a rigid, tripod-shaped molecule with a large surface area, which was first synthesized by Smith and Martin in 1964. Due to its structure, the momentum of inertia of trioxatricornan is much bigger than it is for the rotator part of the rod rotors discussed here and this might lead to a fast rotation of the the rotator.

In order to probe this hypothesis a series of superstructures were synthesized and the solid-state properties and dynamics of one such structure was investigated. Our studies began with a cubic crystal structure of a phenyl-linked rod rotor which showed a three-fold disorder of the phenyl ring. This led to the assumption, that a dynamic process could lead to the disorder. Therefore, variable temperature X-Ray studies were performed to test this hypothesis. DFT calculations estimated a rotation barrier of 0.3 kcal mol^{-1} for the rotation of the phenyl ring. In order to confirm the calculation atomic displacement parameters (ADPs) from three data sets were studied and found their conclusions to agree with the results of the DFT calculation. To further confirm the very low rotation barrier of the phenyl ring rotation solid state NMR studies were performed. For these experiments a deuterated version of the phenyl-linked rod rotor had to be synthesized in 500 mg scale. The NMR studies showed a surprising result:

mixed dynamics- fast rotating and slower rotating components could be identified. From X-Ray powder diffraction patterns of the sample measured, three pseudo-polymorphs could be identified, explaining the mixed dynamics.

ZUSAMMENFASSUNG

Molekulare Achsenrotoren und ihre interne Festkörperdynamik

von

Fitore Kasumaj

Universität Zürich, 2010

Prof. Dr. Jay S. Siegel, Chair

In dieser Doktorarbeit ist in drei Teilen die Synthese und Charakterisierung einer neuen Klasse von Molekularen Achsen Rotoren beschrieben: 1.) Ein kurzer geschichtlicher Überblick wird gegeben, beginnend mit Browns Beobachtung der Brownschen Bewegung, übergehend zu Einsteins Erkenntnis, der Brownschen Molekularen Bewegung und dem darauf folgenden Gedankenexperiment von Einstein und Smoluchowski, dass man eine Molekulare Maschine bauen könnte, die die Brownsche Molekulare Bewegung erntet und so angetrieben wird. Dieser historischen Einleitung folgt ein kurzer Überblick über Brownsche Molekulare Rotoren in der Natur und in der synthetischen Chemie sowie eine Diskussion der gemessenen Rotationsbarrieren. 2.) Im folgenden zweiten Teil der Arbeit werden physikalische Methoden zur Untersuchung der Festkörperdynamik erläutert. Im letzten Abschnitt wird die Möglichkeit des Messens der Dynamik in Lösung diskutiert. Im 3.) Teil, dem Hauptteil dieser Dissertation, liegt der Fokus auf dem Trioxatricornan. Zuerst wird ein historischer Überblick über dessen Synthese

gegeben und danach werden die physikalischen Eigenschaften von Trioxatricornan besprochen. Nach dieser Einleitung folgt die Beschreibung der eigenen Arbeit: Zuerst wird die Synthese der verschiedenen Molekularen Achsenrotoren mit Trioxatricornan Statoren beschrieben, danach ihre physikalischen Eigenschaften und zum Schluss wird die interne Festkörperdynamik eines Systems, einem phenyl-verbrückten Achsenrotor, diskutiert.

Molekulare Achsenrotoren bestehen aus drei unterschiedlichen Teilen: Dem Stator, der Achsel und dem Rotator. Unser Design basiert auf einer neuen Klasse Statoren, den Trioxatricornanstatoren. Trioxatricornan ist rigide, besitzt eine Dreibein Form, hat eine grosse Oberfläche und wurde 1964 zuerst von Smith und Martin synthetisiert. Dank seiner strukturellen Eigenschaften, besitzt Trioxatricornan im Vergleich zu möglichen Rotatoren (z. Bsp.Phenyl), ein hohes Trägheitsmoment und dies sollte dazu führen, dass sich der Rotator im Vergleich zum Stator Teil des Molekularen Achsenrotors schnell bewegt. Um diese Annahme zu überprüfen wurden eine Serie von verschiedenen Substrukturen synthetisiert und und ihre Festkörperstruktur untersucht. Im Falle des phenyl-verbrückten Molekularen Achsenrotors konnten wir die Festkörperstruktur mittels Röntgenstrukturaufklärung einer kubischen Raumgruppe zuweisen. Interessanterweise war der Phenylring dreifach ungeordnet, diese Beobachtung liess uns Vermuten, dass ein dynamischer Prozess zu solch einer Unordnung führen könnte und Röntgenstrukturmessungen bei verschiedenen Temperaturen wurden gemacht um diese Beobachtung zu untersuchen. Währenddessen wurde mittels DFT-Rechnungen eine Abschätzung der Rotations-

barriere berechnet und ergab einen Wert von 0.3 kcalmol^{-1}. Um dieses Resultat zu bestätigen, wurden die atomaren Verschiebungsparameter (Atomic Displacement Parameteres, ADPs) anhand von drei Datensätzen von Röntgendaten, gemessen bei verschieden Temperaturen, untersucht. Der Wert der DFT-Berechnungen konnte bestätigt werden. Als dritte physikalische Methode zur Untersuchung der sehr tiefen Rotationsbarriere wurden Festkörper NMR Studien gewählt. Dazu musste zuerst die phenyl deuterierte, analoge Verbindung des phenylverbrückten Molekularen Achsen Rotors im grossen Massstab (500 mg) synthetisiert werden. Die anschliessenden Festkörper NMR Studien zeigten jedoch nicht das erwartete Resultat. Es stellt sich heraus, dass ein gemischter dynamischer Prozess vorlag mit sowohl sehr schneller Rotation als auch langsameren Rotation. Ein näheres Betrachten der gemessenen Verbindung mittels Pulverröntgen brachte die Erklärung: Es stellte sich heraus, dass wir eine Mischung von drei Polymorphen gemessen worden war. Dieses Resultat erklärte das gleichzeitige Vorliegen unterschiedlich schneller Rotationen.

Acknowledgement

PROF. JAY S. SIEGEL

for the opportunity to join this group and his support and encouragement

PROF. KIM K. BALDRIDGE

for her outstanding calculations, helpful discussions and always having a positive attitude.

PROF. HANS-BEAT BÜRGI

for enormous help with the ADP studies, his patience, his encouragement and his cheerful personality.

PROF. RETO DORTA

for being in my commitee

PROF. NATHANIEL S. FINNEY

for constant help with XRD studies and other questions

PD ANTHONY LINDEN AND SASCHA BLUMENTRITT

for the elucidation of an enormous amount of crystal structures!

DR. JACCO VAN BEEK, ETH ZÜRICH

for the SSNMR studies and helpful discussion.

DR. FABIA GOZZO, PSI VILLIGEN

for XRD studies at PSI.

PETER UEBELHART

for always helping with every question

PD LAURENT BIGLER, URS STALDER JEAN-CHRISTOPH PROBST

for the measurement of mass spectra.

SIMON JURT, NADJA BROSS

for solving all NMR issues.

ROMAN MAAG, SIMON DUTTWYLER, ANNE D. BOWEN, CELINE AMOREIRA, MIKE PACKARD

BECKY ABRAMSON, DERIK FRANTZ, SILVIA ROCHA, EOIN QUINLAN, ARIF KARIM, DAVIDE

BANDERA, JAMES NOYES,

for their friendship and support through all the years & all the good moments beyond chemistry

MOM, DAD, ADRIAN, BESNIK, FISNIK AND CHRISTOPH

for their constant support, patience and love

ALL SIEGEL, FINNEY, AND BALDRIDGE GROUP MEMBERS PAST AND PRESENT

Contents

List of Figures

List of Tables

Chapter 1

Brownian Molecular Machines

1.1 Introduction

A machine is a complex device, consisting of a number of interrelated parts, each having a definite function, together applying, using, or generating mechanical or electrical power to perform a certain kind of work.[1] According to this definition, the simplest known machine would be a wheel or a lever. When external force is applied to the wheel, it starts to move and loads can be transported by using a rotational force. In the case of the lever we have a translational force. If the machine has to be really small, smaller than a hair, as small as a molecule, the concept becomes more complicated and we need to use an extended concept.[2]

1.2 Brownian Motors

In the early 20^{th} century, the theory of molecular Brownian motion was elaborated independently by Einstein[3] and by Smoluchowski.[4] Both scientists explained Brownian motion to be a result of collisions between suspended particles and the molecules of the surrounding solvent molecules, and both arrived at almost the same quantitative predictions, albeit *via* different approaches.

Einstein and Smoluchowski provided also mathematical tools for quantifying Brownian motion. Both researchers based their work on Browns observation that pollen in water, when examined under the microscope, displayed a very rapid, highly irregular, zigzag motion.[5]

In 1912 Marian Smoluchowski presented his "gedankenexperiment" and this was the start for theoretical research on Brownian motors in which universal thermal energy is used to perform useful work.[6] In his "gedankenexperiment" Smoluchowski hypothesized a ratchet as schematically shown in (Fig. 1.1, T=T'). This ratchet is connected by an axle with a paddle wheel and with a spool, which lifts a load. The whole device would be surrounded by a gas at thermal equilibrium (T=T'). So, if it could freely turn around, it would perform a rotatory Brownian motion, due to random impacts of gas molecules on the paddles. Smoluchowski envisioned a device which would be able to lift the load by a saw-tooth motion of the pawl (only "forward" collisions should be harvested, "backward" motion would be excluded).

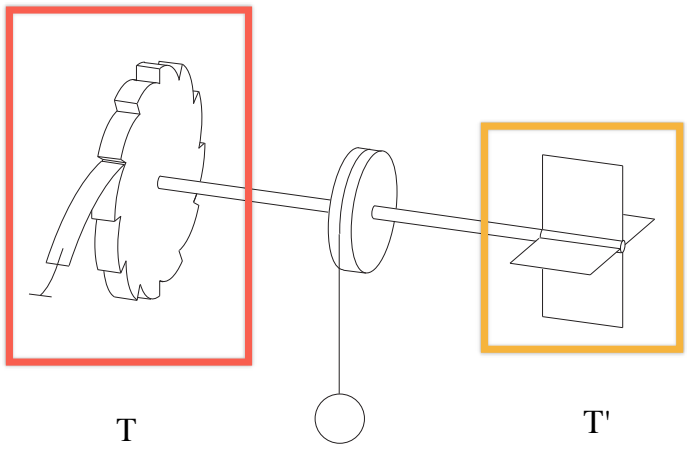

Figure 1.1: Smoluchowski-Feynman ratchet and Feynman-ratchet, in which the ratchet and the wheel are kept at different temperatures.[7]

In the Smoluchowski system, the system is kept at thermal equilibrium, which would imply a break of the second law of thermodynamics and the existence of a *perpetuum mobile* of the

second kind. This would imply the existence of a machine, which would be able of spontaneously converting equilibrium thermal energy into mechanical work, when the whole system is in a single heat reservoir. In order improve this system, Richard Feynman extended the "gedankenexperiment" (50 years later) and showed that Smoluchowski hypothesized experiment could work,[8] if the system is removed from thermal equilibrium. This could be done by placing the paddles and the ratchet shaped wheel and pawl in separate heat baths (Fig. 1.1, T≠ T'). Feynman showed that with this configuration it is possible to rectify unbiased thermal motion if T (rachet) < T' (paddle). By bringing the system out of thermal equilibrium the second law of thermodynamics is not violated.

In the 90's Kelly and coworkers[9–11] tried to realize experimentally, Smoluchowski and Feynman's ratchet and pawl by synthesizing triptycene[4]helicene. This molecule incorporates all essential components: the triptycene "paddlewheel" functions simultaneously as circular ratchet and as paddles (Fig. 1.2); the helicene represents the pawl and provides the necessary break. The two parts of the system are connected by a single C–C bond, which results in only one degree of internal rotation freedom. By performing a VT NMR spin polarization experiment Kelly and coworkers found a rotation barrier of 25 kcal mol^{-1}. Furthermore, they wanted to investigate if the rotation is unidirectional or bidirectional and if this system is a molecular ratchet which would be able to harvest thermal energy and convert it in constant motion. This question was challenging the second Law of Thermodynamics and would be support Smoluchowski "gedankenexperiment".

In order to determine the directional preference of the synthesized system (Fig. 1.2) Kelly and coworkers made use of the fact that triptycene rotation is slow on the NMR timescale and that three aromatic signals can be observed for triptycene. This fact allowed them to selectively

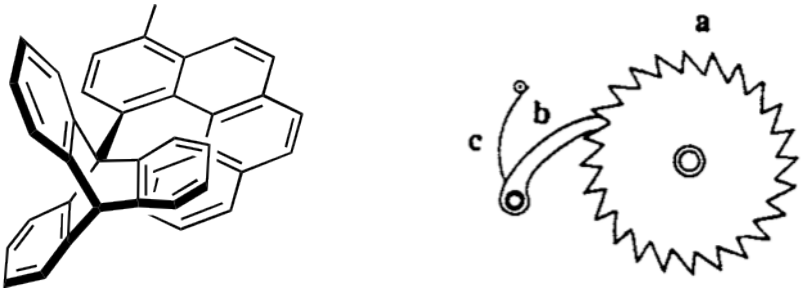

Figure 1.2: Triptycene "paddlewheel", which functions simultaneously as circular ratchet and as paddle.

polarize one proton of the triptycene and then observe the spectrum after a delay. Unidirectional rotation of the triptycene would transfer the polarization to only one of the two other signals, whereas a rotation with no directional preference would transfer polarization to the two other signals at equal rates. Against their expectations, the designed ratchet showed no directional preference.[9–11] In subsequent work, unidirectional rotation was achieved, but they had to use bond-making-and-breaking technology (subsequent reactions) to achieve unidirectional motion, thus leaving the field of Brownian molecular machines.

1.3 Molecular Brownian Machines in Nature

> *Nature uses only the longest threads to weave her patterns, so that each small piece of her fabric reveals the organization of the entire tapestry.* -R. P. Feynman

Every significant biological process in Nature uses molecular machines, which are in general driven by chemical reactions *e.g.* the ATP synthase (Fig. 1.3) which uses the cellular proton pump for the synthesis and hydrolysis of ATP and performs a stepwise rotatory motion while doing this.[12, 13] Biological motors are typically responsible for intracellular transport of cargoes, such as large protein molecules, to locations in the cell where they are needed. It is likely that motor proteins harness Brownian ratcheting to achieve directional motion. The protein kinesin,

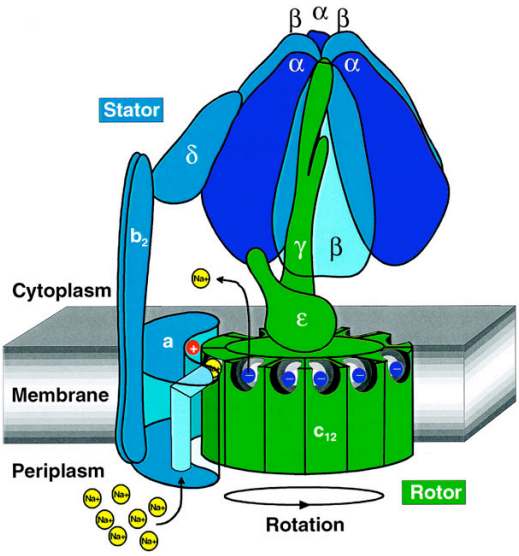

Figure 1.3: Schematic Representation of the ATPase, with a stator and rotator part and the mechanism of rotation.[14]

for example, is a two two-headed motor protein that drags organelles as it moves stepwise along microtubules; it uses the binding of one of its two 'legs' to the track to bias the diffusional search of the other leg for a binding site in the forward direction(Fig. 1.4).[15]

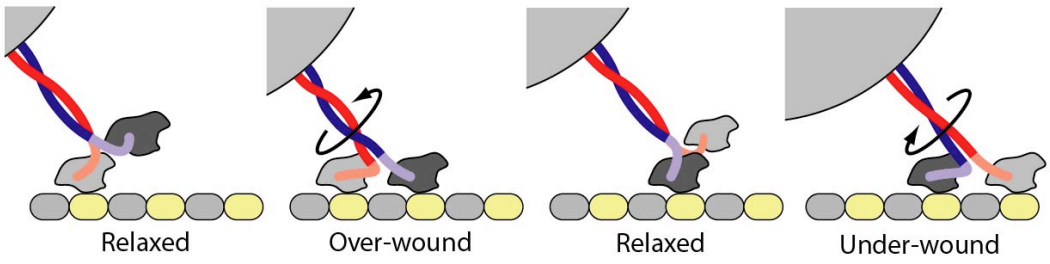

Figure 1.4: Stepwise movement of kinesin along microtubules.[16]

Biological motors convert chemical energy to motion, in order to effect stepwise linear or rotary motion, and are essential in controlling and performing a wide variety of biological functions. Linear motor proteins are central to many biological processes including muscle contraction, in-

tracellular transport, signal transduction, and are also involved in the synthesis and hydrolysis of ATP[?] .

Mimicking such a complex biological machinery as the ATP synthase has been and still is a challenging task for scientist over decades. In order to be able to start mimicking Nature a basic understanding of each small piece of natures molecular designs is necessary. One can try to achieve this by designing small model molecules, which perform a distinct physical operation, as for example a rotational or translational movement. The investigation of such small model compounds, artificial molecular machines, is a growing area of contemporary research at the interface of chemistry, physics, materials science, and biology. In this thesis we will focus on simple molecular rotor model compounds, which are really simple systems compared to Natures architecture. In contrast to the complex natural systems, the molecules we will focus on in this thesis are not molecular rotary machines, driven by a reaction or light. Instead, we will investigate a very simple molecular machine - a Brownian molecular rotor, driven by Brownian motion. In order to gain a better understanding of rotors, in the next chapter we will take a closer look at molecular rotors.

Chapter 2

Molecular Brownian Rotors

2.1 Introduction

In general, we can define a machine as a device which performs a task by transmitting or modifying force or motion.[1] In order to transfer this concept from the macroscopic to the microscopic world the definition has to be altered and simplified. In the macroscopic we can hypothesize that the device is the (molecule-)structure and the task is the function of the structure and that structure and function would be linked by a physical operation. If we narrow down this concept as having a rod structure and a rotational movement we are in the field of molecular rotors. Specifically we consider a rod structure with two caps and a rotating part linked by an axle. The caps are defined as "stators"[17] the rotating part as "rotator",[17] the two parts are connected by axles (Fig. 2.1)

Molecular rotors are molecules with a rotational degree of freedom about a bond, Michl defined molecular machines in the context of nano-science[18] as molecules, consisting of two parts that can rotate relative to each other.[17] In this description the two parts also are distinguishable by their moments of inertia and consist of a rotator and a stator part. We only focused on systems in which the rotator and the stator part are covalently linked to each other, this means

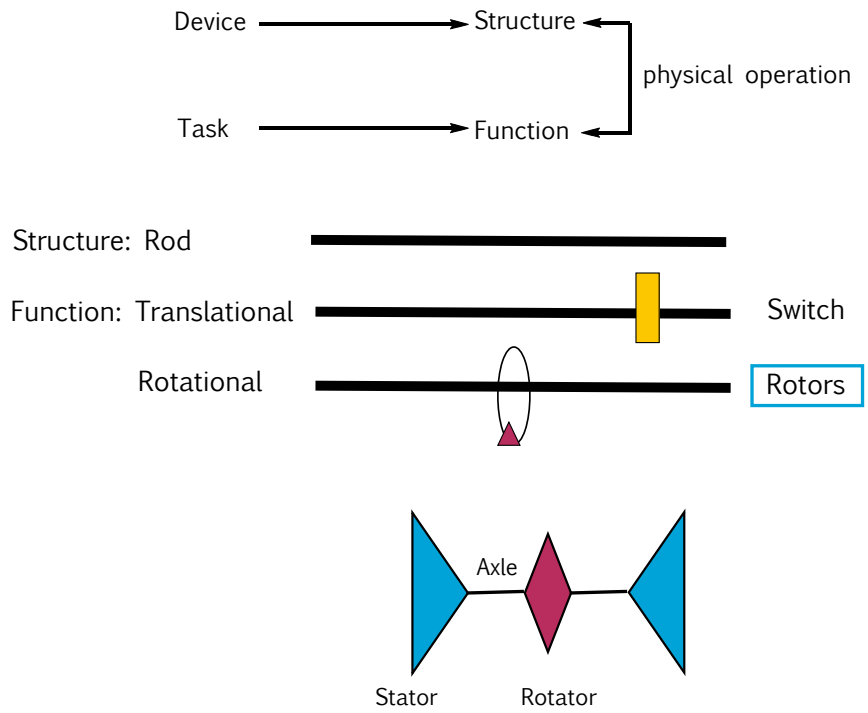

Figure 2.1: Molecular Rotors, schematic simplification

systems like rotaxanes or catananes[19–21] (stator and rotator are not covalently attached) will be excluded from discussion.

2.2 Rotation around a single Bond

2.2.1 Ethane bond rotation

A prototypical example of bond rotation and torsional strain is the ethane molecule.[28] Its eclipsed conformation connects two sp^3 hybridized C atoms at a conformational energy maximum and is approx. 3 kcal mol^{-1} higher than the staggered conformation, which connects two sp^3 hybridized atoms at a conformational energy minimum; the potential energy varies with the angle of rotation in a sinusoidal manner (Fig. 2.2).

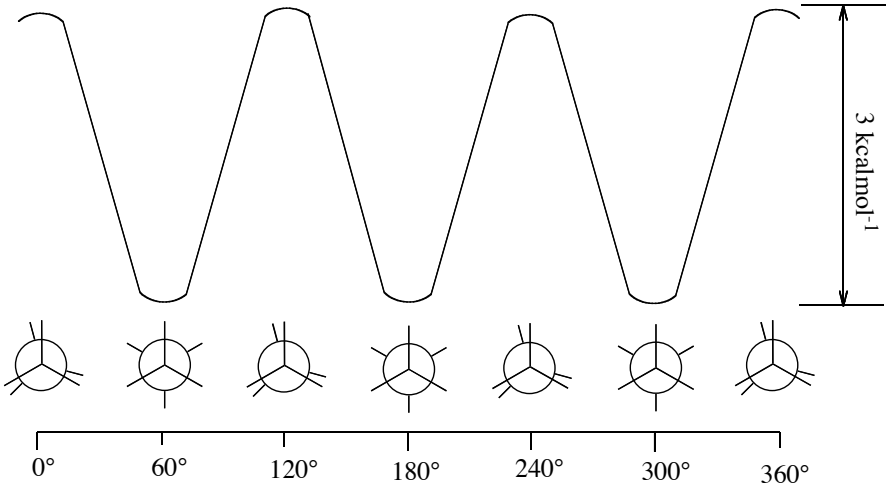

Figure 2.2: Ethane Bond Rotation, the staggered conformation represents a energy minima, whereas the eclipsed one represents a energy maxima.[29]

In 1929 Ebert[22] and then in 1931 Wagner[23] propose a hindered rotation in ethane. Their hypothesis was based on measurements of the molar heat capacity of ethane. There foundings were but were supported by quantum theoretical computations by Eucken, Teller and Weigert[24, 25] in 1933. In 1936 Pfitzer and Kemp[26, 27] showed that by directly applying the third law of thermodynamics to low temperature heat capacity measurements, one could obtain entropy values to be used in thermodynamical calculations. With this method they could show the existence of a barrier in ethane of approximately 3 kcal mol^{-1}. After this experiment many more experiments in this field were done, all confirming the rotation barrier of ethane to be approximately 3 kcal mol^{-1}. In 1949 Smith[30] was able to show that the staggered conformation of ethane is the lower energy one. In the 60's Pople[31–33] corroborated this observation by performing ab initio calculations.

Scientist still discuss the cause of this small energy difference. In ethane the C–C bond length is 154 pm and the Van der Waals radius for hydrogen is 120 pm, this implies that the hydrogen atoms at opposite ends of ethane are not in each others way. Possible origins of the

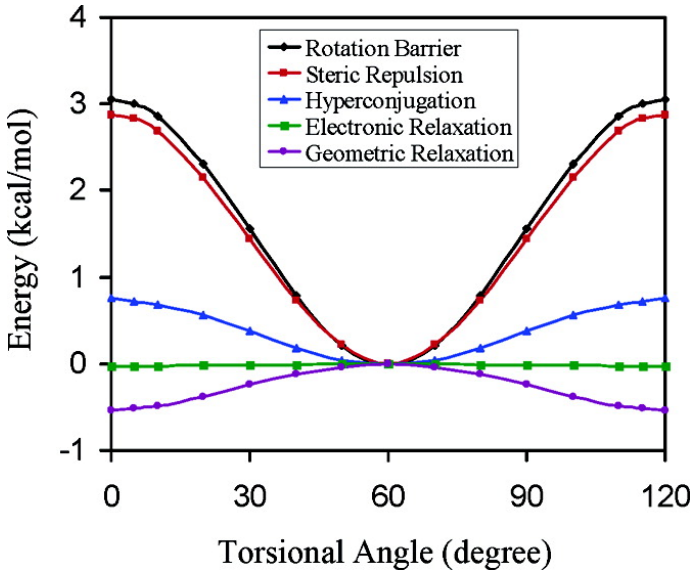

Figure 2.3: Contributions to the rotation barrier in ethane, including steric repulsion, hyper-conjugation, electronic relaxation, and geometric relaxation energy with respect to the torsional angle. (Graphic reproduced from ref.[38])

rotational barrier in ethane could be: a strong hyper-conjugation which would stabilize the staggered conformation compared to the eclipsed one, or a torsional barrier originating from greater electron repulsion in the eclipsed configuration from the overlap of two filled C–H bond orbitals. Most textbooks still explain the rotation barrier as a steric effect.[34] At the end of the 90's Pophristic and Goodman[35–37] showed by using a computational method that the staggered conformation is preferred electronically, they were able to probe this by "swichting off" steric repulsions and still obtaining a rotational barrier[34–37] of about 3 kcal mol^{-1}.

Yirong and Gao[38] performed in 2007 a similar theoretical analysis of this problem, they also discussed the possible origins of the rotational barrier in ethane as summarized in Fig. 2.3. The controversy about the origin of the rotational barrier in ethane centers around the question, whether it is the result of stronger hyper-conjugative stabilization of the staggered conformation compared to that in the eclipsed form or whether the torsional barrier originates from greater

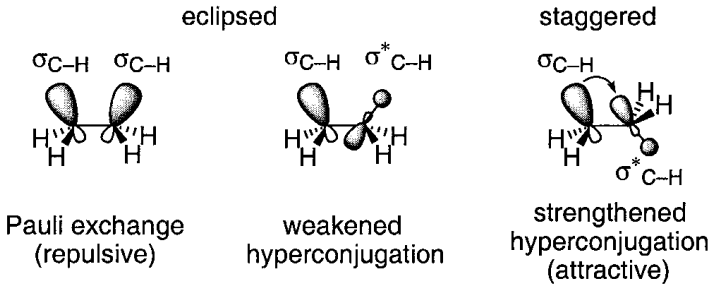

Figure 2.4: Steric as well as quantum-mechanical models for explaining the preference for the staggered form of ethane. (Graphic reproduced from ref.[34])

steric repulsion in the eclipsed configuration due to electrostatic and Pauli exchange interactions. In this account, recent studies led to a consistent conclusion, that hyper-conjugation (Fig. 2.4) controls the ethane barrier.[34–37]

2.2.2 Atropisomerism

When talking about rotation around single bonds, atropisomerism has to be introduced. The term atropisomerism was introduced by Kuhn[39] to describe isomers, which do not interconvert due to restricted rotation around single bonds. He derived the term form the Greek **a**, meaning not, and **tropos**, meaning turn. The first example of resolved atropisomers was 6,6' -dinitro-2,2'-diphenic acid in the early 1920s by Kenner and Christie.[40, 41] By using bulky ortho groups on a biphenyl moiety they were able to prevent rotation about the C–C single bond of the biaryl and to resolve two axial enantiomers which are stable even at room temperature. The family of sterically hindered biaryls is mostly mentioned, when speaking of atropisomerism, but this class of isomerism is found more widely in chemistry.[42] Atropoismerism is also found in other found in hindered biaryls, triaryls, diarylacetylenes, 1,1'-binaphyls as well as non aryl species such as, sulfoxides and 9-substitued triptycenes[43] *etc.*

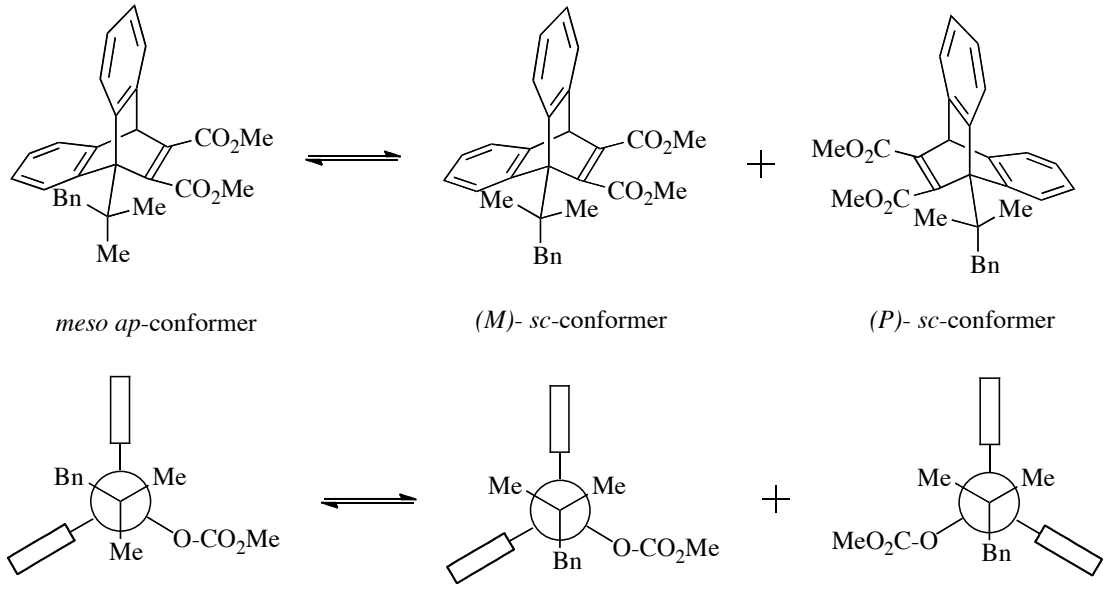

Figure 2.5: Atropoisomerization of dibenzobicyclo[2.2.2]octadiene with rotational barrier[44] of 33.2 kcal mol^{-1}. (Graphic reproduced from ref.[44])

In Fig. 2.5 the atropoisomerization of dibenzobicyclo[2.2.2]octadiene is depicted as an example. It shows the isomerization of the meso conformer (antiperiplanar) to the M- and P-conformers (synclinal) which can be separated.[42, 43]

2.2.3 Biphenyls

In biphenyl, hindered rotation about the sp^2-sp^2 C–C single bond is found. In the gas-phase biphenyl is twisted, with a dihedral angle of approximately 45°. In the crystalline state at ambient temperature, as well as at 100K, biphenyl appears planar.[46] By incorporating more sterically demanding substituents than H in the 2- and 2'-position of the biphenyl core the rotation barrier increases. The preferred ground state conformation of substituted biphenyls is an *anti*-conformation, in which the two aryl moieties are neither coplanar nor orthogonal. Only 2,2' dihalobiphenyls have been reported to prefer the *syn*- conformation.[47, 48] This can be explained by a compromise between resonance stabilization and steric destabilization. In Fig. 2.6

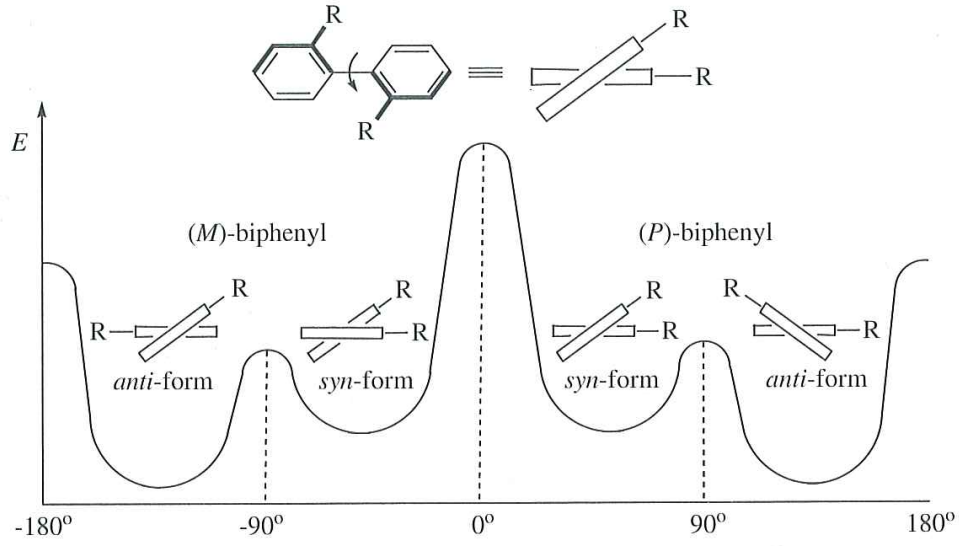

Figure 2.6: Energy profile of 2,2'-disubstituted biphenyls. (Graphic Reproduced form ref.[45])

the energy profile for the rotation of 2,2'-disubstituted biphenyls is depicted. If we start at the ground state and proceed to the syn-state, the substituted biphenyl passes through a high-energy state with increased steric repulsion. In order to achieve another 90° turn, the coplanar situation of the 2,2'-disubstituted biphenyls has to be passed, this is the highest energy state after which further rotation leads to the mirror *cis*-state seen previously.

Charbonneau and Delugeard[46] showed in 1976 that the planar structure of biphenyl in its crystal structure is a time-averaged structure, being caused by a rotation of the two rings in a double minimum potential and that the observed planar structure is the statistically averaged arrangement of two non-planar structures. As the temperature is lowered, a phase transition starts to occur at 40K. This phase transition leads to twisted biphenyl with a dihedral angle of about 10°.

The twist angle for ortho-substitued biphenyls is higher than 10° suggesting a higher rotation barrier.[49] Grein calculated the rotation barriers for a set of ortho-substitued biphenyl in 2002 of

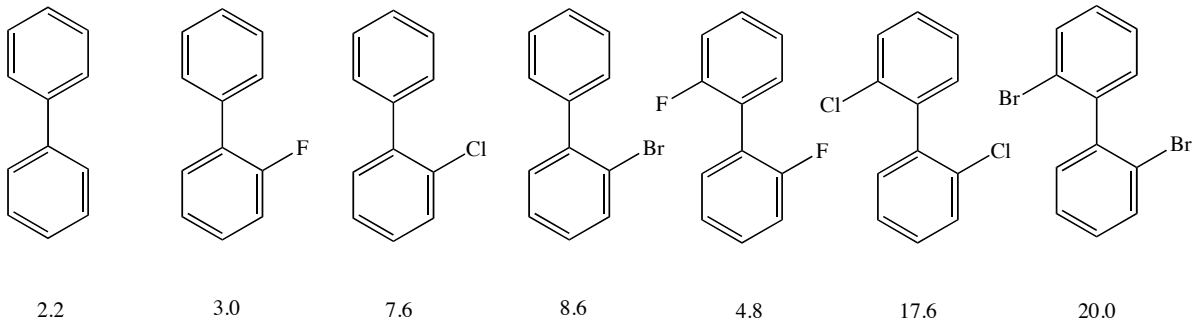

Figure 2.7: Rotation barriers of Biphenyl derivatives[50] in kcalmol^{-1}. (Graphic reproduced from ref.[50])

B3LYP6-311 + G* level of theory[50] (Fig. 2.7). He showed that including functional groups such as halogens in the ortho position of biphenyl, leads to an increase of the conformational stability as a result of steric interactions in the coplanar transition states and therefor higher rotational barriers occur .

Already in 1922 Christie and Kenner[40, 41] had experimentally shown that atropisomeric biaryls[40, 41] can be separated by introducing bulky substituents in the 2, 2' positions. They demonstrated that 6,6'-dinitrobiphenyl-2,2'-dicarboxylic acid and its 4,4',6,6'-tetranitrobiphenyl-2,2'-dicarboxylic acid can be separated into enantiomers while biphenyl-2,2'-dicarboxylic acid undergoes rapid razemization at room temperature.

2.3 Rotation around a Triple Bond

2.3.1 Diphenylacetylene (Tolan)

In tolan, the distance between the two phenyl rings is larger than in biphenyl (Fig. 2.8). As a result, interactions between substituents on the phenyl groups are smaller and hardly influence the rotation barrier around the triple bond.[51–54]

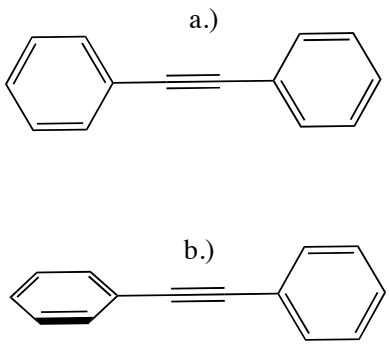

Figure 2.8: Tolan in its a.) coplanar conformation and b.) perpendicular conformation

For predicting the ground state of tolan and its geometry the molecular orbitals have to be considered. In the first case the π-orbitals of both phenyl rings can overlap with the same π-orbital in the alkyne, leading to a planar geometry. In the second case, the π orbitals of one phenyl ring overlap with one π-orbital of the alkyne and the π-system of the other ring interacts with the other π-orbital of the alkyne, leading to a perpendicular geometry. A third possibility is that there is no strong preference for either geometry, leading to essentially free rotation. A truly free rotation is only achieved if, both the coplanar and the perpendicular geometries have the same energy. (Fig. 2.8). In early studies Liberles and Matlosz[51] had calculated a rotation barrier between 0.4 and 0.7 kcal mol^{-1} favoring the planar form,[51] slightly.

Ito and coworkers[52] found in 1984 an experimental value of 0.6 kcal mol^{-1} for the barrier height (derived from electronic spectra in a supersonic free jet). This low value indicates a nearly free rotation of the phenyl groups, considering the three possible geometries of the tolan. This low barrier height was later confirmed by calculations performed by Xu and Cooksy using ab initio B98/cc-pVDZ level[53] of theory.

The crystal structure of tolan shows a planar structure with D_{2h} symmetry;[55–58] however as in biphenyl, this may be the result of a packing effect rather than a reflection of the preferred ge-

ometry. The absorbance spectra of tolan were compared to the spectra of phenylacetylene as well as *E*- and *Z*- stilbene.[51] Tolan does not have absorbances in the same region as phenylacetylene, however there is significant peak overlap with the stilbenes. Tolan is therefore generally thought to be planar in solution because the UV-spectrum more closely resembled stilbene rather than two independent phenylacetylene units. Calculations,[52] indicated a very small rotational barrier in tolan, only slightly favoring the planar species.

2.3.2 Sterically Congested Alkynes

Althought tolan has a nearly free rotation Toyota and coworkers looked to isolate rotational isomers of aryl alkynes by inducing steric interactions and isolated rotational isomers by introducing sterical bulky groups.[60–64] In their first example in 2000 they investigated bis(1,4-disubstitued 9-triptycyl)-ethynes, which have a 3-fold symmetry comparable to that of ethane (rotation barrier 3 kcalmol^{-1}). The distance between the triptycene groups sustained by the alkyne spacer basically eliminates steric interactions (as in tolan). In order to increase the rotational barrier Toyota and coworkers introduced peri substituents on the triptycene core[60] (Fig. 2.9) leading to *ap* and *sc* rotational isomers of bis(1,4-disubstitued 9-triptycyl)-ethynes with measurable rotational barriers in solution phase.

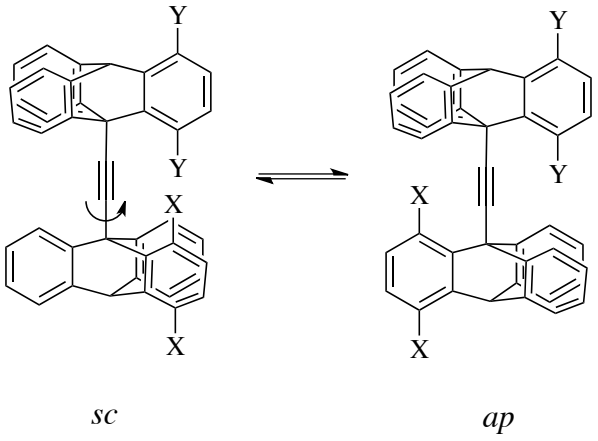

Figure 2.9: Representation of *ap* and *sc* rotational isomers of bis(1,4-disubstitued 9-triptycyl)-ethynes representing a sterically congested alkyne.[60, 61]

Table 2.1: Van der Waals radii and rotational barrier of different sets of *ap* and *sc* rotational isomers of bis(1,4-disubstitued 9-triptycyl)-ethynes.

Entry	prefered Isomer	Substituent Y	Substituent X	Van der Waals radii of X Å	Rotational Barrier kcalmol^{-1}
1	*ap*	CH_3	H	1.20	10.1
2	*ap*	CH_3	OCH_3	1.52	12.7
3	*ap*	CH_3	CH_3	1.80	15.4
4	*sc*	CH_3	F	1.47	11.6
5	*sc*	CH_3	Cl	1.75	14.7
6	*sc*	CH_3	Br	1.85	16.7
7	*sc*	CH_3	I	1.98	17.3
8	*ap*	CH_3	Ph	1.82	15.7
9	*ap*	CH_3	Mes	2.13	18.8

Rotational barriers for a series of bis(1,4-disubstitued 9-triptycyl)-ethynes were measured using variable temperature NMR. Rotational barriers in the range from 9 to 17 kcalmol^{-1} correlated linearly with the van der Waals radii of the substituents.[60, 61] The results are summarized in table 2.1.

In order to have an even more congested system Toyota and coworkers changed to different aryl and phenethynyl groups.[62] Entering a simple phenyl substituent lead to a similar rotational barrier as entering a -CH_3 substituent (table 2.1). The introduction of phenethynyl and napthethynyl substituents increased the barrier to 17.5 and 17.8 kcalmol^{-1}. The highest rotational barrier (to 18.8 kcalmol^{-1}) was achieved by introducing a mesityl group. The authors explained this barrier in terms of the increased rigidity of the mesityl substituent relative to that of the ethynyl groups and concluded that both steric bulk and flexibility must be considered when attempting to hinder rotation.

Toyota and coworkers also reported other classes of congested alkynes bis[di(o-aryl)phenyl]acetylenes as well as bis-diantracene-acteylenes.[63, 64] From VT-NMR measurements, a barrier to restricted rotation about the acetylenic axis of less than 8 kcalmol^{-1} was estimated for bis[di(o-aryl)phenyl]acetylenes. Bis[di(o-aryl)phenyl]acetylenes can be regarded as sterically con-

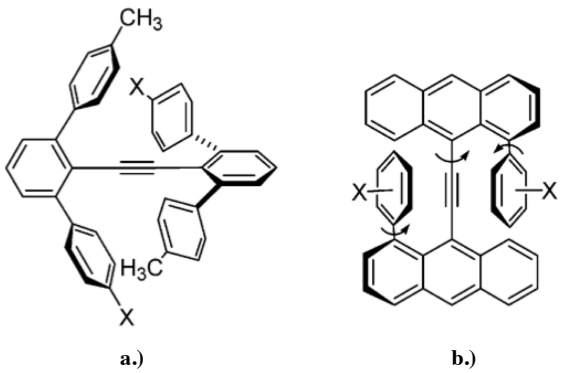

Figure 2.10: a. bis[di(o-aryl)phenyl]acetylenes rotation b. anthracene rotation

gested diphenylacetylenes (Fig. 2.10a.). Toyota and coworkers studied the system in Fig. 2.10a. a congested diphenylacetylene with 4-methylphenyl (tolyl) groups at all ortho positions. Concerning the structure they found that the acetylenic axis is almost linear, and the two axial phenyl groups are tilted by 62.5° out of the coplanar conformation. To obtain kinetic information by

NMR, the system was desymmetrized by functionalization of the methyl groups (converting two of four methyl groups into methyl ethers). The rotation barrier was too low to be measured in solution phase by NMR.

Another example of sterically congested diphenylacetylenes is bis(1-phenyl-9-anthryl)acetylenes. Using VT NMR, Makino and Toyota were able to measure a rotation barrier to rotation about the acetylene bond of 18 kcalmol^{-1} for the sterical hindered substrate ((Fig. 2.10b.) with X= 3,4-(i-Pr)$_2$). They identify two rotational movements, which appeared to be independent of each other: rotation of the two anthracene units about the acetylene axis on one hand and rotation of the phenyl groups about the C-Ar-anthracene bond on the other hand. The second barrier amounted to 10-12 kcal mol^{-1} depending on the substitution of the phenyl ring.[63, 64]

2.3.3 Molecular Turnstiles

In 1995 another example for non-correlated rotary motion was published by Moore and Bedard: a turnstile.[65] It consists of a hexa(phenylacteylene) macrocylic frame (Fig. 2.11: in black) and a an interior spindle (red) linked to the macrocyclic frame with alkyne spacers. This system can also be regarded as a congested diphenylacetylenes. The turnstile has three noteworthy symmetry elements in its architecture: a mirror plane perpendicular to the macrocyclic frame along the rotation axis ($\sigma_{\parallel}$), a mirror plane perpendicular to the macrocyclic frame and the spindle axis ($\sigma_{\perp}$), and a mirror plane contained within the plane of the macrocycle (σ_h).

This architecture was chosen to exhibit conformational bistability (double-well potential energy surface exhibited by a pair of isoenergetic rotational isomers), which allows, depending on the substitution pattern of the macrocycle or the spindle, to relate two rotamers either as homomers, enantiomers, or diastereomers. Of these three possibilities, rotational enantiomers

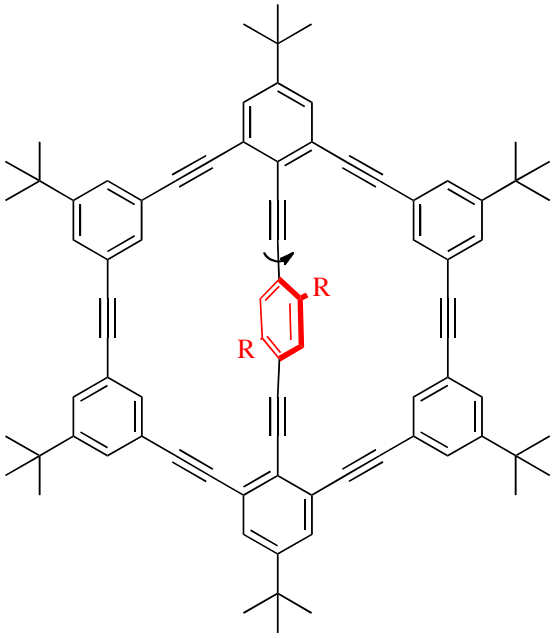

R= CH_2OCH_3 or Ar

Figure 2.11: Molecular Turnstile by Moore and Bedard

are the most interesting since they allow for both polar arrangements of electrical dipoles and true conformational bistability through isoenergetic conformers.

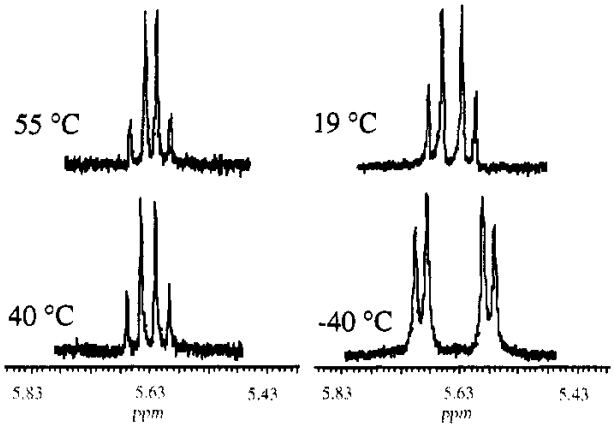

Figure 2.12: Variable-temperature 500MHz ^{1}H NMR spectra in ($CDCl_3$) of a turnstile spindle with R=CH_2OAr in the region of the spindle methylene resonance at the indicated temperatures. (Reproduced from Ref.[65])

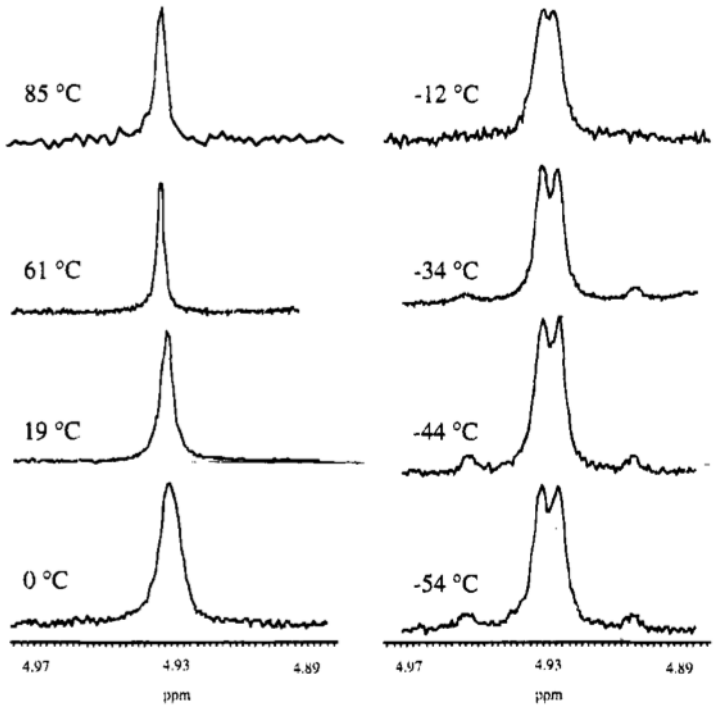

Figure 2.13: Variable-temperature 500MHz ^{1}H NMR spectra ($CDCl_3$) of turnstile spindle with R=CH_2OCH_3 in the region of the spindle methylene resonance at the indicated temperatures. (Reproduced from Ref.[65])

The dynamic behavior of the molecular turnstile was investigated by variable temperature ^{1}H NMR. For R=CH_2OCH_3 and R=CH_2OAr the benzylic protons of the central aryl group (red) become diastereotopic, in the case of slow spindle rotation at the NMR time scale. Therefore two signals are expected for slow rotation and a singlet for fast rotation. (Fig. 2.12) The result for this turnstile confirms that in the case of R=CH_2OAr the turnstile is locked and unable to rotate freely. The estimated rotation barrier for this spindle is approximately 20.6 kcalmol^{-1}. (Fig. 2.13). For R=CH_2OCH_3 spindle rotation can be observed in the ^{1}H NMR. The spectra show a coalescence behavior. At -54°C a doublet is seen, which becomes a singlet with increasing temperature. Studies with molecular models further showed that rotation of the turnstile requires

a distortion of the planar conformation of the macrocyclic frame work. The estimated rotation barrier for the spindle is approximately 13.4 kcalmol^{-1}

2.4 Crystalline Molecular Rotors

2.4.1 Molecular "Gyroscopes" and "Compasses"

In 2002 Garcia-Garibay and coworkers publish the synthesis and elucidation of the internal dynamics of gyroscopes and compasses.[66–69] Garcia-Garibay and coworkers worked towards the synthesis and arrangement of a series of alkyne rotors in a close-packed crystalline molecular assembly. Their intention was to control the rotary motion of this assembly using crystal engineering. Their goal was the realization of a novel concept based on dipolar units expected to reorient under the influence of electric, magnetic, and optical stimuli. The idea was to design a crystaline molecular rotor with a fluorine substituted phenyl rotator part, which is embedded in a static macrocylic part (Fig. **??**). These systems are also congested diphenylacetylene molecules. The strategy of the Garcia-Garibay group was to perform studies on increasingly more congested systems.

The first system they studied was an open system, comparable to other congested diphenylacetylenes, a 1,4-bis(3,3,3- triphenylpropynyl)benzene. The X-ray analysis revealed that it cocrystallized with benzene in a relatively open lattice (Fig. 2.14).[70–72]

By performing variable temperature solid state NMR (^{13}C-CPMAS NMR) the Garcia-Garibay group was able to determine the rates of phenylene rotation in the de-solvated crystal and an approximate rotation barrier of 12.8 kcalmol^{-1}. The phenylene rotation was also measured by VT quadrupolar echo ^{2}H-SSNMR using a model for a two fold flip about the 1,4- axis. Below 295 K, measurements with the benzene clathrate fell within the slow exchange regime (k_{rot}

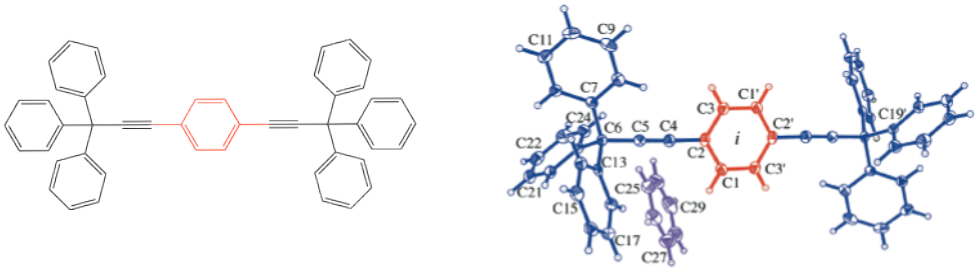

Figure 2.14: 1,4-bis(3,3,3- triphenylpropynyl)benzene with the phenyl rotor part in red and ORTEP diagram of the asymmetric unit of the same compound.[71, 72]

$< 10^{4}$ s $^{-1}$), at higher temperatures the measurements were complicated by the loss of benzene. However, line-shape analysis of spectra measured with desolvated samples between 297 K and 385 K confirmed a two-fold flipping motion with rotation rates ranging between ca. $1.5{\cdot}10^{4}$ s $^{-1}$ and $3.8{\cdot}10^{6}$ s $^{-1}$. From this data an activation barrier for the phenylene rotation of 14.6 kcalmol^{-1} was determined. This value is only 2 kcalmol^{-1} higher than the one for the benzene clathrate, implying nearly no change in the initially porous lattice upon heating. Fig. 2.15 shows the ^{2}H SSNMR VT spectra. On the left the simulated pattern for a two-fold flip are shown,

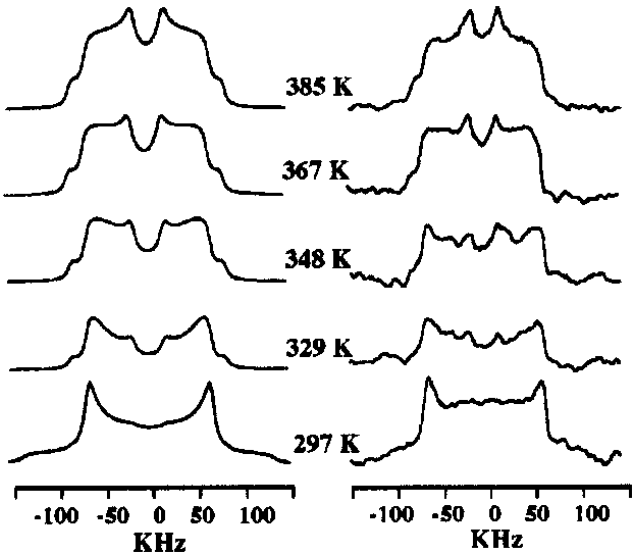

Figure 2.15: Experimental (right) and simulated (left) ^{2}H-SSNMR spectra. (Fig. reproduced from ref.[72])

and on the right the measured spectra. The pattern for the two fold flip of the phenyl ring was clearly recognizable in the experimental spectra. Garcia-Garibay and coworkers concluded from these studies that their molecular frames based on alkyne linkages and trityl groups allow rapid rotation of phenylene groups along their 1,4-axis in the solid state.[72]

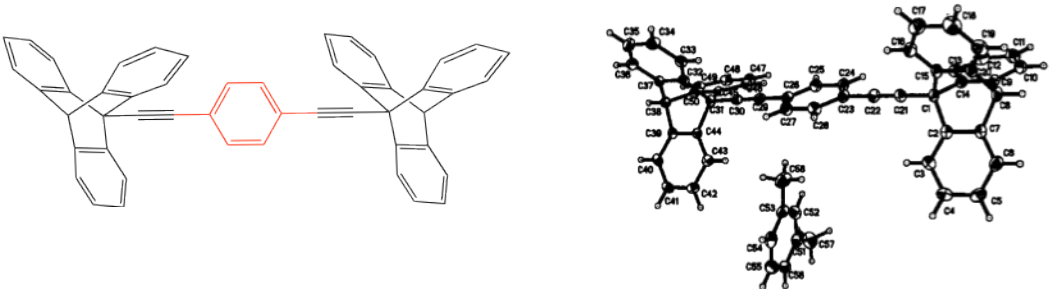

Figure 2.16: Congested system with triptycene stators.[73]

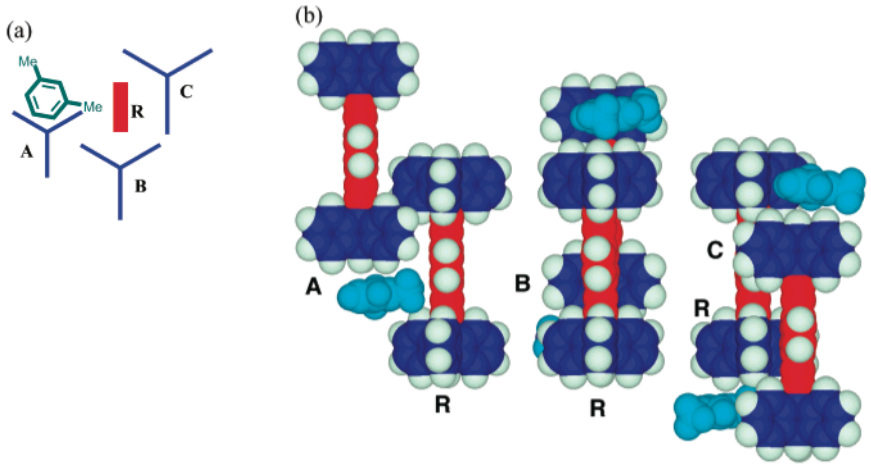

Figure 2.17: Crystal packing of a congested system with tripycene stator parts. (Fig. reproduce from ref.[74])

In order to accelerate the phenylene rotation, Garcia-Garibay and coworkers tried to make the stator part more rigid.[73, 74] To this end the triphenylmethyl stator was replaced by a triptyl framework (Fig. 2.16), in order to sterically shield the phenylene from contact with other molecules in the environment. Semi-empirical calculations with the AM1 method indicate that

rotation about tryptycene-alkyne and aryl-alkyne single bonds are essentially frictionless in the gas phase. The compound crystallized, this time as a clathrate of xylene. In this compound the phenylene ring rotation was strongly hindered in the solid state Fig. 2.17 . All molecules align in the same direction in the packing and molecules fit their protuberances into voids of adjacent molecules, with solvent molecules acting as spacers. This leads to a restriction of the phenylene ring rotation (Fig. 2.17a, red) by the triptycyl groups from three close neighbors (Fig. 2.17a, blue).[74] To avoid this congested packing, the authors suggest substituted triptycenes as a solution as shown in Fig. 2.18.[73] In 2004 the Garcia-Garibay group reported the synthesis of methyl-substituted triptycyl frames and were also able to obtain single crystals for X-ray analysis.[75]

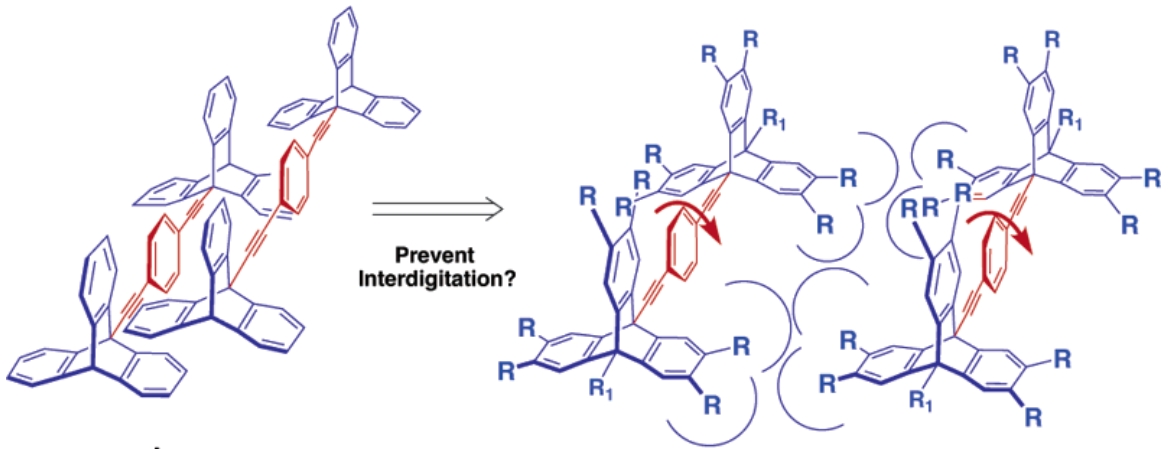

Figure 2.18: Substitution pattern on the triptycene stators, in order to control the crystal packing (Fig. reproduce from ref.[75]).

In the case of 1,4-bis[2-(6,12-dimethyl-2,3,7,13-tetramethyl-10-alkyl-9-triptycyl)- ethynyl] benzenes (Fig. 2.18), the packing was the same as in the original design with the open triphenylmethyl stators. The interdigitation between adjacent molecular rotors is prevented by the

methyl groups on the periphery of the two triptycenes and they also create large cavities between two neighboring rotor molecules. All molecules are oriented in the same direction in the crystal. The local environment around the central phenylene moiety is formed by six solvent molecules (bromobenzene). The bromobenzenes pack in pairs, with a face-to-edge interaction between their aromatic rings.[75] Preliminary dynamic studies on this system were performed by SS ^{2}H-NMR, which indicated that gyroscopic motion in these crystals occurred with a very low rotational barrier.[75–78] Also preliminary analysis of the atomic displacement parameters was undertaken, assuming a two-fold flipping model in a symmetric periodic potential and a simple approximation that involves small excursions lead to a rotational barrier of 3.3 kcalmol^{-1} .

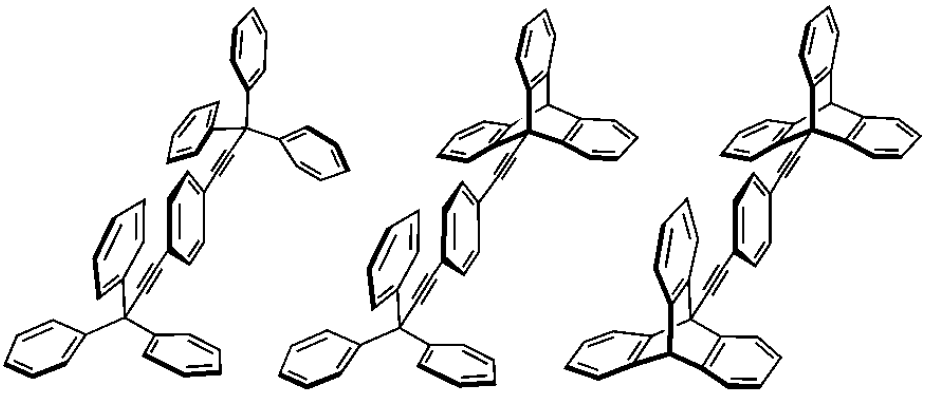

a.) b.) c.)

Figure 2.19: Molecular gyroscopes consisting of a 1,4-diethynylphenylene rotator linked to a.) symmetric bis(trityl) b.) trityl and triptycyl and to c.) bis(triptycyl)stators groups.[80]

In 2006 the Garcia-Garibay group extended their concept for constructing compasses and gyroscopes.[79–81] Their idea was to improve the physical properties and rotational dynamics by making the stator part asymmetric. One stator would be a triptycene and the other a triphenylmethyl moiety.[80] This was based on previous studies on **a** (Fig. 2.18) and **c** (Fig. 2.18) and the remarkable differences in their physical and dynamical properties. **a** (Fig. 2.18) was

soluble in most organic solvents, whereas **c** dissoved only in hot aromatic solvents. The packing of **a** and **c** also differed a lot; in compound **c** phenylene ring rotation was hindered by neighboring triptycene rings (Fig. 2.18), this was not the case in **a**. By mixing the stator parts it was hoped that the packing could be influenced in a positive way (Fig. 2.19). The authors reasoned that the hybrid structure **b** (Fig. 2.18) could have the "desirable sturdiness of **a** , the good solubility of **c**, and the rapid dynamics potentially associated with a lower-density crystal". The mixed gyroscope was then synthesized and analyzed. Even though it tended to give micro-crystalline material the authors were able to obtain a crystal structure - a solvate again, this time of chloroform. The asymmetric unit (triclinic space group) includes one molecule of **b** (Fig. 2.19) and one molecule of chloroform.[80, 81]

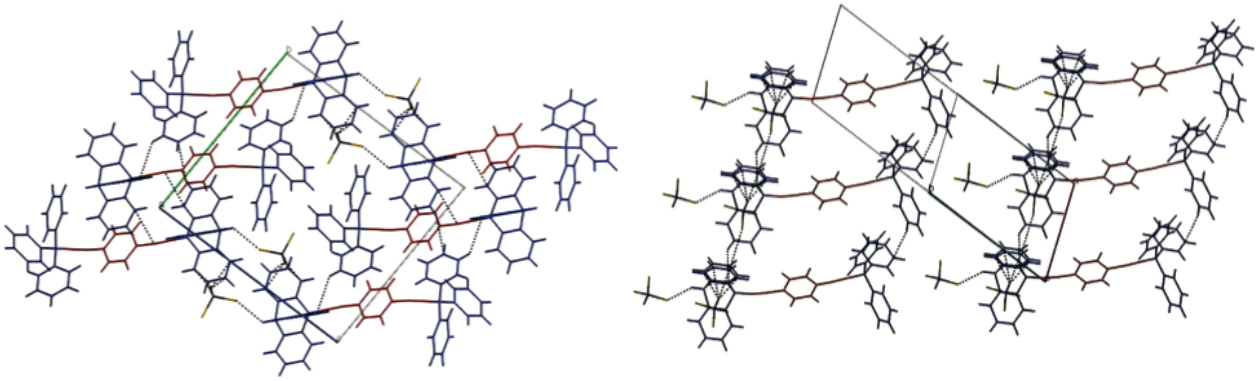

Figure 2.20: Molecular packing of the chloroform solvate of **b** (left) viewed normal to the (1,0,0) plane and (right) normal to the (0,1,-1) plane. Close contacts between neighboring molecules are indicated with dotted lines.(Fig. reproduce from ref.[81])

For the dynamic NMR studies an isotopically labeled sample of **b**-d_4 was prepared and measurements were performed with the solvent free sample giving a rate of rotation (k_{rot}) between $0.5 \cdot 10^6$ and $50 \cdot 10^6$ s^{-1}. By comparing experimental and simulated spectra the authors estimated the rotation barrier to be approx. 8 $kcalmol^{-1}$, this is about 6 $kcalmol^{-1}$ lower than the rotation barrier of compound **a**. The rates of phenylene motion in the solvate are slower than those of the

solvent-free structure. This observation lead to the hypothesis that desolvation occurs without collapse of the lattice.[82, 83] The authors thus concluded, that the asymmetric molecular gyroscope **b**, compared to **a** or **c**, displays a largely improved solubility and dynamic properties, and it represents an interesting lead that highlights the potential properties of solid-state molecular gyroscopes with asymmetric structures.[84, 85]

In 2008 an extended triply-bridged molecular gyroscope was presented.[86–88] Considering that the stator serves as a frame of reference to define the dynamics of the rotator in the crystal, bridged stator should provide high steric shielding, and allow a very fast rotation of the rotator. The triptyl bridged rotors shown in Fig. 2.21 was synthesized and studied,[86] with the idea of extending this design later to a MOF-5 system.

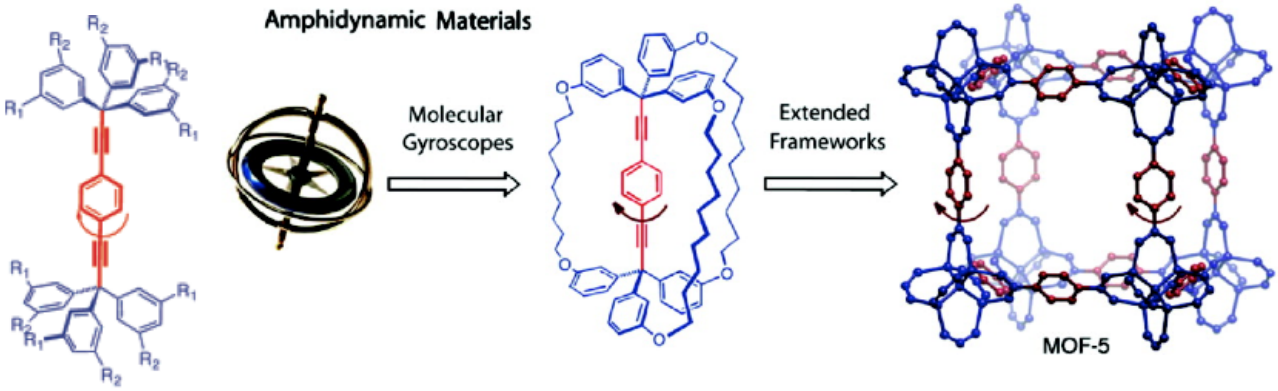

Figure 2.21: Gyroscope consisting of a rotating mass (rotator) linked by an axle to a shielding enclosure (stator). Molecular analogues consist of a phenylene rotator, a dialkyne axle (red), and a bis- trityl stator (blue). Analogs MOF-5. (Fig. reproduced from ref.[86])

The X-Ray structure of a single crystal of the enclosed gyroscope grown in mixtures of toluene and benzene gave a nonstoichiometric mixed solvate. In the crystal structure it was observed, that the steric shielding provided by the three alkyl chains of the gyroscope (Fig. 2.21) is not ideal. Furthermore, the trityl groups of each molecule are arranged in a propeller conformation, with

the aryl groups having different torsion angles. The three bridges as well as the central phenylene are disordered. Concerning the postulated shielding by the three alkyl chains unexpected packing effects occur. Although the three alkyl bridges curve away from the center to maximize the space around the rotator, alkyl bridges from neighboring molecules and solvent molecules fill the free space thus reducing free volume for the rotation of the phenylene. The rotation barrier for this amorphous material was found to be 12 kcalmol^{-1}. From this observation it was concluded, that bulkier and more rigid bridges are needed.[86–89]

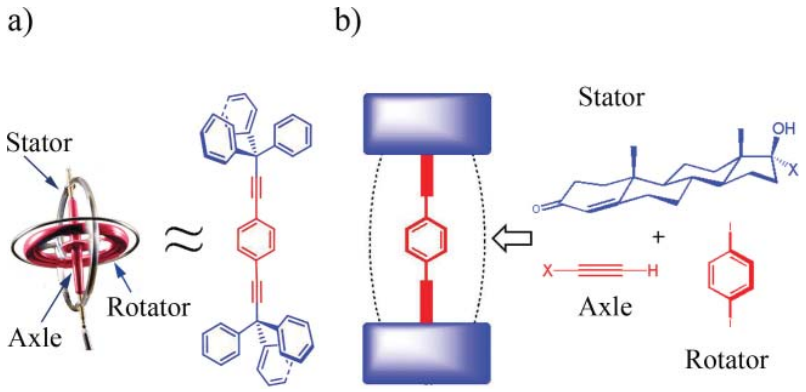

Figure 2.22: a.) A macroscopic gyroscope with its rotator (red), axle and stator (blue). b.) A 1,4-phenylene group (in red) acting as a rotator linked by two alkyne linkages to bulky steroidal groups (in blue) acting as the stator. (Fig. reproduced from ref.[90])

In order to achieve a more shielded system e new strategy was tested. Instead of a molecular rotor system with trityl moieties as stators a new molecular rotor system with 1,4-diethynylphenylene rotators axially linked to two conformationally rigid steroidal norethisterone acetate or ethisterone frames were synthesized[90] and single crystals of the ethisterone frames were obtained. In the case of the ethisterone the system crystallized in a monoclinc space group. The structure expressed very limited conformational degrees of freedom, the structure of the steroidal components in the rotor was very similar to the reported structure for the norethisterone.[90, 91]

The packing arrangement was very dense and showed one-dimensional layers propagating along the plane formed by the a and c crystallographic axis. This arrangement restricted the motion of the central phenylene to a considerable extent. After the synthesis of the deuterium labelled analogues solid state NMR studies were undertaken indicating that the internal dynamics of the ethisterone systeme were very slow in the crystalline state.

2.4.2 Surface Mounted Molecular Rotors

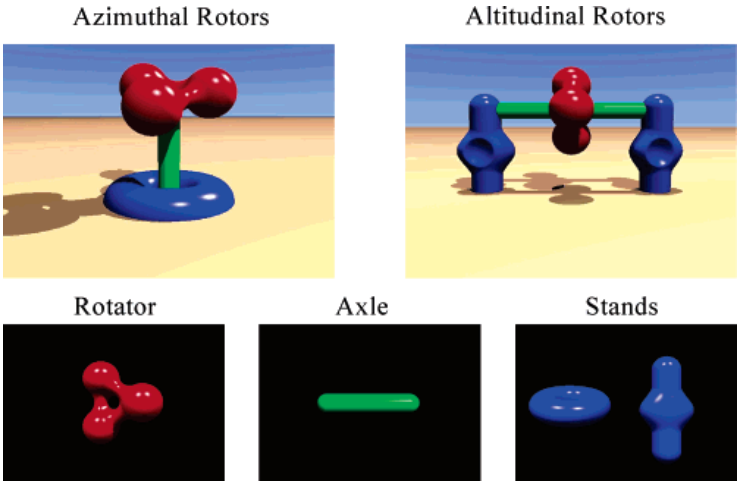

Figure 2.23: Michl's classification system for surface-bound molecular rotors. (Fig. reproduced from ref.[92])

For solution phase rotors the distinction between the rotor and stator is often not clear. Both rotor and stator rotate with respect to each other. However, for surface-mounted molecules, the distinction is unambiguous. Two cases may be distingished: the rotor part is an element of the molecule and the stator part is represented by the surface; alternatively the rotor and the stator are both elements of the molecule, that later can be attached to the surface.[17] Surface mounted rotors can be a further distinguished by whether the axle of rotation is perpendicular (an azimuthal rotor) or parallel (an altitudinal rotor) to the surface (Fig. 2.23).

Michl and co-workers[92] have demonstrated rotation of a polar and dipolar altitudinal rotor mounted on a gold surface (Fig. 2.24). In order to synthesize the suitable system they used the "Molecular Tinkertoys "[93–95] concept of constructing nano-size structures and machinery by covalently binding of molecular rods and connectors. Michl and coworkers were able to synthesize

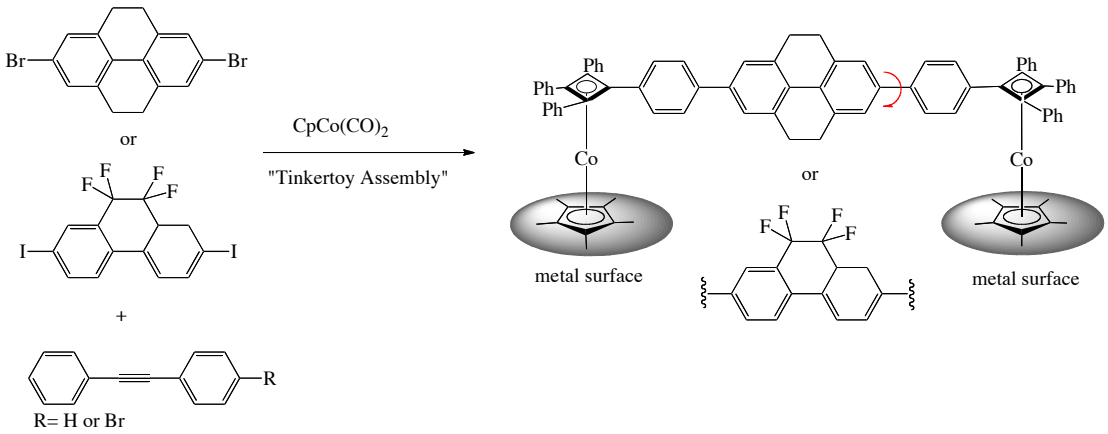

Figure 2.24: "Molecular Tinkertoys". Concept for the synthesis of the altitudinal molecular rotor with nonpolar or polar rotator. .

a dipolar and a non-polar altitudinal molecular rotor[96] which they mounted on a Au (111) surface. STM imaging was used to characterize the structure and monitor molecular dynamics. In order to detect the rotation of the rotor part of the mounted molecules the STM tip was used to measure the work function between the tip and the surface. Michl and Horinek found that one-third of the surface-mounted rotors are free to flip in the direction of their dipole in response to an external electric field and to turn rapidly and randomly at room temperature. The other two-thirds of the rotors appear to be in a blocked state but over time can change to a free state, or from a free state to a blocked state. This work represents an advance in surface-mounted rotors and opens up the prospect to construct closely packed surface-mounted devices that could exhibit correlated motion in response to external stimuli (magnetic, electric, or physical).

Chapter 3

Methods for the Characterization of Rotation Barriers

3.1 Introduction

In order to investigate a rotation barrier of a desired system, different experimental methods have to be considered, depending on the rate of the rotation. There is not a single experiment which allows access to all the time scales of motion. In the case of really fast rotation solid state experiments might be the right choice, since the rotation in solution phase could be too fast to detect. Furthermore working in the crystal engineering field implies solid state quantification. In the following sections the methods used in this project are explained.

3.2 Variable Temperature (VT) X- Ray Analyis

Debije in his famous three papers *"Über den Einfluss der Wärmebewegung auf die Interferenzerscheinung bei Röntgenstrahlen"*, *" Über die Intensitätsverteilung in den von Röntgenstrahlen erzeugten Interferenzbildern"*, and *"Spektrale Zerlegung der Röntgenstrahlung mittels Reflexion und Wärmebewegung"*[97–99] explained in 1913 that increasing the temperature of an X-Ray diffrac-

tion experiment reduces the intensity of the Bragg diffractions, whereas the position and witdhs of the peaks remains nearly unchanged. This effect becomes especially prominent at large scattering angles. It is due to the increase of amplitudes of atomic vibrations about their average positions, the so-called dynamic disorder.[97–99]

In the 50s Cruickshank introduced the anisotropic Gaussian displacement parameters (ADPs) and reported that for aromatic systems ADPs could be interpreted as resulting from rigid body motion.[100, 101] Many crystallographers later contributed to the better understanding of ADPs, and made analyses of molecular motion from X-Ray diffraction data feasible. In the 80's Dunitz, Bürgi, Schomaker, Maverick and Trueblood influenced the way chemists use crystallographic ADPs for the understanding of molecular motions in crystals. They extended Cruickshank's rigid-body model, to allow the distinguishing of different atomic motions[102–107] and the estimation of rotation barriers from VT X-Ray studies.

3.2.1 ADP

The atoms in a crystal are not stationary and vibrate about their mean positions. The structure determined from a difractogram is a time average of this motion. This effect is the so-called dynamic disorder. The atoms may also be distributed randomly over different sets of positions from one unit cell to another, this is the so-called static disorder. It is the mean atomic positions as well as the probability density functions of the individual atoms that are obtained from diffraction studies. The density function represents the time-averaged displacements from their mean position, averaged over all the repeating unit cells. Both kinds of informations are expressed in the well known "ellipsoid" picture of the molecules (Fig. 3.1).[102–107]

The pictures are based on numerical parameters, which contain quantitative information on the rigidity of molecules in crystals, as well as the nature of the molecular rigid body motions,

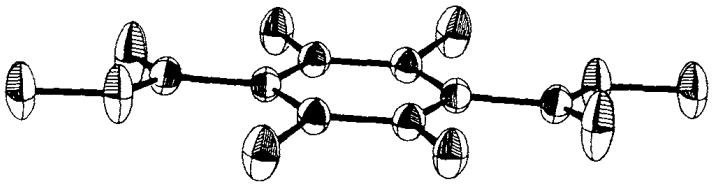

Figure 3.1: Thermal ellipsoids for all atoms in 2,5-dichloro-1,4-dihydroxyterephthalate, except hydrogens in the molecule of dimethyl. Hydrogen atoms are omitted for clarity. The whole molecule can be regarded as a rigid body which is rocking around its pivot atoms of the phenyl ring. (Fig. reproduced from ref.[105])

and even about internal motions of supposedly rigid fragments in nonrigid molecules.[103] From the obtained data it is possible to derive quantities such as rotation barriers, by using a few rather simple assumptions.[103] The following approximation can be used:

If we take a particle in a one-dimensional quadratic potential, V (x)=fx^2/2, its classical Boltzmann distribution (Eq. 3.1) of displacements from equilibrium is given by a Gaussian (Eq.: 3.2) .

$$p(x) = (2\pi kT/f)^{-1/2} \cdot exp(-fx^2/2kT) \tag{3.1}$$

$$< x^2 >= kT/f \tag{3.2}$$

For many crystals the second moments of the atomic pdfs are approximately proportional to the absolute temperature over a considerable range. The second moment for a harmonic quantum oscillator is: Eq. 3.3.

$$< x^2 >= (h/8\pi^2\mu\nu)\coth(h\nu/kT) \tag{3.3}$$

In this equation ν is the oscillator frequency and μ its reduced mass, which in the case of a rotational oscillation is the moment of inertia I. For $h\nu \gg 2kT$, the cotangens hyperbolicus

(coth) factor is 1 and the expression reduces to (Eq.: 3.4):

$$< x^2 >= h/8\pi^2\mu\nu \tag{3.4}$$

In the case of $h\nu \ll 2kT$ the coth factor becomes kT/$h\nu$ and leads to a linear dependence for $< x^2 >$ on T. Its temperature dependence is than given by eq. 3.2 and eq. 3.3.

From experimental values of $< x^2 >$, which can be derived from the principle mean square atomic displacements parameters of the ellipsoids and a knowledge of the temperatures at which they were measured. Effective quadratic force constants f (or frequencies) for the mean-field motions in question may be estimated with eq. 3.2 and eq. 3.3. A more accurate model is needed to calculate rotational barriers. The mean-field potential associated with a given type of motion can be obtained, at least conceptually, by following the potential energy variation when an atom (or molecule) is gradually displaced from its equilibrium position (or orientation), with all neighboring atoms (or molecules) in their equilibrium positions. This is an over- simplified picture. A more realistic model allow for the ways in which the instantaneous displacements of different atoms (or molecules) are correlated. This is achievable from a complete lattice-dynamical treatment, but only at the cost of considerable additional mathematical complexity and loss of conceptual simplicity. In lattice dynamics a suitable force field is used to solve the equations of motion for the whole periodic ensemble of molecules that constitute the crystal structure. The calculation yields the frequencies of all the normal modes of vibration of the crystal.[103–107]

3.2.2 Calculating Rotation Barriers from ADPs

In order to calculate the rotation barrier the harmonic potential is replaced by a more appropriate sinusoidal potential. For such a potential, classical Boltzmann averaging leads to a distribution of

angular displacements given by eq.: 3.5 , in which B is the barrier height and N is a normalization factor.

$$p(\phi) = Nexp(-B(1-cosn\phi)\cdot 2RT) \tag{3.5}$$

$$\langle \phi^2 \rangle = \frac{2RT}{Bn^2} \tag{3.6}$$

$$< \phi^2 >= \frac{\int \phi^2 exp\{-B(1-cosn\phi)/2RT)\}d\phi}{\int exp\{-B(1-cosn\phi)/2RT)\}d\phi} \tag{3.7}$$

The quadratic function (3.6) can only be used if $< \phi^2 n^2 >$ is much smaller than unity, this means when B is several times larger than RT. Otherwise eq. 3.7) must be evaluated numerically as a function of RT/B (Fig. 3.2).

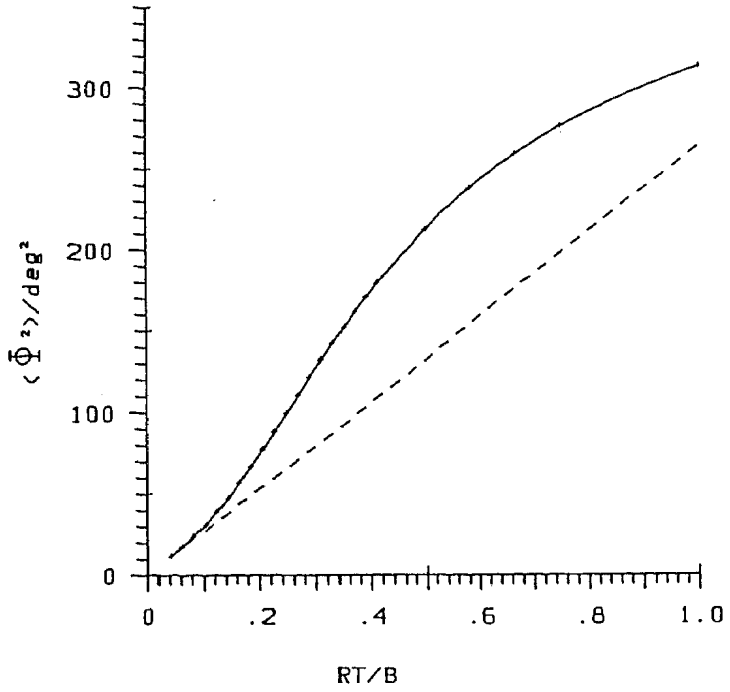

Figure 3.2: Full curve (Eq.: 3.7 , n=5): Variation of mean-square libration amplitude $< \phi^2 >$ with RT/B for a fivefold periodic sinusoidal restricting potential with barrier height B. For the dashed curve $< \phi^2 >$ for harmonic oscillator potential with the same quadratic force constant. At very low temperatures, both curves should run parallel to the horizontal axis at the nonzero value of $< \phi^2 >$ corresponding to the zero-point motion. (Fig. reproduced from ref.[105])

After having the sin-plot Fig. 3.2 in hand the rotational barrier can be obtained by entering a $<\phi^2>$ value from experiments reading the corresponding RT/B value from the plot and calculating the rotational barrier B nummericaly.[102]

3.3 Solid State NMR

In solution phase NMR spectroscopy, anisotropic NMR interactions are averaged out by rapid molecular tumbling, which leads to very sharp transitions (peaks) in the the spectra. In contrast, in solid state NMR the anisotropic or orientation-dependent interactions, *i.e.* chemical shift anisotropy (CSA) and the dipolar and quadrupolar couplings, lead to a broadening in the spectra. Thus the resonance frequency of a given nucleus within a particular crystallite depends on the orientation of the crystallite relative to the direction of the magnetic field.[112, 113]

On the one hand, these anisotropic interactions lead to a significant reduction of the resolution in the spectra but, on the other hand, theses anisotropic interactions contain valuable structural and dynamic information. Moreover, the CSA and quadrupolar interactions together with the dipolar couplings offer a formidable way to probe dynamic processes: VT quadrupolar SSNMR can detect really fast dynamic processes, such as fast rotation in the range of 10^4-10^8 Hz.

3.3.1 Quadrupolar Solid State NMR (^{2}H SSNMR)

The applications of ^{1}H SSNMR is usually relate to the investigation of dynamic processes. In general, one of the most important facets of solid-state NMR, is its ability to probe molecular dynamics. This ability to probe dynamics is a direct consequence of the orientational dependence of the NMR resonance frequency: a given motional process leads to a particular crystallite experiencing a range of different orientations and hence a range of different frequencies.[108, 109] The motion is thus reflected in a marked change in the NMR spectrum as compared to the static

case, with an extreme example of this phenomenon being the complete removal of anisotropic broadening as a consequence of isotropic molecular tumbling in solution. Notably, solid-state NMR spectra are not only sensitive to the rates of dynamic processes but also the geometry.[110]

Compared to ^{1}H (spin I = $\frac{1}{2}$ nucleus), ^{2}H (spin I = 1 nucleus) has a relatively low gyromagnetic ratio ($\sim \frac{1}{7}$ that of ^{1}H). Based on this one would expect a small chemical shift range and therefore narrow line widths for ^{2}H SSNMR spectra. Contrary to expectation a normal line width of $\sim$ 100Hz is normally found for a static ^{2}H SSNMR spectrum. This can be explained by the charge distribution of the nuclei (Fig. 3.3). Quadrupolar nuclei possess a non-spherical charge distribution, which is able to couple to electric field gradients, which are present in most solid state materials.

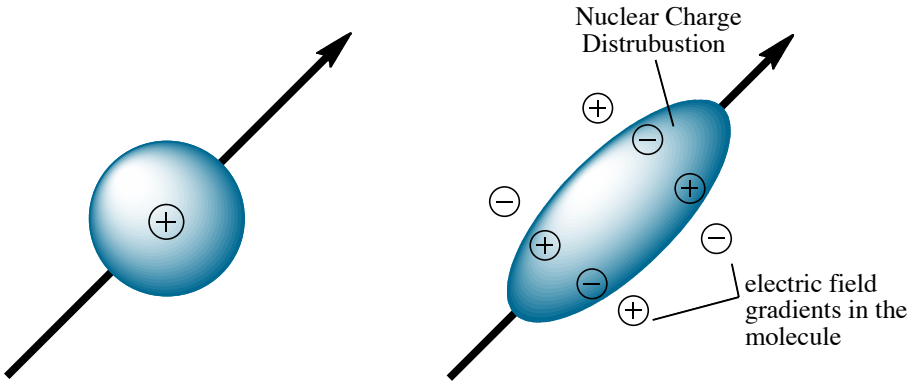

Figure 3.3: Comparison between a spin $\frac{1}{2}$ nucleus and a quadrupolar nucleus.

Although the ^{2}H quadrupolar coupling ($\sim$ 100 kHz) is relatively small as compared to other quadrupolar nuclei, it still dominates the other anisotropic interactions. The quadrupolar coupling depends on the molecular orientation with respect to the magnetic field. A reorientation of the molecule influences the shape of a ^{2}H spectrum and can lead to a reduction of its width. This anisotropic behavior makes the quadrupolar coupling a sensitive measure of internal molecular

motion. By recording a series of spectra at variable temperatures, kinetic parameters and the activation energy, as well as the motional mechanism for the dynamic process, can be investigated. This is done by means of line-shape analysis based on computer simulations. In Fig. 3.4 examples of different simulations are shown. In (a.) a chemical shift anisotropy (CSA) pattern is shown for a static case, a two-site jump and a three- site jump. For the case of a three-site jump, *i.e.* a methyl group rotation, the case of different correlation times is shown in (c.). In (b.) and (d.) ^{2}H powder pattern for molecular motion are shown. The change in the shape of the powder pattern for different molecular motion is also shown. *i.e.* for a two site jump the powder pattern is much wider than that for a three site jump. Moreover, such investigations are aided by the fact that the experiment can be performed over a very wide temperature range, because the sample is in the solid-state (i.e., there is no problem with a solvent freezing or evaporating).

Quantitatively the molecular motions are characterized by the correlation times τ_c and the activation energies ΔE_a. τ_c represents the time it takes for a molecule to reorient by 1 degree, this reorientation requires structural changes in the immediate immediate environment and can be written in the Arrhenius form:[111] $\tau_c = \tau_o exp\frac{E_a}{RT}$.[111] If a molecule undergoes an internal molecular motion, regular powder patterns will be observed only if its correlation time, τ_c, is much longer than the inverse of the anisotropy factor (δ) of the spin interaction. (Eq. 3.9) Under static conditions the NMR Hamiltonians can be written as (Eq. 3.8):

$$\omega = \omega_{iso} + \omega_{aniso}(\theta,\phi) \tag{3.8}$$

$$= \gamma B_0 \left\{ R_{iso} + \frac{\delta}{2}\left(3cos^2\theta - 1 + \eta sin^2\theta cos2\phi\right) \right\} \tag{3.9}$$

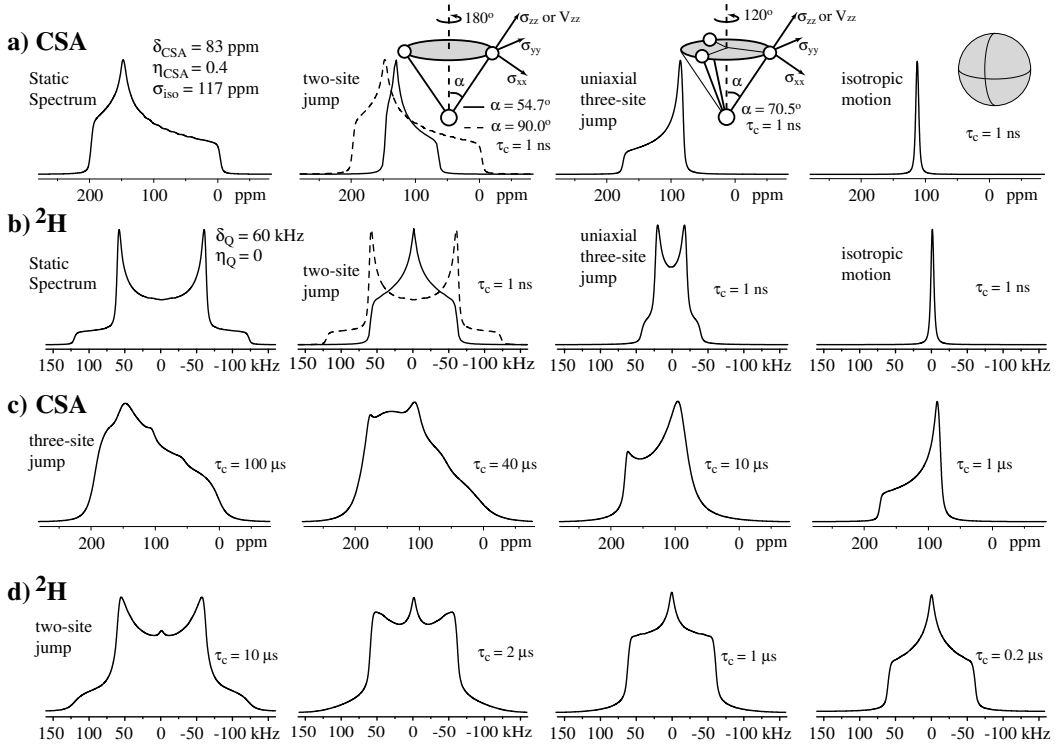

Figure 3.4: Series of CSA and quadrupolar (^{2}H) powder patterns simulated for different kinds of molecular motions. a) CSA powder patterns. b) ^{2}H powder patterns. c) CSA powder pattern for three-site jump with $\alpha = 70.5^\circ$ (methyl rotations) and different correlation times. d) ^{2}H Powder pattern for two-site jump with $\alpha = 54.7^\circ$ and different correlation times. (Figure reproduced from ref.[112])

In 3.9 R_{iso}: isotropic term, δ: anisotropy factor, η:asymmetry parameter, ϕ and θ: Euler angles, τ_c : correlation time

In the slow exchange regime we have:

$$\delta \cdot \tau_c \gg 2\pi$$

At larger motional rates in the intermediate exchange regime we have:

$$\delta \cdot \tau_c \sim 2\pi$$

At fast motional rates in the fast exchange regime:

$$\delta \cdot \tau_c \ll 2\pi$$

A big advantage of ^{2}H SSNMR, besides quadrupolar coupling, is the wide temperature range in which it is applicable. It is possible to go down to 5 K. This capability makes it possible to obtain the static case for a molecule that shows "free rotation" i.e barriers comparable to kT.[112–114]

3.4 Solution Phase Dynamic ^{1}H-NMR Spectroscopy

Sometimes a broad band, instead of a sharp signal can be observed in a ^{1}H-NMR spectrum. This phenomenon might be caused by an exchange process between nucleus sites at given measurement conditions. If, on raising the temperature, the broad signals becomes sharper a dynamic process is occurring, with a fast exchange between sites . The sample can also be cooled, in order to test whether freezing a dynamic process is causing a broadening. Cooling of the sample should then lead first to further broadening and eventually to a splitting of the broad signal into two or more signals (Fig. 3.5).[115–117] In order to be able to distinguish the sites their life time τ must be longer than that shown in Eq. 3.10 ($\Delta\nu$ is the difference in frequencies).[115]

$$\tau = \frac{\sqrt{2}}{2\pi \cdot \Delta\nu} \tag{3.10}$$

Analysis of line shapes provides information about the rates of exchanges of sites. An example for line shape analysis is the rotation of the amide bond in *N*,*N*-Dimethylaformamide (DMF). DMF has a planar molecular geometry and rotation about the amide bond is high. The high rotation barrier leads to magnetically nonequivalent N-methyl groups. Due to the restriction of rotation in DMF the N-methyl groups give rise to two separate NMR signals at room temperature. With increasing temperature, rotation rates increase and cause the two signals two become broader and merge more and more. As the temperature is increased, eventually the amide has enough energy to rotate about the C-N bond fast enough to make the methyl groups equivalent, and

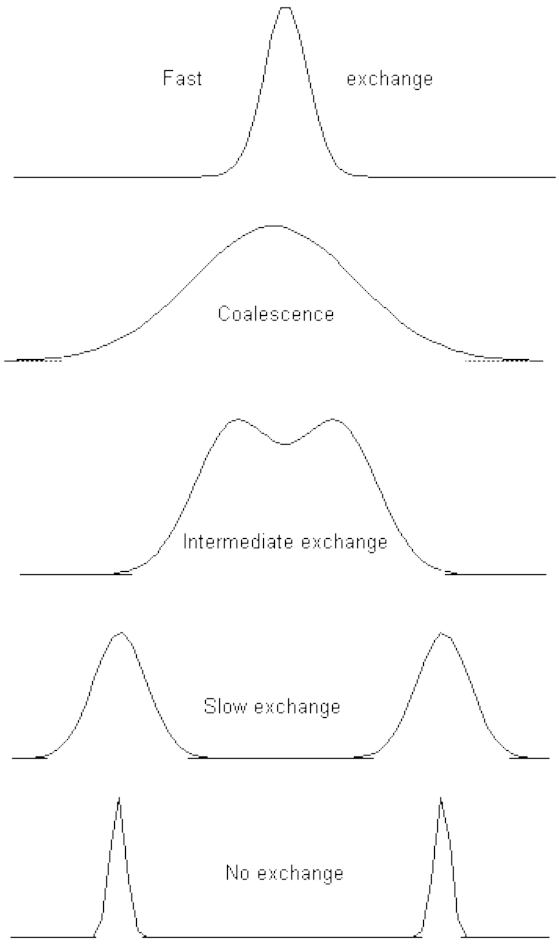

Figure 3.5: Schematic coalescence spectra

the two singlets coalesce into one singlet. The temperature where two signals coalesce is defined as coalescence temperature T_c. In 1956 Gutowsky and Holm[118] solved the Bloch equation and calculated the exchange rate in an uncoupled AB system with equal population (Eq. 3.11).

$$k_c = \frac{\pi}{\sqrt{2}}\Delta\nu = 2.222\Delta\nu \tag{3.11}$$

This equation strictly only holds at T_c. For an uncoupled AB system with non-equal population (Eq. 3.12) was given. $\Delta\nu_0$ is the separation when the exchange rate is negligibly small and $\Delta\nu$ is

the observed separation.

$$k_c = \frac{\pi}{\sqrt{2}}\sqrt{\Delta\nu_0^2 - \Delta\nu^2} \tag{3.12}$$

The above discussion shows that it is quite simple to measure rotation barriers by dynamic ^{1}H-NMR spectroscopy. The method is well established and widely used. In the field of Brownian molecular rotors this method is often not applicable: for really low rotation barriers it can't be used, since the coalescence temperature are so low that most of common used NMR solvents are frozen, thus suppressing the required fast tumbling proicess. Dynamic ^{1}H-NMR spectroscopy is very valuable for rotation barrier around 20 kcalmol^{-1}; for lower barriers it becomes increasingly more difficult to find the experimental conditions that achieve the desired goal.[115–118]

Chapter 4

Triangulenes

4.1 First attempts to synthesize Triangulenes

Clar and Steward introduced in 1953 the term triangulene for a large and diverse class of compounds, consisting of six-membered rings fused in a triangular fashion. This class of substances has a dibenzopyren structure, is rigid, has a large surface area of about 50 Å and is proposed to be flat. The numbering of the triangulene framework as well as the systematic name 4H,8H-dibenzo[cd,mn]pyrene is based on Clar's and Steward's work in the 50's .[119, 120]

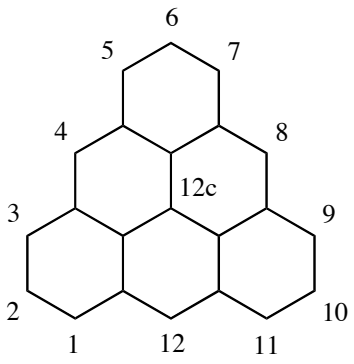

Figure 4.1: Numbering of the trinagulene Framework with its dibenzopyrene structure

Clar and Steward's goal was to synthesize a non-Kékule hydrocarbonsystem (Fig. 4.2 a.)), also known as Clar's hydrocarbon. It is a system, which contains an even number of π- electrons, but the topology of the system makes it impossible to write a resonance structure in which each π- electron is paired with one on a neighboring carbon.[120]

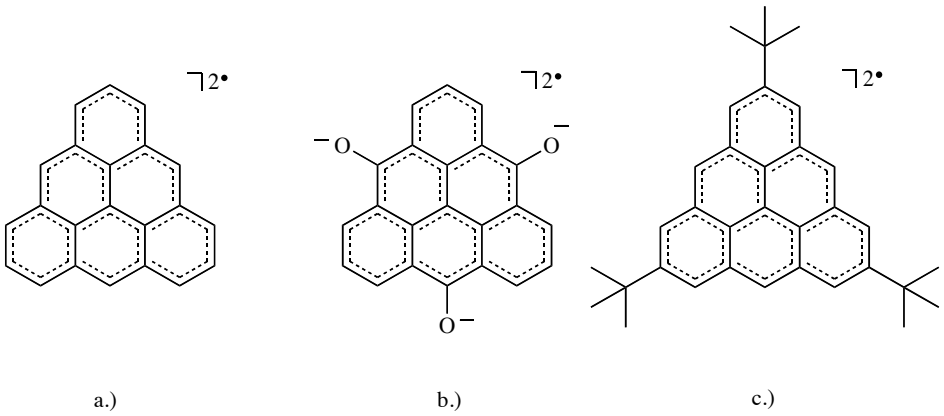

a.) b.) c.)

Figure 4.2: Non-Kékule Triangulenes: a.) Clar's hydrocarbon b.) trioxytriangulene by Bushby c.) 2,6,10-tri-tert-butyltriangulene by Nakasuji.

Clar and Steward did not succeed in the synthesis of the non-Kékule system, but were able to synthesize the first triangulene, a triangulenequinone. Their conclusion was that the non-Kékule system is too unstable to be isolated. 40 years later Bushby and coworkers[121] succeeded in the synthesis of the non-Kékule trioxytriangulene and were able to perform NMR, IR, ESR and X-Ray studies. They confirmed a non-Kékule diradical with a triplet ground state, which is highly sensitive to oxidation (Fig. 4.2 b.)). The Nakasuji group reported in 2001 the first successful attempt to synthesize and detect Clar's hydrocarbon. The group synthesized 2,6,10-tri-tert-butyltriangulene (Fig. 4.2 c.))and was able to detect the non-Kékule diradical with a triplet ground state by ESR.[122]

4.2 Trioxatriangulene Synthesis

In 1963 Martin and Smith synthesized the best known triangulene, the oxygen bridged trioxatriangulenium ion, which they called sesquixanthydrol. Their strategy was to start with 1,3- dimethoxybenzene which was lithiated with phenyllithium in benzene before quenching the adduct with diethylcarbonate to yield the open carbinol. Martin and Smith's approach was straightforward and led, in three steps, to the desired product. Ring closure was performed in the melt of py · HCl and after basic workup 12c-hydroxy trioxytrianguelene (Scheme. 4.1, **3**) was obtained.[123]

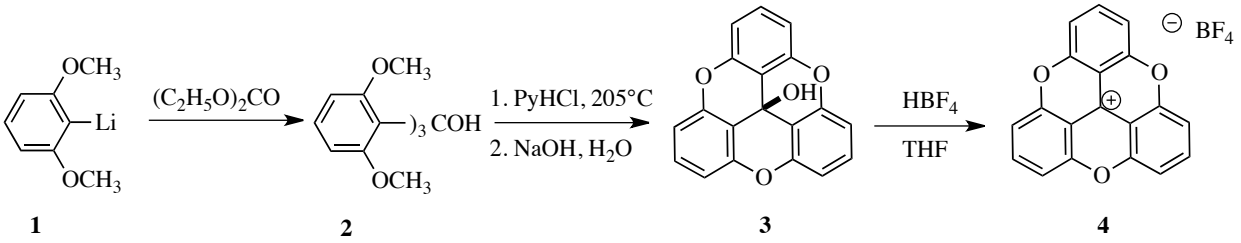

Scheme 4.1: Synthesis of Trioxatriangulene by Martin and Smith. Compound **4** is often called $TOTA^+$ or Martin's salt.

The scientist's motivation for the synthesis of this family of molecules was the study of different triarylmethanols, especially bridged triarylmethanols. Highly stable carbon cations and free radicals of triarylmethanols and triarylmethyl derivatives had already been studied extensively.[124–128]

Compared to other compounds of the triphenylmethane familiy the trioxatriangulenium ion, $TOTA^+$ (Scheme 4.1, **4**), has some unique properties. First of all it is planar and has a high symmetry (D_{3h}). Due to its planarity, dimerization under reductional conditions is very fast. Studies of this dimerization have been performed using ESR techniques.[129–132] For $TOTA^+$ it

also was found that it is less reactive than other carbocations with similar structures.[133] The stability of $TOTA^+$ has also been investigated by means of electrochemical reduction in sulfuric acid.[134] The Rieke and also the Nemcova group compared $TOTA^+$ also to triphenylmethane and compared steric effects and physical properties.[135, 136]

4.3 Structure and Physical Properties of $TOTA^+$

4.3.1 pK_{R^+} of Trioxatriangulene

Triarylmethanol are considered to ionize in acid media *via* protonation and subsequent loss of water. Martin and Smith investigated the high stability of the generated cation ($TOTA^+$), by meassuring the pK_{R^+} value of $TOTA^+$. The pK_{R^+} value expresses the reactivity of the cation toward hydroxide ions. For example a pK_{R^+} value of 9 means, a cation is 50% converted into its carbinol at pH=9.

$$pK_{R^+} = pH + log\frac{[R_3C^+]}{[R_3COH]} \tag{4.1}$$

Martin and Smith[123] reported a pK_{R^+}= 9.05 for $TOTA^+$. This value shows that the stability of $TOTA^+$ is in the range of crystal violet (CV) which has a pK_{R^+}= 9.36 and was one of the most stable know carbon cations[137, 138] until then.

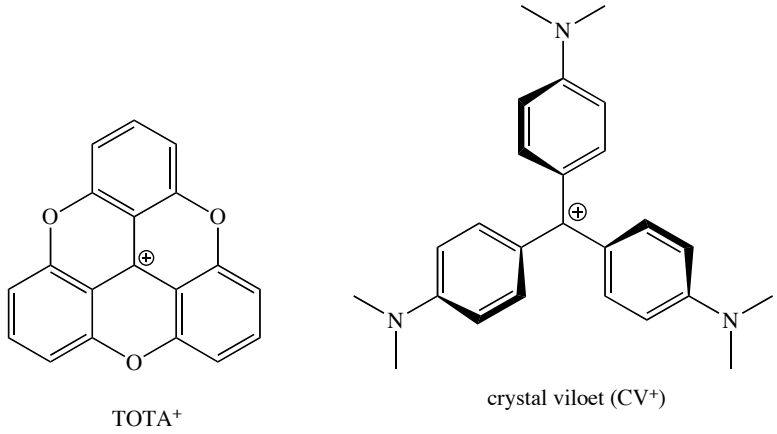

Figure 4.3: TOTA$^+$ and CV structure

Only in 1988 Okamoto and coworker[139] found a more stable carbon cation than CV, a stabilized tropylium ion annelated with three bicyclo[2.2.2]octane, which had a measured pK_{R^+} of 13. In 1994 Asao and coworkers were able to synthesize a series of substituted triazulenyl carbenium ions with pK_{R^+} values in the range of 14 (and even beyond, but not quantified)[140] , which are the highest pK_{R^+} values known.

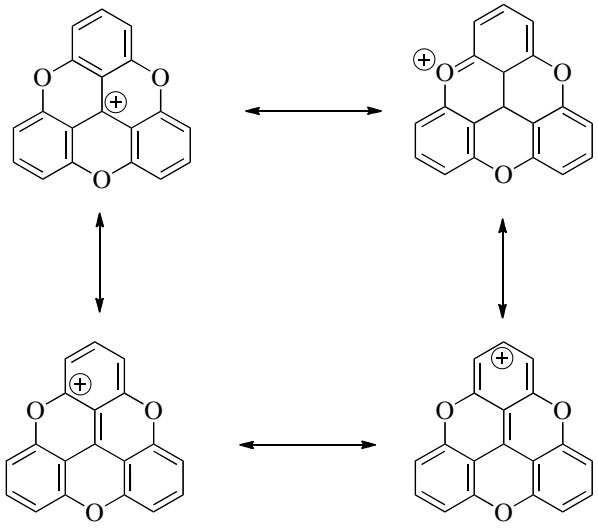

Figure 4.4: Resonance Stabilization of TOTA$^+$

In the case of the CV cation the high stability can be explained by the strong electron donating ability of the three dimethylamino substituents, which allows the delocalization of the charge. A good correlation between the pK_{R^+} value and the electron-donor strength of the para substituents is often found in substituted triarylcarbenium ions. For tris-(4-methoxyphenyl)carbenium ion the pK_{R^+} is much lower ($pK_{R^+} = 0.82$). This implies that the the high stability of the $TOTA^+$ cation does not only rely on the presence of the three oxygen atoms but also on the flat structure of $TOTA^+$, which allows substantial delocalization of the positive charge (Fig. 4.4). The reaction on the central atom in the framework becomes even more unfavorable due to destabilization of the corresponding product *i.e.* carbinol, by additional strain when the atom is forced in to sp^3 hybridization.

4.3.2 Solid State Structure of Trioxatriangulene (=Trioxatricornan*)

In 1999 Frederik C. Krebs and coworkers presented an extensive study of the solid state structure of trioxatricornan and tri-*tert*-butyl Trioxatricornan, they investigated the effect of the counter ion on the $TOTA^+$ structure by crystallizing the $TOTA^+$ cations with 12 different mono- and bivalent anions[141] . In all investigated systems the core structure of $TOTA^+$ was planar. The different salts crystallize in different space groups (Table 4.1):
Furthermore, the crystallographic study confirmed that the $TOTA^+$ system is very rigid, the structure of the cationic moiety and the packing was not effected by the nature of the anion. The packing showed a zig-zag motive.

*Due to the simular structure and shape of trioxatriangulene to tricornan, the term *trioxatricornan* was introduced by the Siegel group[148] in the 90's.

Table 4.1: Solved X-Ray structures of trioxatriangulenes[141]

Triangulene	Anion	Lattice System	Space group
TOTA$^+$	BF_4^-, AsF_6^-, I^-	Orthorombic	$Pbca$
	PF_6^-	Trigonal	$R\bar{3}c$
	$HNO_3 \cdot NO_3^-, CF_3SO_3^-$	Monoclinic	$P2_1/n$
	$Mo_6Cl_{14}{}^{2-}$	Monoclinic	$C2/c$
	$S_2O_6{}^{2-}$	Triclinic	$P\bar{1}3$
^{t}Bu$_3$TOTA$^+$	$PF_6^- \cdot CH_3CN, Mo_6Cl_{14}{}^{2-}$	Monoclinic	$P2_1/n$

4.3.3 Reactivity of Trioxatriangulene

Due to the planar and stable structure of TOTA$^+$, the central carbenium atom is easily accessible for attack by nucleophilices or free radicals. Compared to non bridged triarylmethanes reactions take place at a very high rate. The steric hindrance provided by the ortho hydrogenes in the propeller shaped triarylmethanes structure makes the attack on the central carbon atom difficult. In 1966 Diffenbacher and his coworkers reported that the the reaction between the carbenium and hydroxide ion is 104 times faster for TOTA$^+$ ($pK_{R^+} = 9.05$) compared to CV$^+$ ($pK_{R^+} = 9.36$), even though both compounds have very similar pK_{R^+} values.[138]

By comparing the dimerization of the neutral radicals, generated by one-electron reduction the difference in reactivity between bridged and non bridged triarymethanes becomes comprehensible. The planar TOTA$^+$ dimerizes very fast yielding a dimer connected by its two central C atoms (Fig. 4.5 a.)). The propeller shaped triarylmethane reacts very slowly and dimerizes differently, the para position of one of the three aryl rings dimerizes with the central ring of the second triarylmethane (Fig. 4.5 b.))[124, 129–131, 143, 144]

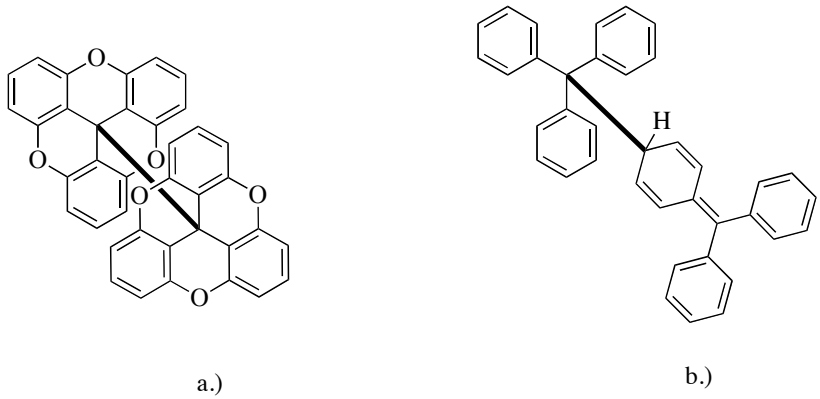

Figure 4.5: Dimerization product of a.) $TOTA^+$ and of b.) Triarylphenyl

4.3.4 Trioxatriangulene as Starting Molecule for cavitants and cryptands

Besides the high stability, the large surface area of 50Å, the tripod-shaped form (when substituted in the central C-Atom), the solubility and it's synthetic availability make Martin's salt a molecule of interest for various purposes. In the 90s the Siegel group began to work with $TOTA^+$.

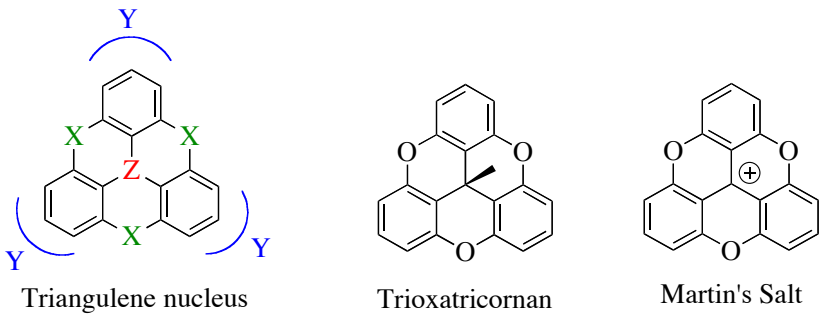

Figure 4.6: Trioxatriangulene and its regions

In their preliminary studies, the Siegel group found, that $TOTA^+$ becomes bowl-shaped, when substituted on the central C atom. They investigated this behavior by synthesizing different $TOTA^+$ derivatives and looking at their solid state structure, and also by calculations. Furthermore, the Siegel group developed the reactivity of the different regions of $TOTA^+$. The trioxatriangulene structure consist of three variable regions X, Y, and Z (Fig. 4.6). The X region

mediates the π electronics of the whole systems and, X= O is the most basic version of the known triangulene systems. The Y region controls the symmetry. Substitution of trioxatricornan at position 2, 6, and 10 yields an achiral product with C_{3v} geometry. Substitution at positions 1, 5, 9 to a chiral C_3 geometry and 3, 5, 9 substitution to an achiral C_1 geometry. The Z region controls the solubility of the system and substitution at the central atom leads to a bowl-shaped molecule.

Lofthagen used the qualities of TOTA$^+$ for the development of three dimensionally arrayed macrocylic ensembles in a controlled fashion. TOTA$^+$ was substituted on the aromatic region such that it would provide three points for attachments in order to yield a polycyclic cyclophane. The goal was to achieve well-defined three dimensional systems which could be interesting for guest host interaction studies. In the 90s he published the synthesis of the such a three dimensional macrocycle and dynamic studies of the host /guest interaction.[145–148] One of the first synthesized macrocycles is depicted in Fig. 4.7

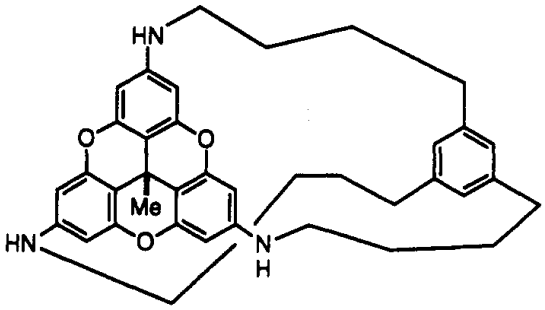

Figure 4.7: Three dimensionally arrayed macrocylic structure by Lofthagen[145]

VernonClark studied used the reactivity of the central carbenium ion of $^+$citeVernonClark. He synthesized centrally substituted derivatives of trioxatricornan and studied their solid state structure, supported by calculations. My thesis is based on the two PhD theses of Lofthagen[145]

and

VernonClark.[149]

Chapter 5

Synthesis of Molecular Rod (Rotors) with Trioxatricornan Stators

5.1 Aim of the Project

The aim of this PhD project was to design, synthesize and analyze a new family of molecular rod rotors based on $TOTA^+$. It was anticipated that the reactivity discussed in chapter 4 could be used to synthesize a molecular rotor based on $TOTA^+$

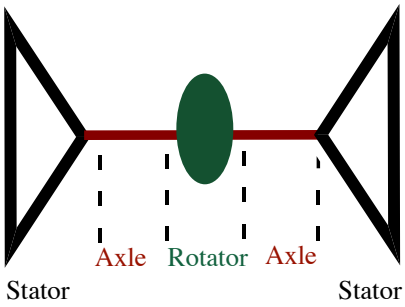

Figure 5.1: Concept for a molecular rotor with three distinguished regions, the "stationary" stator, the axle and the "rotating" rotator

A molecular rotor has two parts which are connected by an axle.[150] One part has a large moment of inertia compared to the other and is considered to be stationary, these are the

stators, in our case $TOTA^+$. The other part is the rotator, with a small moment of inertia. The distinctions between the two parts is not completely unambiguous, especially in the solution state. A part from the rotator moving relative to the stators the letter may move relative to each other. However, the hypothesis is, that the rotator will move much faster than the stators. In Fig. 5.1 the principle is depicted.

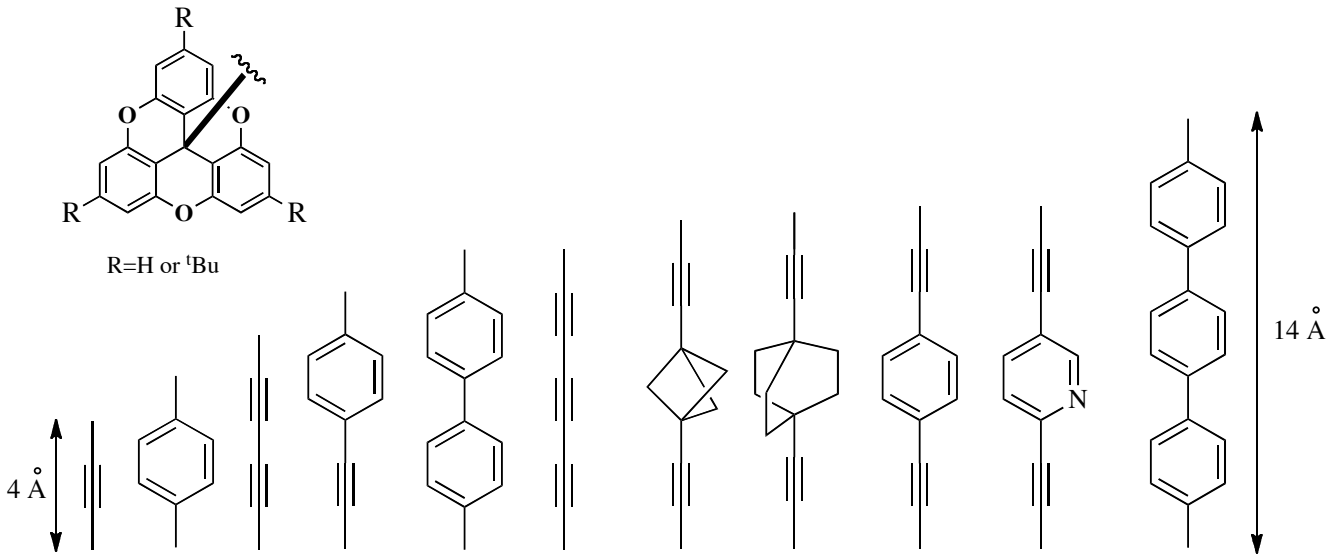

Figure 5.2: Design of molecular rod rotors and rods, with distinct distances and two trioxatriangulene caps.

In order to make the system even less ambiguous our design includes working on solid state rotors. To achieve solid-state rotor molecules the idea was to synthesize a library of molecular rods, which are capped by trioxatriangulenes on each side and contain a potentially fast rotating part in it. To keep the system simple and linear, only C–C and -C–C≡C–C- bonds were used as axles, furthermore it was taken into account that the linear rod structure is preserved by using linear rotator parts such as phenyl, pyridinyl, and bicyclo[2.2.2]octane fragments. A propellane was also considered as a rotating part. Besides linearity, it was also desirable to have a set of

molecules with comparable rod lengths and this could be achieved by the combination of the above mentioned building blocks (Fig. 5.2).

5.2 En route to the Building Blocks - Synthesis of the Trioxatricornan Caps

5.2.1 Synthesis of the tri-*tert*-butyl-Trioxytriangulenium cation[151]

The eight-step synthesis of the tri-*tert*-butyl-trioxtriangulenium cation was performed by starting with commercially available 2,6-dimethoxyphenol, which was tert-butylated by using Friedel-Crafts conditions. The 2,6-dimethoxy-4-^{t}butyl phenol **6** (scheme 5.1) then was converted to the diethyl phosphate **7** which was subsequently reduced with Li in liquid ammonia to give 2,6-dimethoxy-4-^{t}butyl benzene **8** in quantitative yield. Bromination of 2,6-dimethoxy-4-^{t}butylbenzene with bromine gave the 1-bromo-2,6-dimethoxy-4-^{t}butyl adduct **9** also in quantitative yield. Subsequent lithiation with *tert*-butyl lithium for one hour and quenching with diethyl carbonate and further refluxing for 48 hours yielded the open tris-phenyl carbinol **10** , which was recrystallized in hexane. For the closure to the macrocyle, the open carbinol was mixed with pyridine hydrobomide in a vessel with an over-head stirrer and heated to 205 $°C$ the melt was stirred for 3 hours until the color of the melt changed from deep purple to intense red. The reaction was quenched with water and the suspension filtered. In order to obtain a clear mother liquor a very fine glass filter (pore 4) was used. It was recognized, that by that by dissolving the filter cake another three times in water and sonicating it before filtering again the final yield can be improved dramatically by 30%. The combined mother liquor was basified with 1M NaOH. The red solution became colorless and formation of a white participate was observed. The white powder was recrystallized from refluxing EtOH to yield the tri-*tert*-butyl-12c-ethoxy-trioxytriangulene **11** as a white powder in a good yield (78-90%).

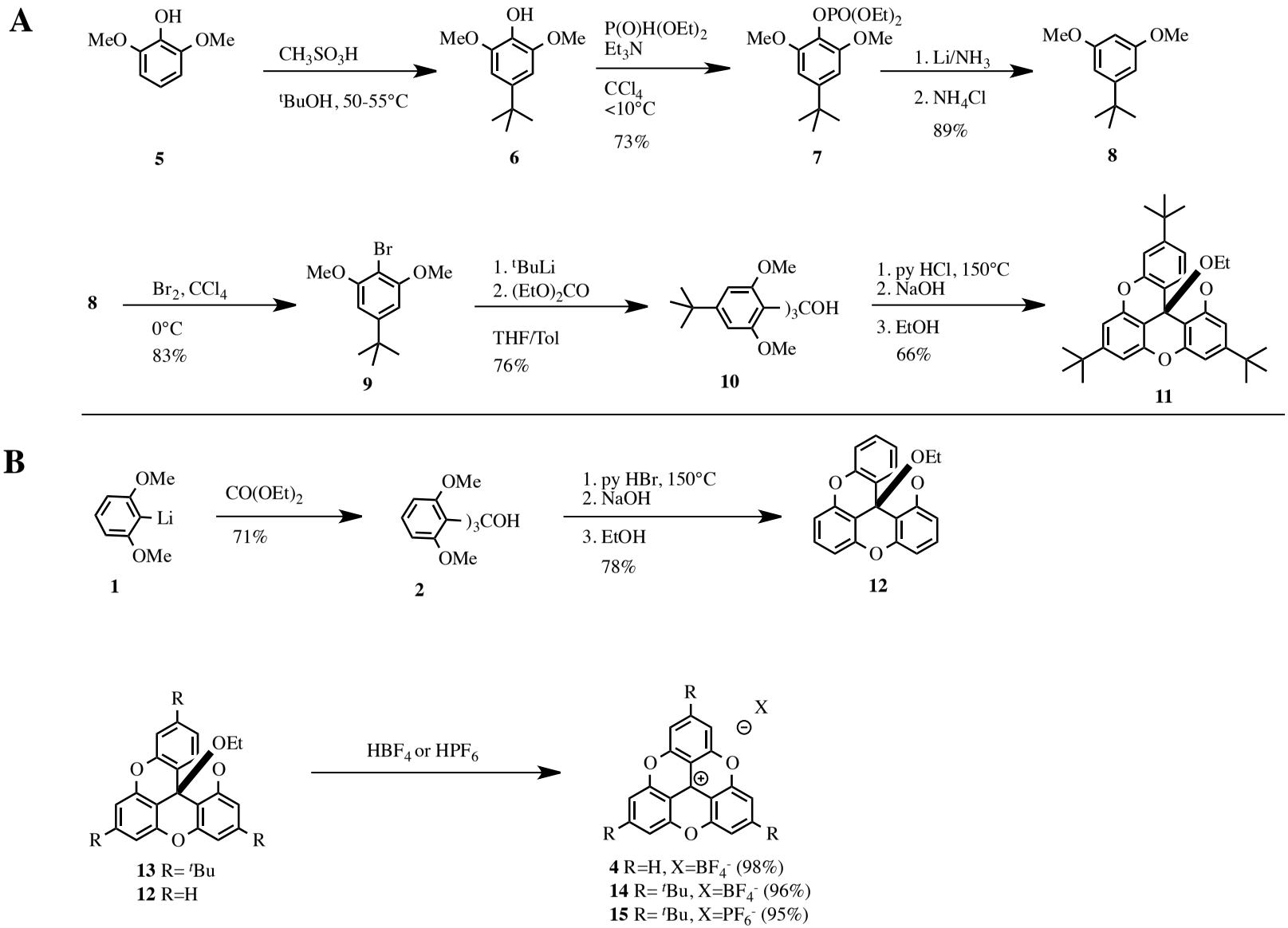

Scheme 5.1: Synthesis of tricornan caps.

Then tri-*tert*-butyl-12c-ethoxy-trioxytriangulene **11** was dissolved in ether and aqueous HPF_6 was added slowly, yielding deep yellow participate, tri-*tert*-butyl-trioxytriangulenium cation **14** the same procedure with HPF_6 gives the PF_6 salt **15**. After filtration the salt can be stored for months in a dark sealed tube, and can be used without further purification. The reaction steps are summarized in Scheme 5.1 (A):

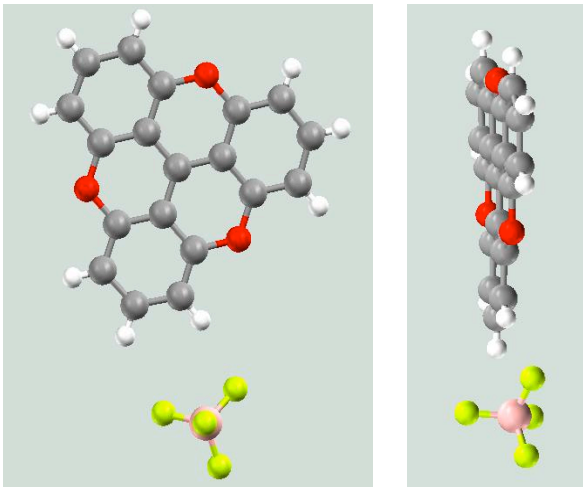

Figure 5.3: X-Ray of Martin's salt ($TOTA^+$ BF_4^-), showing the flat structure

5.2.2 Synthesis of Trioxytriangulenium cation

The three-step synthesis of trioxatriangulene begins also with commercially available 2,6-dimethoxyphenol, which is first lithiated with *n*-BuLi in THF. After one hour the THF was removed by destillation under N_2 atmosphere at 40°C and 330 mbar and replaced by dry toluene. Diethyl carbonate in toluene was then added and refluxed for 48 hours to yield the open tris-phenyl carbinol **2** . In the next step the open carbinol and pyridine · HBr were mixed in a vessel with an overhead stirrer and heated to 205°C. After 2 hours stirring the deep purple melt turned to intense red and was ready for filtration in the same way as described before for the tri-*tert*-butyl-12c-ethoxy-trioxytriangulene. Following filtration the mother liquors are again combined

and basified, to give a clear solution with a white participate. After another filtration a white powder is obtained and recrystallized in EtOH. Then 12c-ethoxy-trioxytriangulene **12** was dissolved in THF and aqueous HBF_4 was added immediately yielding the deep yellow cation **4** in quantitative yield (Scheme 5.1).

5.2.3 Synthesis of the two principle building blocks - alkye and phenyl substituted trioxatriangulenes

5.2.3.1 12c-ethyl-triocaxatricornan

Commercially available trimethylsilylacetylene was dissolved in 5 mL dry THF and lithiated with *n*-BuLi for 30 min in acetone/dry-ice cooledTHF. Then, $TOTA^+$ BF_4^- was added slowly with a spatula and a yellow suspension was obtained*. The reaction was monitored by GC/MS showing the completion of the reaction within 1 hour†.

The workup involved quenching the reaction with water and performing an ether extraction (3x). After combining the organic layers they were dried over $MgSO_4$, filtered and evaporated to give the protected alkyne **16a**. After a short filter column, the deprotection was performed by dissolving the protected alkyne in THF/MeOH (1:1), adding K_2CO_3 and stirring at ambient temperature. Here too the deprotection was monitored by GC/MS (especially since the educt and product have nearly the same R_f value). For the largest scale experiment (1g), completion of the deprotection required 3 hours. The work up was performed by doing an ether extraction, combining the organic layers, drying over $MgSO_4$, filtration and evaporation. The white solid product **16b** was used without further purification (Scheme 5.2).

*The addition by spatula was chosen due to poor solubility of $TOTA^+$ BF_4^- in THF, for the tert butyl substituted cation the solubility is better and it can be dissolved in THF and added by cannula to the lithium salt.

†It was recognized that, if the reaction is left to proceed longer and the temperature raised above 0°C the yield decreases significantly and a side product m/z =$TOTA^+$ + 1 is observed. Therefore the reaction was always left to proceed below 0°C and monitored by GC/MS.

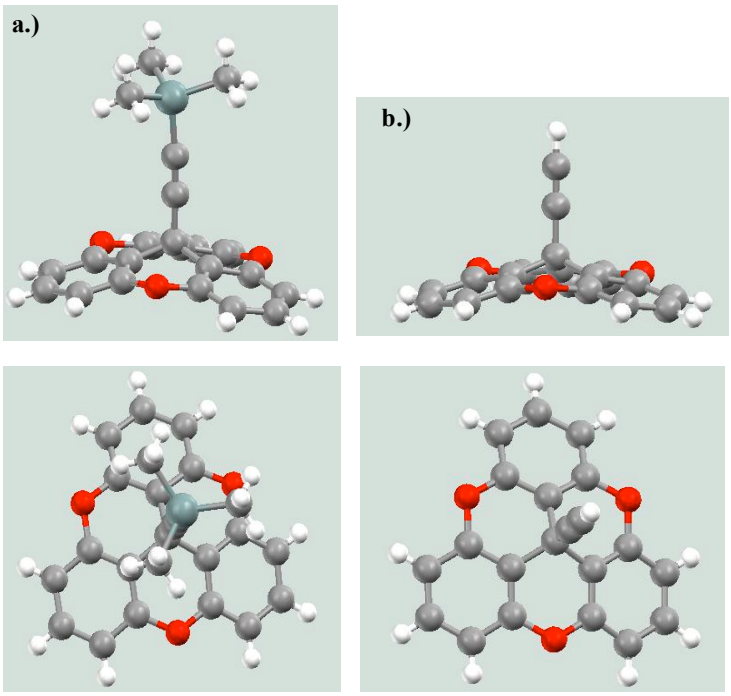

Figure 5.4: X-Ray structures of a.) TMS-alkyne derivative, triclinic P1(#2) R=0.069 b.) alkyne derivative, cubic Pa3(#205) R=0.062.

5.2.3.2 12c-bromophenyl-trioxatriangulene and 12c -iodophenyl-trioxatriangulene

This class of precursors of molecular rod rotors was synthesized by lithiation of 1,4 disubstituted benznes followed by addition of $TOTA^+$ $BF_4{}^-$. For the phenyl derivative different approaches were tried. 1,4-dibromobenzenzene, 1,4-diiodobenzene or 1-iodo-4-bromobenzene were used as starting materials. In the beginning the Grignard reaction was the reaction of choice, but since the yield was never better than 30% new routes had to be explored. Therefore lithiation reactions with diiodobenzene and dibromoenzene were tried leading to a maximum yield of 40%. As this yield was not satisfying and the purification of the product mixture also turned out not to be trivial, the next possible route was tried. 1-Iodo-4-bromobenzene was used as starting material and lithiated with *n*-BuLi at -78°C, the lithiation was allowed to proceed for 30 min before

$TOTA^+$ BF_4^- was added with a spatula[‡]. The yellow suspension was stirred for 1 hour at -78°C and then allowed to reach ambient temperature within 2 hours. After a further 4 hours of stirring the reaction mixture was quenched with aq. NH_4Cl solution and extracted with ether. The combined organic layers were dried over $MgSO_4$, filtered and evaporated. Purification was achieved by a short filter column with hexane as eluent yielding a white powder (**18**) in 80% yield [§] For the iodobiphenyl rod precursor, the reaction procedure was exactly the same as described above, but instead of 1,4 diiodobenzene 1,4' diiodo biphenyl was used as starting material, the reaction yield for this compound **19** was 60% (Scheme 5.2).

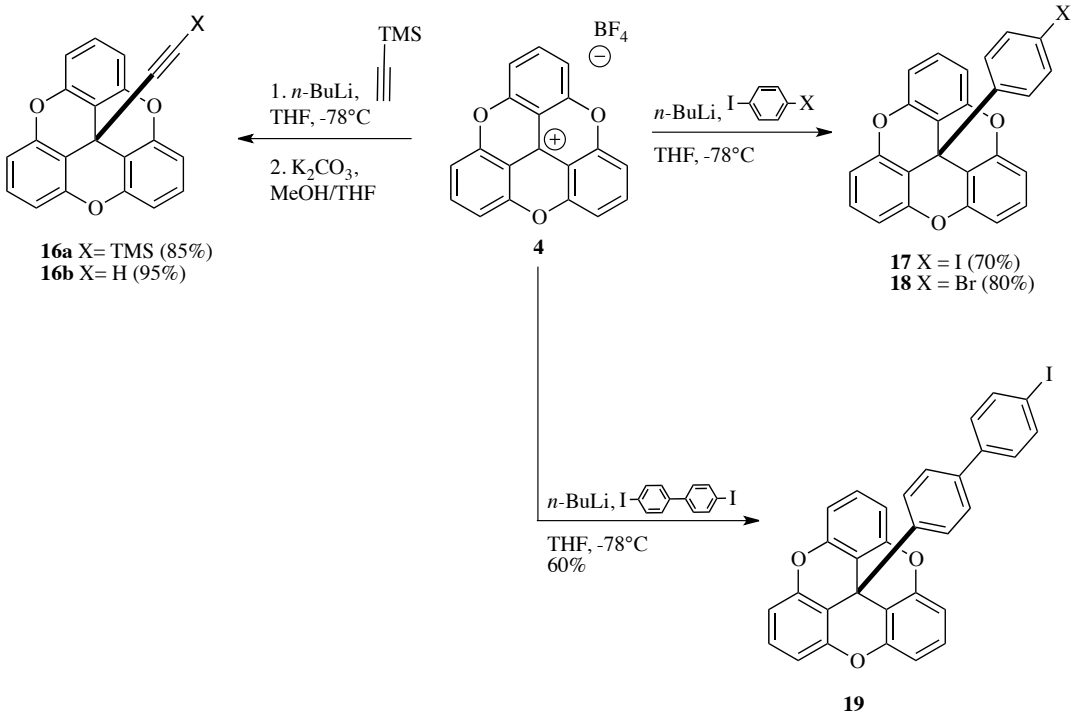

Scheme 5.2: Synthesis of Trioxatriangulene derivatives **16**-**19**, the main building blocks.

[‡]tri-*tert*-butyl $TOTA^+$ was dissolved in cooled THF and added by cannula.

[§]for the tri-*tert*-butyl $TOTA^+$ the route with 1,4 diiodobenzene gives a 70% yield (**17**) and therefore it is the preferred one. In general, it was noticed that the yield for reactions with tri-*tert*-butyl $TOTA^+$ is higher. This can be explained by the increased solubility of tri-*tert*-butyl $TOTA^+$ compared to $TOTA^+$.

5.2.4 Synthesis of the linking parts for the rod structure

The synthesis of two linking parts was done by a Sonogashira reaction, for which the following procedure was used. The reactions were performed in closed vessels equipped with a stirring bar. First the solvent was degassed by bubbling vigorously N_2 trough it for 15min. Then, the substrate, CuI, and the catalyst were added and N_2 was bubbled through for another 5 min before the alkyne was added and the vessel closed. The closed vessel was then put in a oil bath of 80 °C and the reaction was left to proceed overnight. After 16h, the reaction was monitored by GC/MS and left to proceed until no more educt was visible.

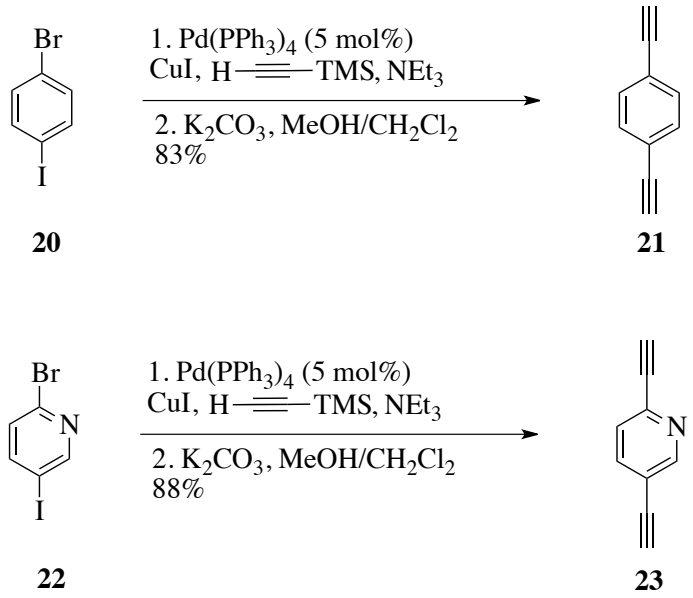

Scheme 5.3: Synthesis of linking parts **21** and **23**.

In the case of the 2,6-diethynylpyridine **23** the reaction was complete overnight and in case of 1,4-diethynyl benzene **21** the reaction was left to proceed for a further 20 hours. The work up was performed by first filtering the cooled suspension through a silica plug and washing the plug with ether, followed by evaporating the solvent. Following an ether extraction and the combined organic layers were dried over $MgSO_4$, filtered and evaporated. Purfication was achieved by

a short filter column with hexane as eluent yielding a white powder. For the deprotection, the white powder was dissolved in CH_2Cl_2 and an equal amount of MeOH added, followed by K_2CO_3. The reaction was stirred for 2 hours at ambient temperature. The work up was performed by doing an ether extraction, combining the organic layers and then drying over $MgSO_4$, filtering and evaporating. The white solid product was used without further purification (Scheme 5.3) and obtained in a good total yield of 83% for **21** and 83% for **23**.

5.2.5 Synthesis of the molecular rods

5.2.5.1 Phenyl linked Molecular Rods

In order to place the second cap on the molecular rod structure, the halophenyl derivative was lithiated with *n*-BuLi in the case of halogen=iodine and with *t*-BuLi in the case of halogen=bromine. After one hour of lithiation at -78°C, $TOTA^+$ BF_4^- was added with a spatula and left stirring at at -78°C for 1 hour. Then the suspension was allowed to reach ambient temperature and stirred overnight. The reaction then was quenched by addition of water and an CH_2Cl_2 extraction was performed. The combined organic layers were dried over $MgSO_4$, filtered and evaporated.

The same approach was used with the tri-*tert*-butyl $TOTA^+$ and 1,4-diiodobenzene leading to the comparable molecular rod with the *tert* butyl groups. The purification of the molecular rods was not trivial. Firstly it was noticed that the compound starts to decompose, if it is exposed for too long to acids. A separation of the different products was obtained only on silica. After realizing this fact, the dry load was done with alox on a silica column using a maximum of 25 g of silica for 100 mg compound silica used. In order to get a good separation a gradient of the eluent, starting with hexane: CH_2Cl_2 (9:1) and increasing the CH_2Cl_2 ratio, was used. Furthermore, very small fractions of 1 mL were collected. This approach led to a white powder which was the

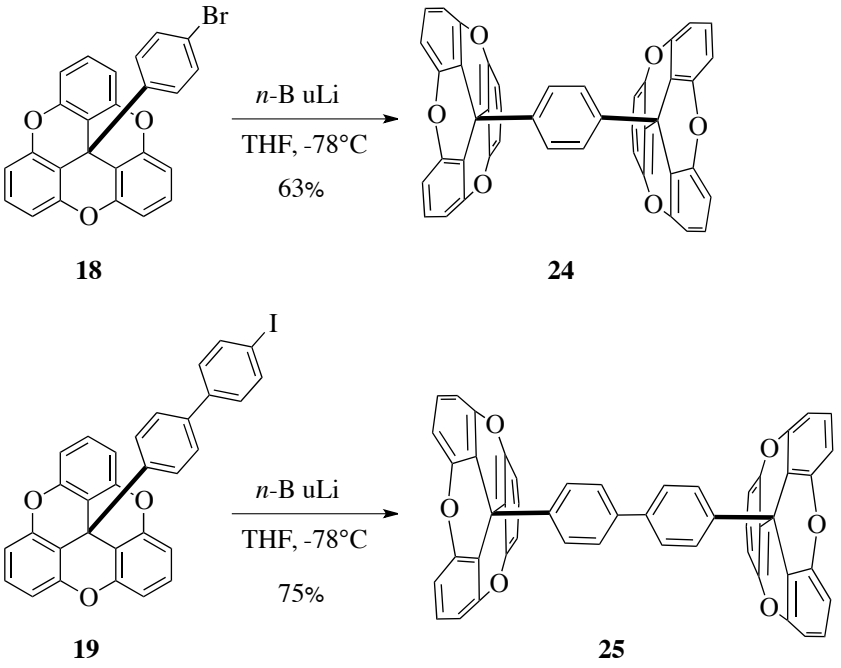

Scheme 5.4: Synthesis of phenyl linked molecular rods **24** and **25**

product **24**, of which also the crystal structure was solved. In order to synthesize the biphenyl rod, the same procedure was used but using *n*-BuLi. Again the purification was tricky and the same approach as for the phenyl rod was used yielding a white powder **25**(Scheme 5.4).

5.2.5.2 Alkyne linked Molecular Rods

To synthesize the mono alkyne molecular rod structure, the precursor **16b** was first lithiated with *n*-BuLi and then stirred for one hour at -78°*C* before $TOTA^+$ BF_4^- was added with a spatula. The resulting suspension was left stirring at -78°*C* for 1 hour and then allowed to reach ambient temperature and stirred over night. The reaction was quenched with aq. NH_4Cl solution and an ether extraction was subsequently performed. The combined organic layers were dried over $MgSO_4$, filtered and evaporated. Purification was performed by a silica column running a

hexane:CH_2Cl_2 gradient starting from a 9:1 (hexane:CH_2Cl_2) ratio and increasing the CH_2Cl_2 fraction. The procedure yielded a white powder of compound **26** (Scheme 5.5).

For the rod structure with two alkyne linkers an *Eglinton Reaction* was performed. The alkyne precursor was suspended in EtOH and $Cu(OAc)_2 \cdot H_2O$ added. The suspension was refluxed for three days, then allowed to cool and diluted with methylene chloride. The mixture was transferred into a separatory funnel and washed three times with water, then dried over $MgSO_4$. Solvent was evaporated under reduced pressure. The product was purified by column chromatography yielding a white powder of bialkynyl rod **27**(Scheme 5.5).

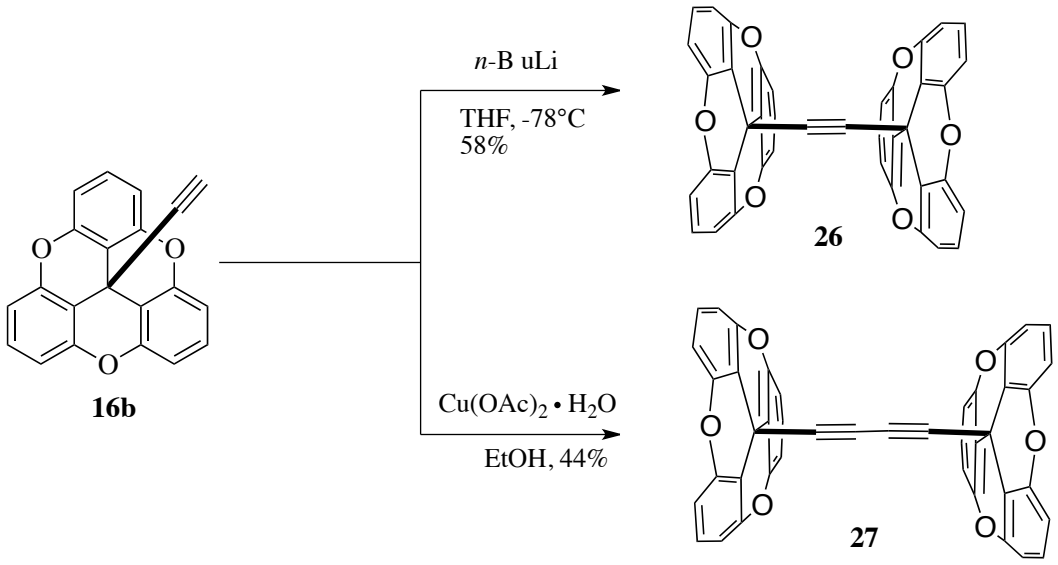

Scheme 5.5: Synthesis of alkyne linked molecular rods **26** and **27**

5.2.5.3 Molecular Rods with mixed Likers

The synthesis of molecular rods, consisting of phenyl alkyne linkers was performed by *Sonogashira Reaction*. The alkyne precursor was dissolved in piperidine and the piperidine solution was degassed by freezing it in liquid N_2 and then applying vacuum while it was melting. This

procedure was repeated twice. Afterwards 1,4-diiodobenzene [¶], $Pd(PPh_3)_2Cl_2$ and CuI was added and the apparatus equipped with a reflux cooler and an N_2 inlet. The suspension kept at refluxed for two days, then cooled to ambient temperature. The work up was performed by first filtering the suspension through a silica plug and washing the plug with CH_2Cl_2, then the solvent was evaporated. Afterwards an CH_2Cl_2 extraction was done and the combined organic layers were dried over $MgSO_4$, filtered and evaporated. Purification was done on a silica column with a hexane:CH_2Cl_2:toluene eluent in a 8:1:1 ratio yielding a white powder (**28** or **29** Scheme 5.6).

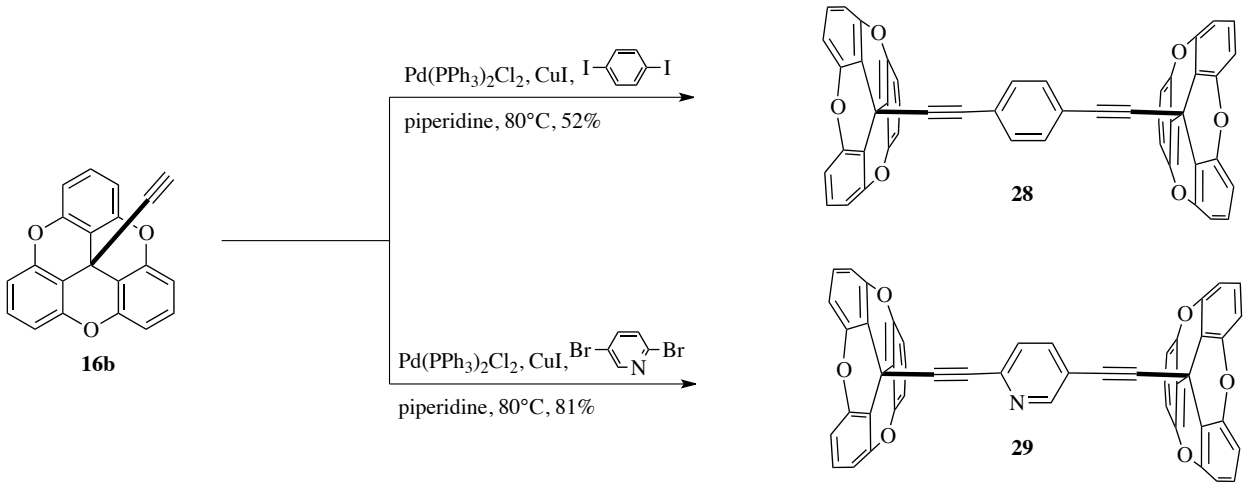

Scheme 5.6: Synthesis of molecular rods with mixed linkers **28** and **29**.

In order to synthesize the tolan linked molecular rod **31**, two subsequent *Sonogashira Reactions* were performed and a deprotection step after the first *Sonogashira Reaction*. In a first step the bromophenyl precursor was dissolved in NEt_3 and then the solution degassed by vigorously bubbling N_2 trough it for 15 min. Then, the catalyst and CuI were added and N_2 was bubbled through for another 5 min before the alkyne was added and the vessel closed. Afterwards, the closed vessel was put in an oil bath at 80 °C and the reaction was left for proceed over night. In the morning the reaction was monitored by GC/MS and left to proceed until no more educt was

[¶] in the case of the pyridine compound 2,5-dibromopyridine was used as reactant and *i*-Pr_2NH as base

visible. The work up was done by first filtering the cooled suspension through a silica plug and washing the plug with CH_2Cl_2, then the solvent was evaporated. Afterwards an ether extraction was done and the combined organic layers were dried over $MgSO_4$, filtered and evaporated. Purification was achieved by a short filter column with hexane as eluent yielding a white powder of compound **30a** (Scheme 5.7).

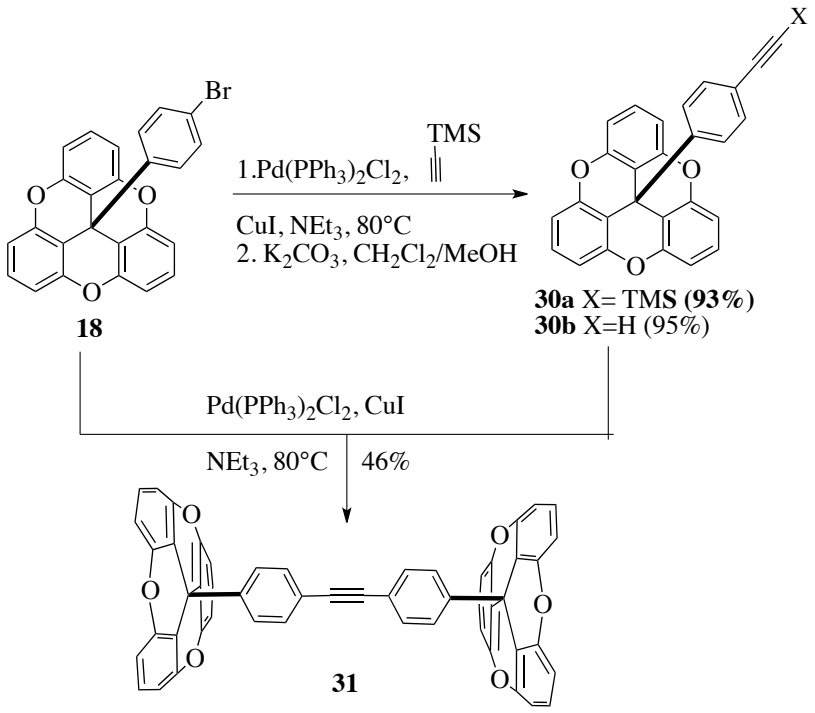

Scheme 5.7: Synthesis of tolan linked molecular rod **31**.

For the deprotection **30a** was dissolved in CH_2Cl_2 and an equal amount of MeOH was added, followed by K_2CO_3, and the reaction was stirred for 2 hours at ambient temperature. The work up was performed by doing an ether extraction, combining the organic layers, drying over $MgSO_4$, filtering and evaporating. The white solid product **30b** was used without further purification for the next *Sonogashira Reaction* and dissolved together with the bromophenyl precursor **18** in NEt_3 followed by the procedure explained above. The reaction was left stirring for two days before the workup which was performed by first filtering the cooled suspension through a

silica plug and washing the plug with CH_2Cl_2. Then the solvent was evaporated. Afterwards a CH_2Cl_2 extraction was done and the combined organic layers were dried over $MgSO_4$, filtered and evaporated. Purification was on a silica column with a hexane:CH_2Cl_2:toluene eluent in a 8:1:1 ratio yielding **31** (Scheme 5.7).

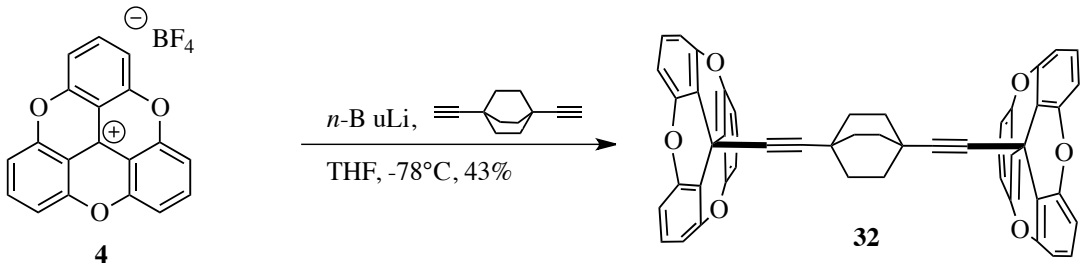

Scheme 5.8: Synthesis of 1,4 diethynyl bicyclo [2.2.2] octane linked molecular rod **32**.

In order to synthesize the molecular rod with a saturated linker, 1,4-diethynyl bicyclo [2.2.2] octane was used as starting material and lithiated with *n*-BuLi at -78°C, the lithiation was allowed to proceed for 30 min before TOTA$^+$ BF_4^- was added with a spatula[‖]. The yellow suspension was stirred for 1 hour at -78°C and then allowed to reach ambient temperature within 2 hours. After a further 4 hours of stirring the reaction was quenched with aq. NH_4Cl solution and an ether extraction was subsequently performed. The combined organic layers were dried over $MgSO_4$, filtered and evaporated. Purification was performed by a short filter column with hexane as eluent yielding a white powder **32** in 80% yield (Scheme 5.8).

5.3 Conclusion and Outlook

In summary three principle strategies were chosen to synthesize the molecular rods (Table 5.1) t

- Lithiation and then quenching with the electrophile (mostly TOTA$^+$ BF_4^-)

[‖]tri-*tert*-butyl TOTA$^+$ was dissolved in cooled THF and added by cannula.

Table 5.1: Summary of Synthesis of Molecular Rod Rotors.

Entry	Educt	Reagents	Yield	Molecular Rod
1	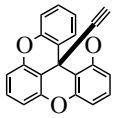 **16b**	1. *n*-BuLi, THF, -78°C 2. $TOTA^+ BF_4^-$	58%	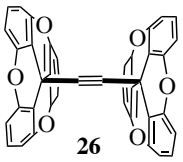 **26**
2	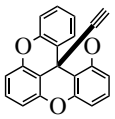 **16b**	$Cu(OAc)_2 \cdot H_2O$ EtOH	44%	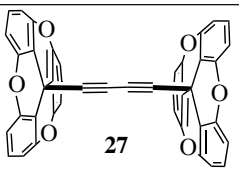 **27**
3	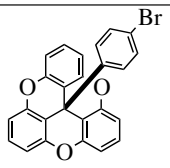 **18**	1. *n*-BuLi, THF, -78°C 2. $TOTA^+ BF_4^-$	63%	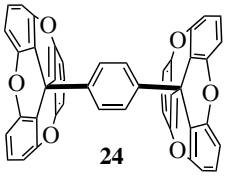 **24**
4	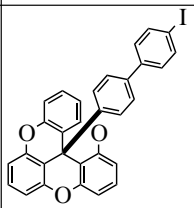 **19**	1. *n*-BuLi, THF, -78°C 2. $TOTA^+ BF_4^-$	75%	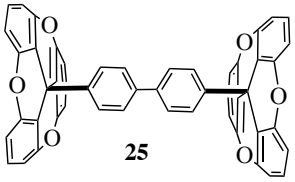 **25**
5	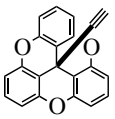 **16b**	$Pd(PPh_3)_2Cl_2$, CuI,  piperidine, 80°C	52%	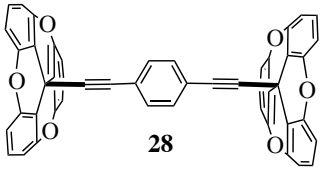 **28**
6	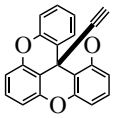 **16b**	$Pd(PPh_3)_2Cl_2$, CuI, 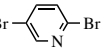 piperidine, 80°C	81%	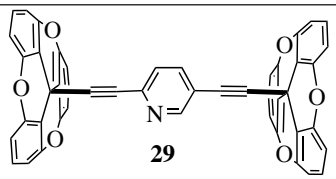 **29**
7	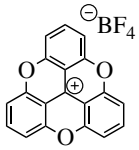 **4**	*n*-B uLi,  THF, -78°C	43%	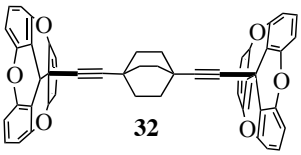 **32**
8	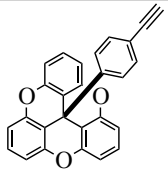 **30b**	$Pd(PPh_3)_2Cl_2$, CuI, **18** piperidine, 80°C	46%	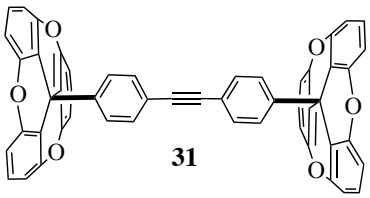 **31**

- Cross coupling

- Mixed strategy of lithiation and cross coupling

With these strategies, three classes of molecular rods were synthesized as summarized in table 5.1. The phenyl linked molecular rod rotor (Entry 3, table 5.1) and the 1,4 diethynyl bicyclo [2.2.2] octane linked molecular rod rotor (Entry 7, table 5.1) were also synthesized with the tri-*tert* butyl TOTA caps on both sides. TOTA X-Ray data could only be obtained from the phenyl linked rod with tri-*tert*-butyl TOTA caps. In the next chapter the X-Ray structure will be discussed. A general trend for the solubility was observed: the longer and the more saturated the molecular rod structure with TOTA caps became, the poorer the solubility. In the case of the biphenyl linked molecular rod CH_2Cl_2, $CHCl_3$, CCl_4, 1,2-dichlorobenzene, benzene, toluene,, xylene, ether,THF, 1,2-tetrachlorethylene, CS_2, DMF and DMSO were used to test the solubility. 1 mg of molecular rod was dissolve in 0.5 mL of solvent but in none of the solvents did the substance dissolve completely. The same solubility problem was faced for all other molecular rod structures excluding the saturated system (Entry 7, table 5.1). In the case of the molecular rod structure with tri-*tert*-butyl TOTA caps the solubility was better, as expected from the handling of the precursors. Another problem during this project was the purification of this class of substances. It appeared that they are acid labile and UV measurements confirmed this assumption by showing the formation of Martin's salt. In order to purify this class of molecules, an alox plug was always applied and it was found that a mixture of hexane: CH_2Cl_2: toluene as eluent in a 8:1:1 ratio achieved the best separation.

5.3.1 Phenyl Linked Molecular Rod Rotor

In the case of the phenyl linked molecular rod structure a clean separation reqiured, running a gradient with hexane:CH_2Cl_2, as an eluent, starting with a 9:1 ratio and increasing the CH_2Cl_2 ratio. After obtaining a single crystal structure of the phenyl liked molecular rod structure (tri-*tert*-butyl-TOTA caps on both sides), we postulated, that the phenyl ring rotates very fast. This assumption was based on a three fold disorder of the phenyl ring in the crystal structure which will be discussed in the next chapter together with further solid state dynamics studies of the phenyl linked molecular rod rotor in Fig. 5.5.

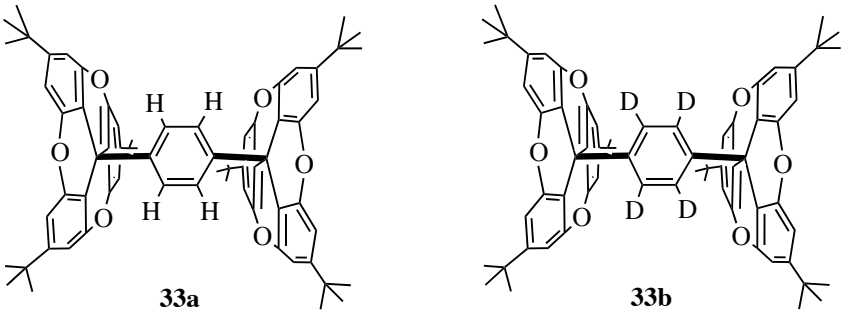

Figure 5.5: Phenyl linked molecular rod rotors, the linking phenyl ring can either be protonated (**33a**) or deuterated (**33b**).

Chapter 6

Solid State Dynamic Studies

6.1 X-Ray Determination of Phenyl Linked Rod Rotors

The first X-Ray structure obtained for the phenyl linked rod rotor with tri-*tert*-butyl $TOTA^+$ caps was cubic and showed a three-fold disorder of the phenyl ring.

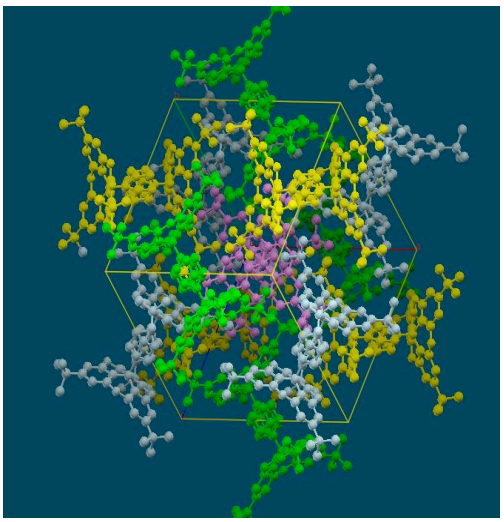

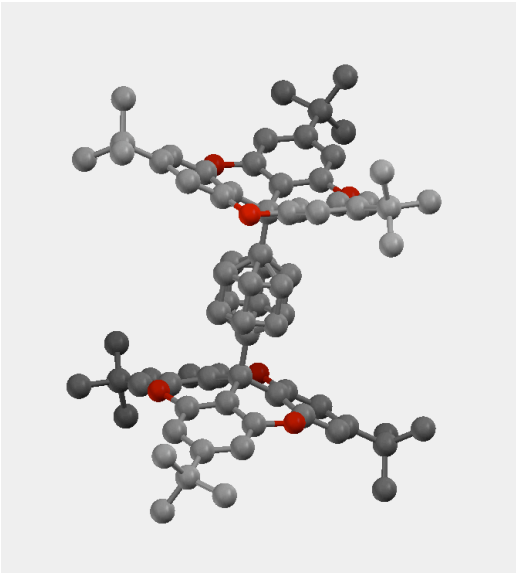

Figure 6.1: X-Ray structure of protonated rod rotor with cubic symmetry (Pa3 #205) . The crystal was grown from CH_2Cl_2 solution

Because the atomic displacement parameters (ADPs) of the phenyl rings seemed larger when compared to the ellipsoids of the the other atoms variable temperature X-Ray diffraction data were taken in order to examine this observation more closely.

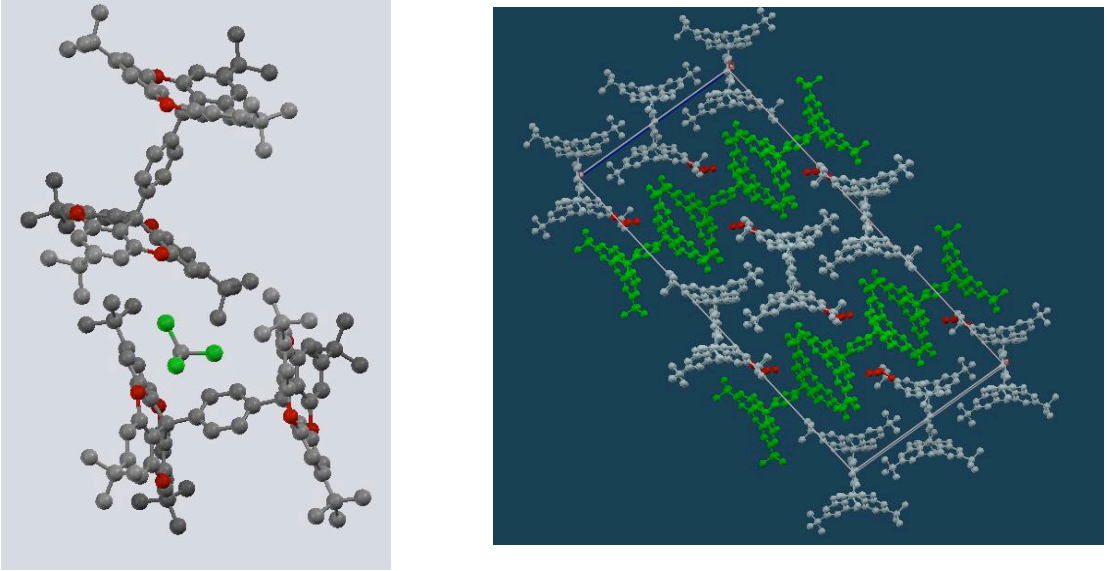

Figure 6.2: X-Ray structure of deuterated rod rotor with monoclinic symmetry C2/c #15. The crystal was grown from $CDCl_3$/hexane

By comparing the change in shape of the ADPs over temperature it was postulated that the phenyl ring of the phenyl linked rod rotor rotates* very fast. Based on that result all dynamic studies were initiated. First of all a deuterated version of the rod rotor was synthesized with four deuterium atoms in the central phenyl ring (Fig. 5.5, **33b**).

In order to do the ADP studies also on the deuterated compound. The first successful attempt led, as mentioned above, to a big surprise. First of all the structure of the d_4- compound **33b** was not showing cubic point group symmetry anymore, but monoclinic. Also there were two molecules per unit cell, instead of one and the disorder of the phenyl ring was not prominent anymore. In order to compared the ADPs visually, electron density difference maps of the

*Rotation does not imply unidirectional motion.

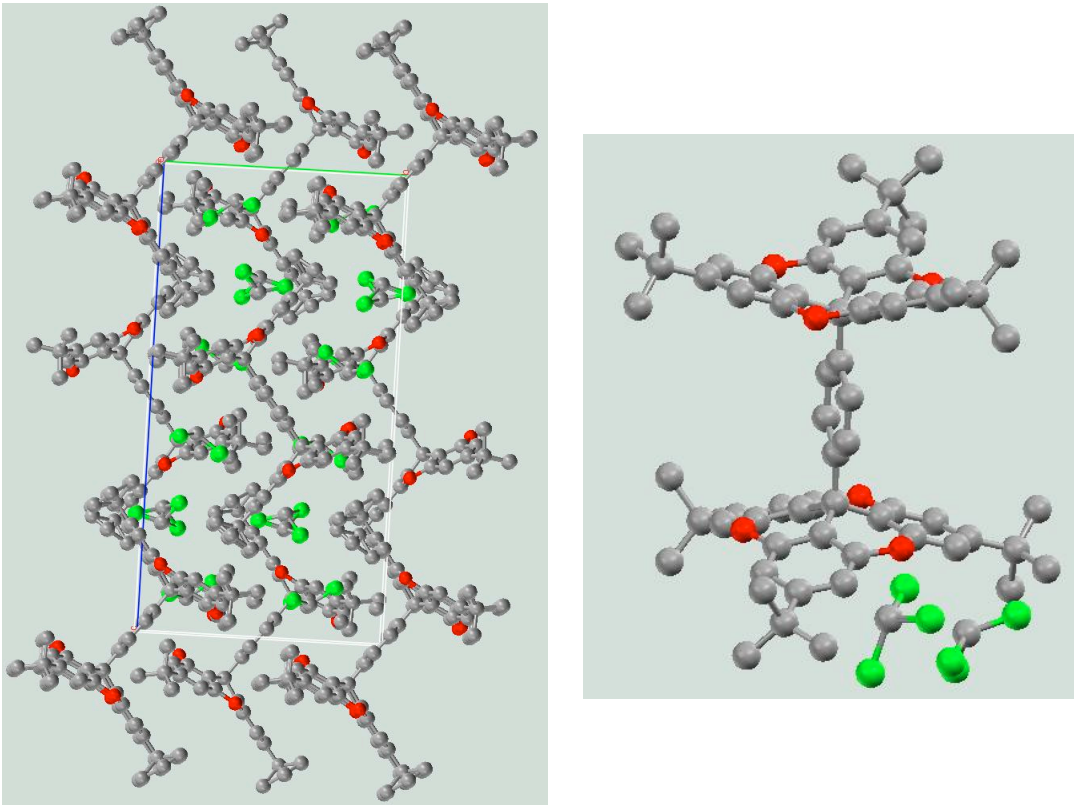

Figure 6.3: X-Ray structure of deuterated rod rotor with orthorombic symmetry Cmca (#64). The crystal was grown from CH_2Cl_2 and $CDCl_3$

monoclinic and cubic structures (Fig. 6.4 and Fig. 6.5) were generated by taking the projection down the yellow line indicated (Fig. 6.4 and Fig. 6.5):

Figures Fig. 6.4 and Fig. 6.5 show electron density contour maps and thermal ellipsoids of the phenyl spaced rotor. The non-deuterated rod rotor was crystallized from CH_2Cl_2 in a cubic point group symmetry. The phenyl ring is disordered and the thermal ellipsoids show a clear increase with rising temperature. Also, the electron density contour map illustrates the allocation of the electron density around the phenyl ring system, indicating a dynamic behavior. In the monoclinic point group symmetry (Fig. 6.5) of the deuterated phenyl spaced rotor (crystallized from $CDCl_3$ /hexane) the electron density difference maps show also a change in the thermal ellipsoid size. In this case, the electron density contour map shows another electron density distribution, due

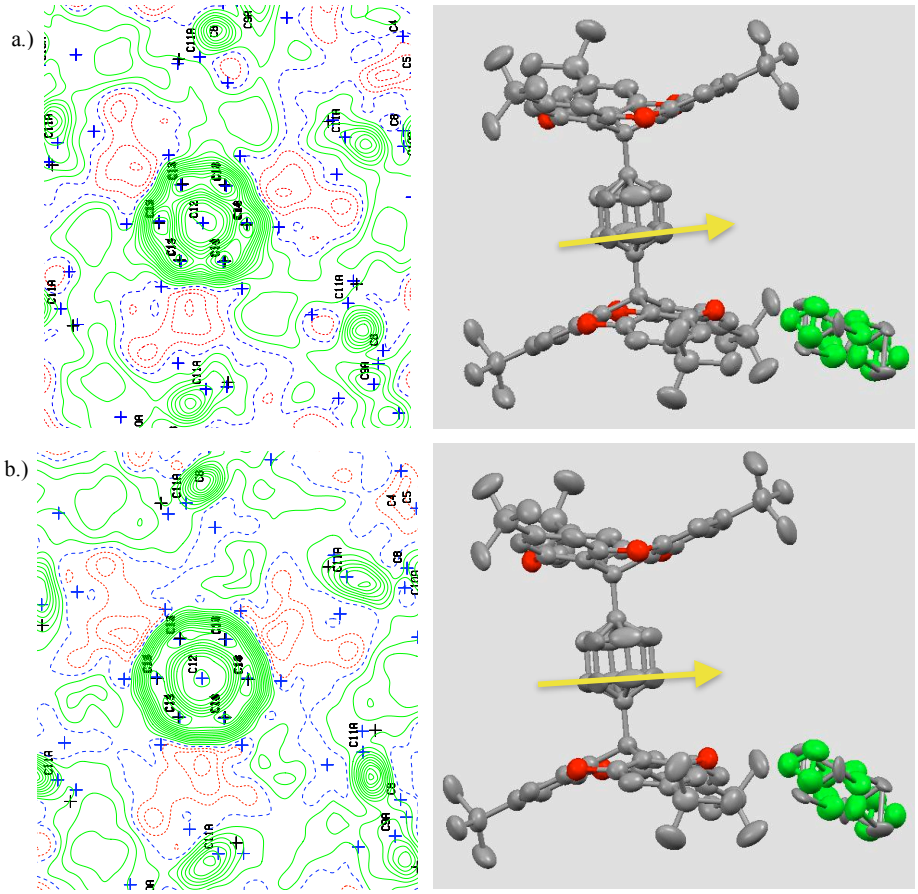

Figure 6.4: Difference map plots and thermal ellipsoid illustration of the phenyl spaced rotor (cubic space group)at a) 100 K and b) 270 K

to the other point group symmetry, the electron density seems to be more smeared out at higher temperatures, whereas at 100K the positions of the atoms are slightly better defined.

After this unexpected observation of having two crystal forms with different point groups symmetries, it was decided to grow more crystals under different crystallization conditions. Crystallization from $CDCl_3$ /hexane for the deuterated as well as for the non deuterated phenyl rod led mostly to monoclinic samples. Only in one case a crystal with orthorhombic point group symmetry was obtained using $CDCl_3$ /hexane as solvent.

Crystallization from CH_2Cl_2 led for the deuterated as well as the non-deuterated case to a cubic point group symmetry. But again an unexpected observation was made: in the case of

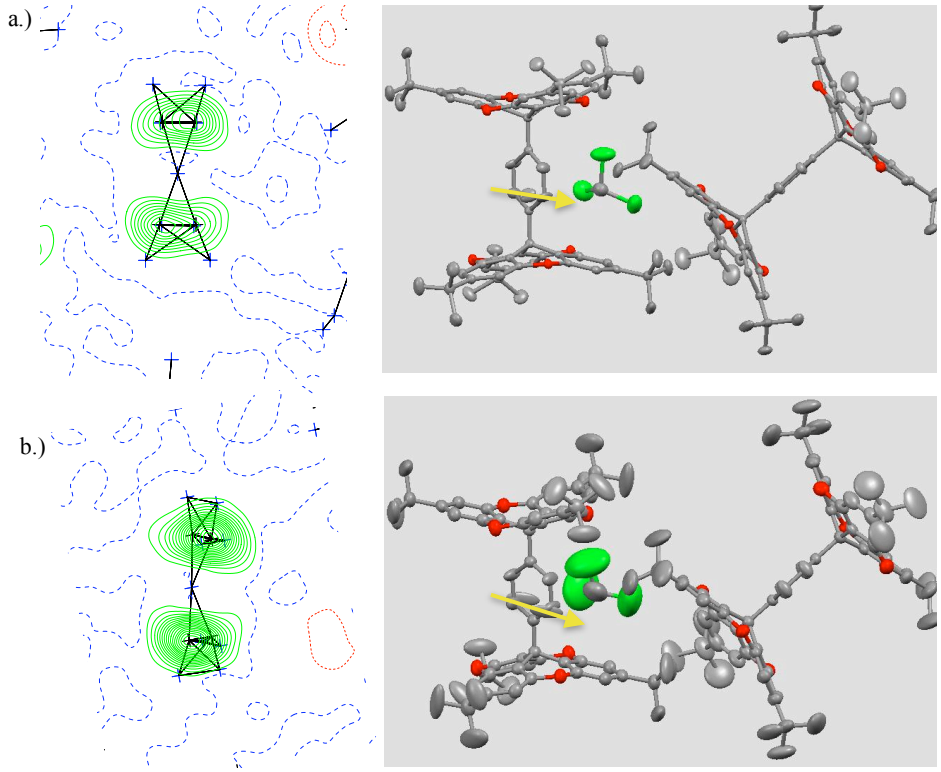

Figure 6.5: Electron density difference maps and thermal ellipsoid illustration of the deuterated phenyl spaced rotor (monoclinic space group) down at a) 100 K and b) 270 K

the deuterated system chlorination of the trioxatricornan ring was observed four times. In order to have a better understanding of the chlorination process HR-ESI-MS spectra were measured from each synthesis step performed in order to have the phenyl rod rotor. No precursor showed chlorination. Chlorination of the trioxatricornan stator was only found in the sample batch used for crystallization. To try to prevent chlorination of the trioxatricornan stators the sample vial with the crystallization solution was kept in the dark to omit radical formation with the result of having less chlorination on the TOTA rings.

6.1.1 Rotation Barriers Calculations from ADP's - Ellipsoid studies

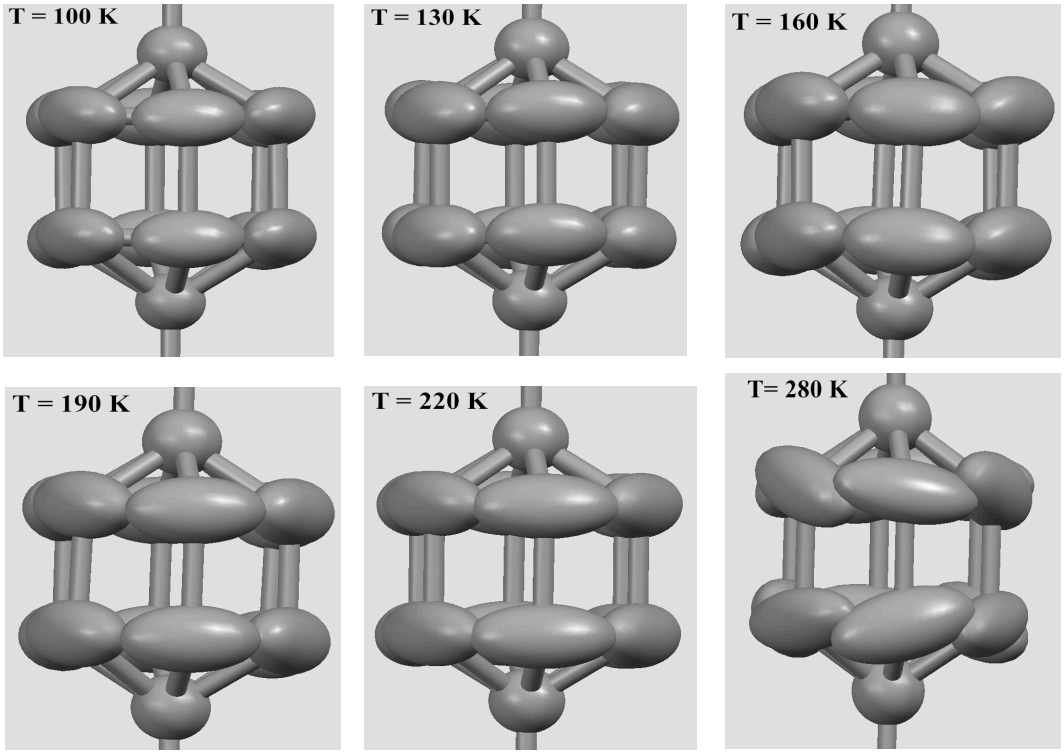

Figure 6.6: X-Ray structures of the phenyl ring part of the phenyl rod rotor at variable temperature, showing the increase of the ellipsoid size with increasing temperature.

Based on the phenyl ring disorder depicted in (Fig. 6.6) of the crystals grown from CH_2Cl_2 in cubic point group symmetry a rotation of the phenyl ring was postulated [†]. This assumption arose from the fact that the ellipsoids of the phenyl ring visibly increase with temperature increased, whereas the ellipsoids of the pivot atoms and the "static" TOTA part show only a little increase, not notable at first sight. Furthermore, the three fold disorder was an additional indication of a fast rotational motion and lead to the assumption of an energy potential with six local minima dependent on the angle of rotation. In order to calculate the rotation potential energy barrier ADP studies were performed at variable temperature starting at 100 K and ending at ambient temperature for three single crystals with cubic point group symmetry and with and

[†]Whereas a possible static or dynamic disorder of the whole system still was considered as a possibility

without deuterated phenyl ring. The refined anisotropic displacement parameters were subjected to rigid-body analysis using the TLS method of Maverick and Dunitz in which the TOTA atoms were considered to be the rigid group.

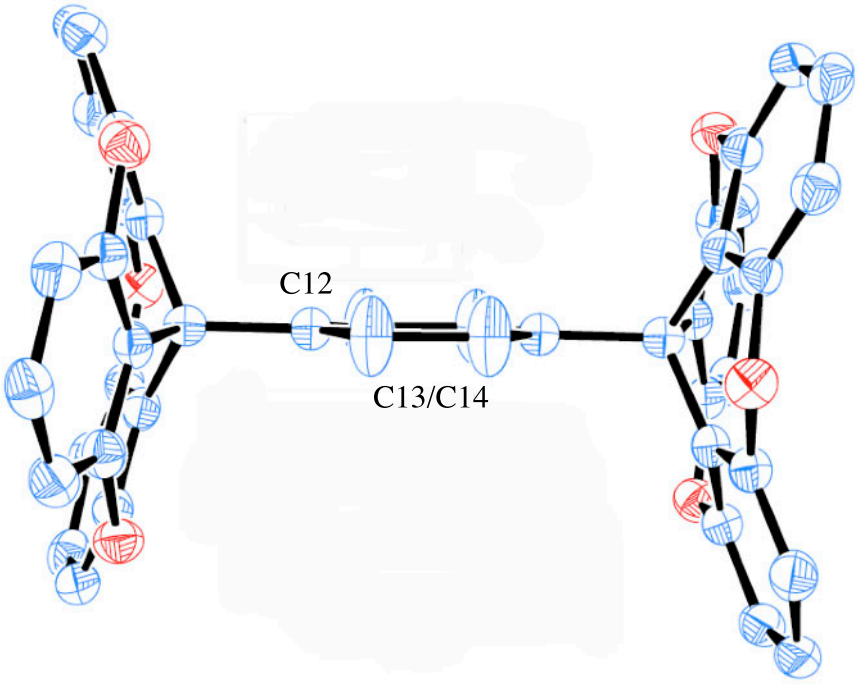

Figure 6.7: ORTEP displacement diagrams of the phenyl rod rotor 100 K, with ellipsoids drawn at the 30% probability level. Hydrogens and *tert*-butyl groups have been omitted for clarity.

The ADP treatment was performed on three data sets (SG0702, SG0927, SG1012). The first X-Ray data set (SG0702) was from the protonated phenyl rod **33a** (Fig. 5.5, Chapter 5) the second and third one (SG0927, SG1012) were from the deuterated species **33b** (Fig. 5.5) and showed both a small fraction of chlorination on the TOTA-phenyl ring. Fig. 6.7 shows ORTEP displacement diagrams of the phenyl rod rotor at 100K for dataset SG0702, already at 100 K it is apparent that the phenyl ring ellipsoids on C13/C14 are larger than ellipsoids in other positions.

For the ADP treatment the largest major axis of the ellipsoid on C13 and C14 was used. In a first step graphical representations of the major axes [‡] (SMA) vs. T were done and showed some interesting trends. The pivot atom (C12) showed less variation with increasing temperatures. For the two non pivot atoms C13 and C14 the trends are different from C12, increasing the temperature leads to increased values in all three data sets Table 6.1, 6.2 and, 6.3. In order to have standardized values C13 and C14 were forced to have identical ADPs. The EADP treatment is chosen here because the disorder implies occupation factors of only 1/3 low scattering power and thus low precision of the ADP. The treatment equates the two sites and therefore we obtain a single set of values for C13 and C14. In a next step, the fact that the SMA of C12 does not vary

Table 6.1: SG0702, Unit Cell Volumes and Principle Mean Square Atomic Displacement $<U^2>$ of SMAs for phenyl linked molecular rod rotor.

Temp [K]	SMA C12 [Å^2]	SMA C13 [Å^2]	SMA C14 [Å^2]	SMA C12 with EADP	SMA C13/14 with EADP	s.u.	C13/14 -C12(IP)	C13/14 -C13/14 (IP)
100	0.0506	0.1403	0.1466	0.0508	0.1454	0.0188	0.1028	0.0417
130	0.0479	0.1411	0.1368	0.0480	0.1387	0.0105	0.0961	0.0350
160	0.0349	0.1500	0.1256	0.0344	0.1365	0.0127	0.0939	0.0328
190	0.0479	0.1477	0.1745	0.0472	0.1599	0.0122	0.1173	0.0562
210	0.0469	0.1561	0.1948	0.0470	0.1750	0.0151	0.1324	0.0713
240	0.0487	0.1641	0.1819	0.0488	0.1711	0.0127	0.1285	0.0674
270	0.0506	0.1881	0.2299	0.0507	0.1924	0.0108	0.1498	0.0887
298	0.0510	0.2003	0.1940	0.0509	0.1918	0.0125	0.1492	0.0881

significantly with temperature was considered by subtracting the y-intercept point (IP), of the best fitted line of the data points of C12 (Fig. 6.8, 6.9, 6.10), from C13/14 as a first correction

[‡]the longest diameter of an ellipse

step. The same was done with the y-intercept point (IP) of C13/C14, it also was subtracted from the SMAs of C13/C14. The data for each set was summarized in tables 6.1, 6.2 and, 6.3) and for better visualization all three data sets are shown in Fig. 6.8, Fig. 6.9, and Fig. 6.10.

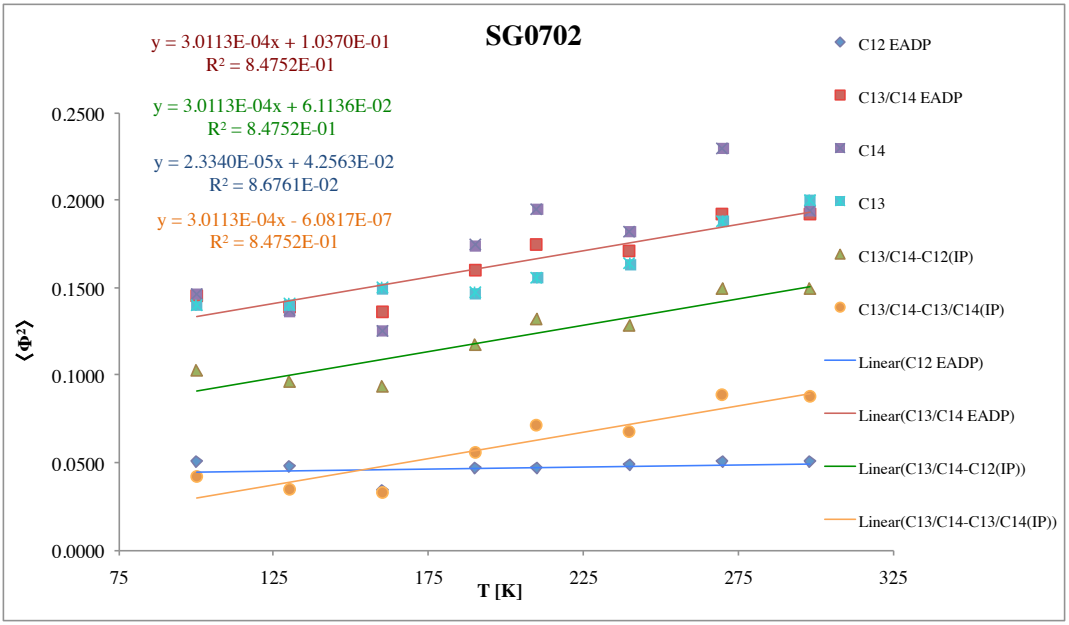

Figure 6.8: SMA vs. T for SG0702

$$\frac{\sqrt{\langle U^2 \rangle}}{d} = tan \left\langle \Phi^2 \right\rangle^{\frac{1}{2}} \tag{6.1}$$

$$artan \frac{\sqrt{\langle U^2 \rangle}}{d} = \left\langle \Phi^2 \right\rangle^{\frac{1}{2}} \tag{6.2}$$

$$f = \frac{k_B \cdot T}{\langle \Phi^2 \rangle} = \frac{R \cdot T}{\langle \Phi^2 \rangle \cdot N_A} \tag{6.3}$$

In order to calculate the rotation barrier first of all SMA values have to be transformed into angular displacements. This is done by trigonometry. By first taking the square root of the SMA values and then dividing it by the half distance of C13 to C14, tan $\left\langle \Phi^2 \right\rangle^{\frac{1}{2}}$ is obtained (Eq. (6.1) and (6.2)) and by transforming the equation $\left\langle \Phi^2 \right\rangle^{\frac{1}{2}}$ is then easily obtained. This treatment was performed on the normalized SMAs C13/14-C12 (IP). In a next step the quadratic approximation

Table 6.2: SG0927, Principle Mean Square Atomic Displacements U

Temp [K]	SMA C12 [Å^2]	SMA C13 [Å^2]	SMA C14 [Å^2]	SMA C12 with EADP	SMA C13/14 with EADP	s.u.	C13/14 -C12(IP)	C13/14 -C13 (IP)
100	0.0448	0.1248	0.1392	0.0449	0.1334	0.01051	0.0910	0.02948
130	0.0442	0.1146	0.1762	0.0443	0.1438	0.00826	0.1014	0.03988
160	0.0472	0.1637	0.2189	0.0473	0.1841	0.01537	0.1417	0.08018
190	0.0483	0.1615	0.2013	0.0485	0.1816	0.01092	0.1392	0.07768
220	0.0496	0.1927	0.1892	0.0494	0.1888	0.01044	0.1464	0.08488
250	0.0508	0.1875	0.2239	0.0510	0.2101	0.01299	0.1677	0.10618
270	0.0512	0.1674	0.2141	0.0514	0.1896	0.01016	0.1472	0.08568
300	0.0539	0.2239	0.2465	0.0542	0.2175	0.01483	0.1751	0.11358

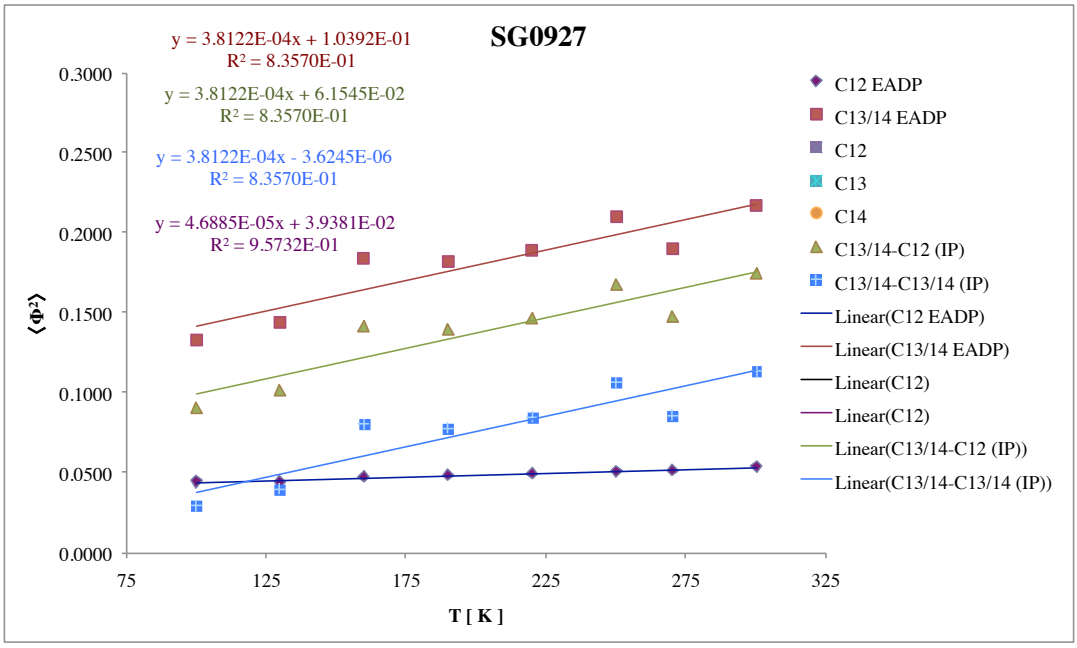

Figure 6.9: SMA vs. T for SG0927

Table 6.3: SG1012, Principle Mean Square Atomic Displacements U

Temp [K]	SMA C12 [Å^2]	SMA C13 [Å^2]	SMA C14 [Å^2]	SMA C12 with EADP	SMA C13/14 with EADP	s.u.	C13/14 -C12(IP)	C13/14 -C13/14 (IP)
100	0.0536	0.1466	0.1359	0.0535	0.1410	0.00471	0.0882	0.03292
130	0.0604	0.1609	0.1563	0.0603	0.1587	0.00474	0.1059	0.05062
160	0.0596	0.1592	0.1839	0.0597	0.1711	0.00559	0.1183	0.06302
190	0.0620	0.1888	0.1820	0.0619	0.1858	0.00511	0.1330	0.07772
220	0.0582	0.1873	0.2159	0.0582	0.2017	0.00727	0.1489	0.09362
250	0.0611	0.1989	0.2030	0.0611	0.1996	0.00559	0.1468	0.09152
280	0.0638	0.2102	0.2092	0.0638	0.2115	0.00657	0.1587	0.10342

with $V(x) = fx^2/2$ to the *cos*-potential, Eq. (6.4), is considered and the force constant f of this quadratic potential is calculated by using Eq. (6.3).

$$V(\Phi) = \frac{B}{2} - \frac{B \cdot (cosn\Phi)}{2} \tag{6.4}$$

$$\frac{\partial V(\Phi)}{\partial \Phi} = \frac{B \cdot n}{2} \cdot sin\Phi \tag{6.5}$$

$$\frac{\partial^2 V(\Phi)}{\partial \Phi^2} = \frac{B \cdot n^2}{2} \cdot cos\Phi \tag{6.6}$$

$$f = \frac{B \cdot n^2}{2} = \frac{RT}{\langle \Phi^2 \rangle} \tag{6.7}$$

$$B = \frac{2 \cdot RT}{n^2 \cdot \langle \Phi^2 \rangle} \tag{6.8}$$

For the calculation of the rotation barrier we can now make use of the fact that f and B are proportional. If Φ=0 the second partial derivative of $V(\Phi) = \frac{B}{2} - \frac{B \cdot (cosn\Phi)}{2}$ is equal to $\frac{B \cdot n^2}{2}$ and

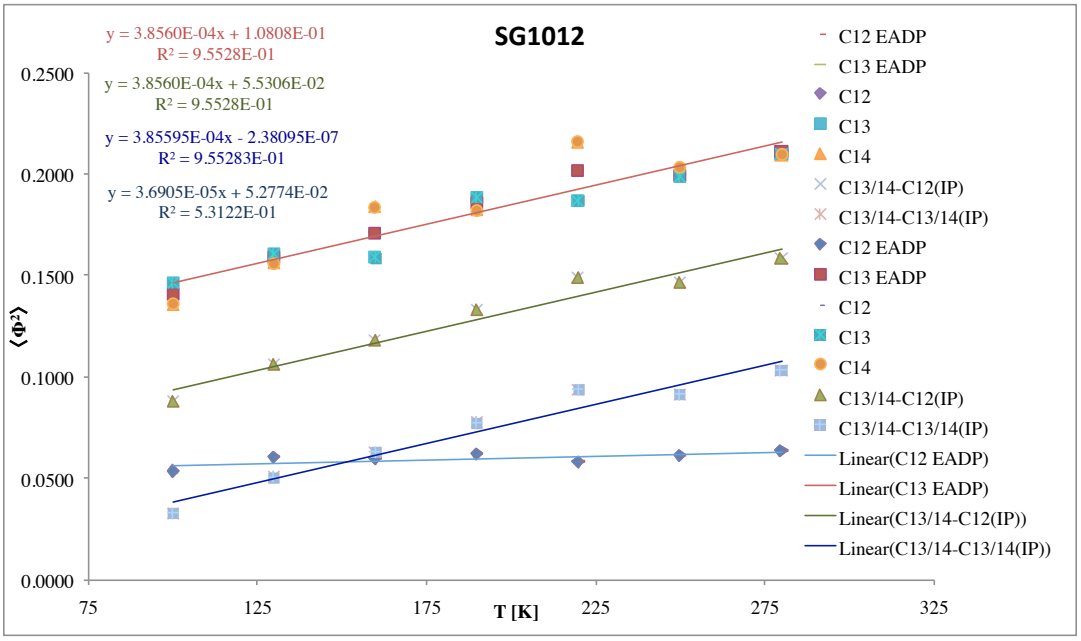

Figure 6.10: SMA vs. T for SG1012

this is equivalent to $\frac{RT}{\langle\Phi^2\rangle}$ (Eq.(6.4)- (6.7)). This approach leads us to the rotation barrier for the harmonic oscillator model and uses a gaussian probability distribution. By using Eq. (6.8) and n = 6 (energy potential with six local minima) rotation barriers for all three data sets were obtained and summarized in table 6.4, table 6.5,and table 6.6. The values for the barriers for all data sets lie between $5{\cdot}10^{-5}$ kcal/mol and $1.1{\cdot}10^{-4}$ kcal/mol which would be basically a free rotation.

In order to have a more accurate model to calculate the rotation barrier a sinusoidal potential is considered. For a sinusoidal potential, classical Bolzmann averaging leads to a mean square angular displacements given by eq.: 6.9, in which B is the barrier height and n is the multiplicity of the barrier. The mean square amplitude of libration $< \phi^2 >$ of the central phenyl ring is obtained by the expression in eq.: 6.9.

$$< \phi^2 >= \frac{\int_0^{\pi/n} \phi^2 exp\{-B(1-cosn\phi)/2RT)\}\, d\phi}{\int_0^{\pi/n} exp\{-B(1-cosn\phi)/2RT)\}\, d\phi} \tag{6.9}$$

Table 6.4: Calculation of the rotational barrier for SG0702

T [K]	C13/14-C12 [Å^2]	(C13/14-C12)$^{1/2}$ [Å]	tan (Φ)	$<\Phi>$ [rad]	$<\Phi>$ [°]	$<\Phi^2>$ $[deg^2]$	f $\left[\frac{cal}{deg^2}\right]$	B $\left[\frac{cal}{mol \cdot deg^2}\right]$
100	0.103	0.321	0.265	0.259	14.82	219.6	$5.45 \cdot 10^{23}$	0.050
130	0.09613	0.310	0.256	0.250	14.35	205.9	$7.55 \cdot 10^{23}$	0.070
160	0.0939	0.306	0.253	0.248	14.19	201.4	$9.50 \cdot 10^{23}$	0.088
190	0.117	0.343	0.283	0.275	15.78	249.1	$9.12 \cdot 10^{23}$	0.084
210	0.132	0.364	0.300	0.292	16.71	279.3	$8.99 \cdot 10^{23}$	0.083
240	0.129	0.359	0.296	0.288	16.48	271.5	$1.06 \cdot 10^{24}$	0.098
270	0.150	0.387	0.319	0.309	17.71	313.7	$1.03 \cdot 10^{24}$	0.095
298	0.149	0.386	0.319	0.309	17.68	312.6	$1.14 \cdot 10^{24}$	0.11

Table 6.5: Calculation of the rotational barrier for SG0927

T [K]	C13/14-C12 [Å^2]	(C13/14-C12)$^{1/2}$ [Å]	tan (Φ)	$<\Phi>$ [rad]	$<\Phi>$ [°]	$<\Phi^2>$ $[deg^2]$	f $\left[\frac{cal}{deg^2}\right]$	B $\left[\frac{cal}{mol \cdot deg^2}\right]$
100	0.091	0.302	0.269	0.263	15.06	226.8	$5.27 \cdot 10^{23}$	0.048
130	0.101	0.318	0.284	0.277	15.86	251.5	$6.18 \cdot 10^{23}$	0.057
160	0.142	0.376	0.336	0.324	18.56	344.5	$5.55 \cdot 10^{23}$	0.051
190	0.139	0.373	0.333	0.321	18.41	338.8	$6.71 \cdot 10^{23}$	0.062
220	0.146	0.383	0.341	0.329	18.84	355.1	$7.07 \cdot 10^{23}$	0.068
250	0.168	0.410	0.365	0.350	20.07	402.6	$7.12 \cdot 10^{23}$	0.068
270	0.147	0.384	0.342	0.330	18.89	356.9	$9.05 \cdot 10^{23}$	0.083
300	0.175	0.418	0.373	0.357	20.47	1172.7	$3.04 \cdot 10^{23}$	0.080

Table 6.6: Calculation of the rotational barrier for SG1012

T [K]	C13/14-C12 [Å^2]	(C13/14-C12)$^{1/2}$ [Å]	tan (Φ)	$<\Phi>$ [rad]	$<\Phi>$ [°]	$<\Phi^2>$ $[deg^2]$	f $\left[\frac{cal}{deg^2}\right]$	B $\left[\frac{cal}{mol \cdot deg^2}\right]$
100	0.0882	0.297	0.265	0.259	14.84	220.2	$5.43 \cdot 10^{23}$	0.050
130	0.106	0.325	0.290	0.283	16.19	262.0	$5.93 \cdot 10^{23}$	0.055
160	0.118	0.344	0.307	0.298	17.06	290.9	$6.58 \cdot 10^{23}$	0.060
190	0.133	0.365	0.325	0.315	18.02	324.7	$7.00 \cdot 10^{23}$	0.065
220	0.149	0.386	0.344	0.331	18.99	360.7	$6.96 \cdot 10^{23}$	0.067
250	0.147	0.383	0.342	0.329	18.87	356.0	$8.06 \cdot 10^{23}$	0.077
280	0.159	0.398	0.355	0.341	19.56	382.7	$8.44 \cdot 10^{23}$	0.081

A plot of $<\phi^2>$ as a function of RT/B for n = 6 was then generated and is depicted in Fig. 6.11. At very low values of RT/B eq.: 6.9 does not hold and a quantum mechanical expression for $<\phi^2>$ must be considered. For temperatures higher than T=160 K description of the atoms becomes less and less appropriate because the atomic ellipsoid shape become more and more "banana-shaped". This observation meant for our research that only the first three temperature could be used from each data set. With the plot in hand we could obtain RT/B values for all three data sets for two to three temperatures. Technically this was done by entering the calculated $<\phi^2>$ in deg^2 (Table 6.1, 6.2 and, 6.3) and reading the corresponding RT/B value from the simulated function derived from eq. 6.9 (Fig. 6.11). From this value the rotation barrier was calculated.

In table 6.7 the results for all data sets are summarized. In order to have an upper and lower limit of the rotation barrier the treatment performed on the SMAs was also redone with SMA

plus standard uncertainty and SMA minus standard uncertainty leading to $<\Phi^2>+s.u.$ and $<\Phi^2>-s.u.$ values respectively from which a upper and lower limit of the rotation barrier was calculated.

Table 6.7: Summary rotation barriers for the three data sets, including the upper and lower barrier of rotation.

Data set	Temp [K]	$<\Phi^2>$ $[deg^2]$	B_0 $\left[\frac{kcal}{mol \cdot deg^2}\right]$	$<\Phi^2>+s.u.^*$ $[deg^2]$	B_+ $\left[\frac{kcal}{mol \cdot deg^2}\right]$	$<\Phi^2>-s.u.^\dagger$ $[deg^2]$	B_- $\left[\frac{kcal}{mol \cdot deg^2}\right]$
SG0702							
	100	219.6	0.19	249.8	0.12	189.1	0.26
	130	205.9	0.30	223.0	0.23	188.8	0.34
	160	201.4	0.37	220.4	0.30	182.4	0.45
SG0927							
	100	195.4	0.25	217.0	0.19	173.6	0.30
	130	216.8	0.26	233.6	0.20	199.8	0.40
	160	297.7	-	-	-	297.7	-
SG1012							
	100	189.6	0.27	199.3	0.24	179.9	0.29
	130	225.9	0.23	235.6	0.19	216.3	0.26
	160	239.8	0.18	262.3	-	239.8	0.22
Avarages (s.u.)			0.26(6)		0.21(6)		0.32(8)

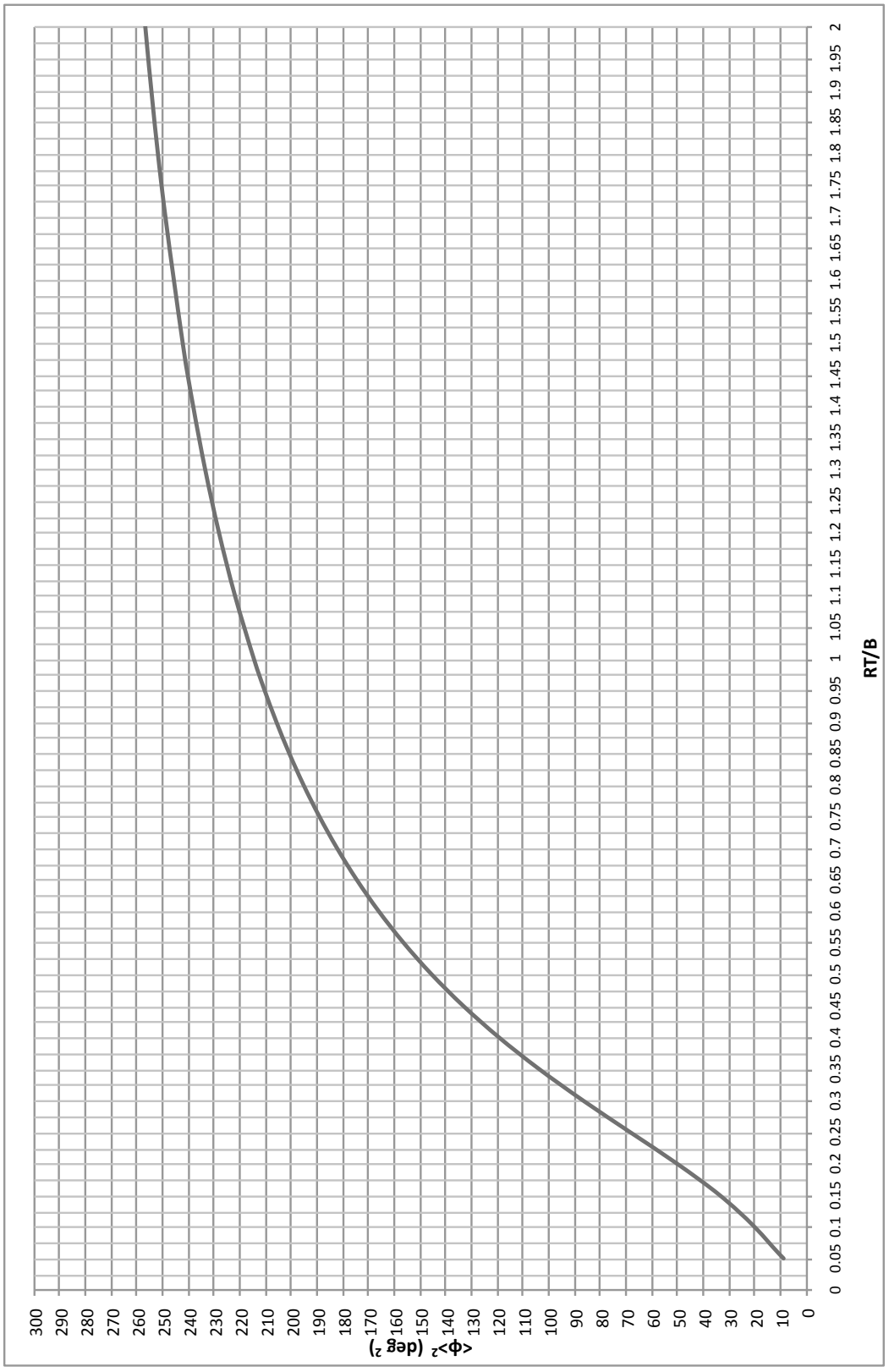

Figure 6.11: $< \phi^2 >$ as a function of RT/B for n = 6

In table 6.7 a very low barrier for the phenyl ring rotation of 0.3 kcal/mol is found. The lower limit lies around 0.2 kcal/mol and the upper limit around 0.4 kcal/mol. In the dataset SG0927 the rotation barrier at 160 K could not be obtained, the $<\Phi^2>$ values were already in an area of the plot (fig. 6.11) were the model we used is not applicable.

Table 6.8: Summary of rotation barriers for three data sets with derived $<\Phi^2>$ values from linear regressions.

Data set	Temp	$<\Phi^2>$ $[\text{Å}^2]$	$<\Phi^2>$ $[deg^2]$	B_0 $\left[\frac{kcal}{mol \cdot deg^2}\right]$
SG0702				
linear regression		$<\Phi^2>= 3.10 \cdot 10^{-4} \cdot T + 0.061$	$R^2 = 0.85$	
	100	0.091	195.3	0.25
	130	0.10	213.8	0.26
	160	0.11	232.2	0.24
SG0927				
linear regression		$<\Phi^2>= 3.81 \cdot 10^{-4} \cdot T + 0.062$	$R^2 = 0.84$	
	100	0.1	213.8	0.20
	130	0.11	236.2	0.19
	160	0.12	260.1	0.15
SG1012				
linear regression		$<\Phi^2>= 3.86 \cdot 10^{-4} \cdot T + 0.055$	$R^2 = 0.96$	
	100	0.094	201.5	0.23
	130	0.11	234.2	0.19
	160	0.12	248.4	-
Avarages (s.u.)				0.21(4)

In order to confirm the barrier the linear regression of the SMA values (Fig. 6.8, 6.9, 6.10) of C13/C14-C12(IP) was used from all three data sets. From the obtained regression $<\Phi^2>$ values for T= 100K, 130K as well as T=160K were calculated and then first transformed to deg^2. From

these $< \Phi^2 >$ values the rotation barrier were obtained. The most reliable values for all data sets are at 100K, were $< \Phi^2 >$ are still in a good region of the curve (not yet on the flat part). The barrier from this calculations is 0.2-0.3 kcal/mol. The results are summarized in table 6.8.

6.1.2 Conclusion X-Ray studies

Several single crystals of the phenyl linked rod rotor were obtained and showed in total three different point groups depending on crystallization conditions. During the ongoing project a reproducible way of obtaining cubic crystals was achieved. It was noticed that fast crystallization tends to lead to monoclinic crystals rather than cubic ones. Crystallization was preferably performed in NMR-tubes and at a scale of 5 mg in 1.5 mL solvent; in order to dissolve the phenyl linked rod rotor the ultrasonic bath was used, the tube was then sealed by putting teflon band around the lid for slower evaporation. The crystallization was done in the dark (to avoid/ reduce chlorination of the trioxatricornan rings) and took 2-3 months on average.

In summery VT X Ray studies of three single crystals were obtained and ADP studies were performed. The ADP studies of the three data sets lead in the case of a harmonic potential model to a barrier of 0.4 kcal/mol. In the case of a sin potential values for the different data sets varied more, obtained values for the barrier are between 0.2 -0.4 kcal/mol. This variation is due to the curvature of the plot (fig. 6.11) in the sin potential. At 100 K $< \Phi^2 >$ values in all three data sets amount to $\sim$200 deg^2 and we are already in a region of the plot (fig. 6.11), were the curve starts to flatten and this model becomes worse for higher temperature. This can be explained by the changing shape of the ellipsoids with temperature, the higher the temperature the more banan shaped the ellipsoid become. This change of shape would imply the use of a different model at high temperature. For our purpose the ADP model was a good choice, similar values for the rotation barrier from three data sets and three temperatures for each sets were

obtained. This results lead to the conclusion that the synthesized phenyl linked rod rotor shows a nearly free rotation. In order to proof this finding DFT calculations and solid state NMR studies were performed and are presented in the next sections.

6.2 DFT Calculations

6.2.1 Electrophilic (HOMO) and Nucleophilic (LUMO) frontier density surfaces.

For a better understanding of the X-Ray data and the molecular rod rotor, DFT calculations (including dispersion parameter) were performed[§]. In a first step the dynamic and static symmetry of the system were visualized.

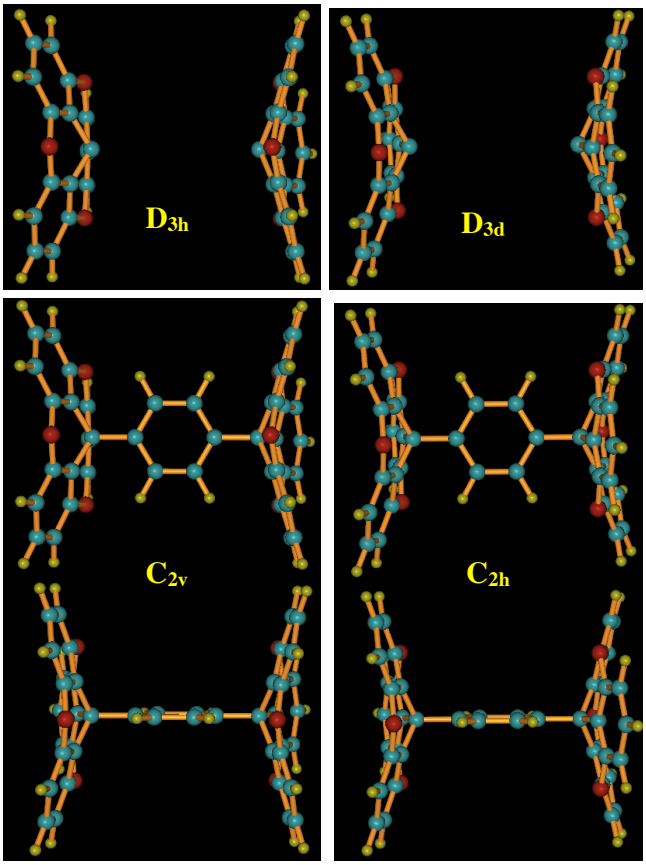

Figure 6.12: Static Symmetry of the phenyl rod rotor

In Fig. 6.12 the static symmetry of the two trioxatricornan rings is depicted. Either both caps face each other such that the oxygen atoms of one cap unit are in the same mirror positions as the oxygen atoms of the second cap (D_{3d} geometry) and in the second case the oxygen atoms of one cap are aligned such that they are facing aromatic sp^2 C atoms of the

[§]by Prof. Dr. Kim K. Baldridge, from the University of Zurich

second cap (D_{3h} geometry). In the first case ("mirror caps") the dynamic symmetry is C_{2v} x C_3 (three distinguishable positions for the phenylen ring) and in the second case C_{2h} x S_6 (six distinguishable positions for the phenylene ring).

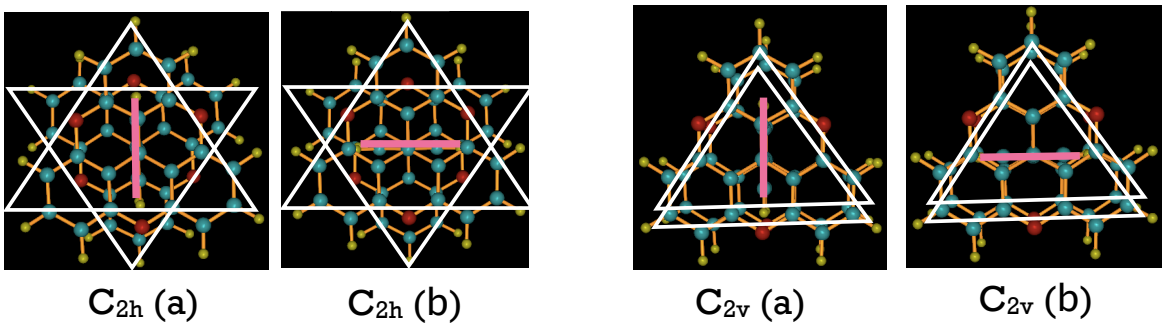

Figure 6.13: Top view of the different possible geometries of the caps and the minima and maxima position of the phenylene rotator

For these geometries the frontier density surfaces were computed by using the magnitudes of the MOs, which are possibly attacked by a nucleophile, radical, or electrophile. The results are visualized in Fig. 6.14 for the C_{2h} geometry ,and in Fig. 6.15 for the C_{2v} geometry. A color pattern for the molecular orbitals and the electrostatic potential was used; the interpretation key is summarized in table 6.9.

In Fig. 6.14 the results for the C_{2h} geometry are depicted. As expected the electrophilic (HOMO) frontier orbital density surface around the oxygen atoms in the caps is blue, which indicates that this region is most susceptible to attack by an electrophile. In the visualization of the nucleophilic (LUMO) frontier density surface the area around the oxygen atoms is less likely to be attacked by a nucleophile than the surrounding carbon atoms and therefor more red. In this representation the phenylene rings, especially at the pivot atoms, is now the most susceptible place to be attacked by an nucleophile. When looking at the molecular orbitals of the molecular rod rotor, we astonishingly find a delocalization of the π- system over the whole molecule, this is

Table 6.9: Color Interpretation of the frontier density surfaces[152]

Surface	Color	Interpretation
Molecular Orbital	Red/Blue	occupied orbital
	Green/Yellow	unoccupied orbital
Electron Density	Gray	isosurface
Electrostatic Potential	Red	negative region
	Blue	positive region
Electrophilic (HOMO) Frontier Surface	Blue	region most susceptible to attack by an electrophile
Nucleophilic (LUMO) Frontier Surface	Blue	region most susceptible to attack by a nucleophile

observed in the LUMO as well as in the HOMO. This delocalization indicates a high reactivity of the the molecule, *i.e.* susceptibility towards attacks by nucleophiles, electrophiles ,and radicals.

In Fig. 6.15 the results for the C_{2v} geometry are depicted. The results are comparable, also in the C_{2v} geometry conformation the electrophilic (HOMO) frontier density surface around an oxygen atoms in the caps are blue and the most susceptible to attack by an electrophile. For the nucleophilic (LUMO) frontier density surface the pivot atoms of the phenylene ring are blue and the most susceptible to attack by a nucleophile. Like in the C_{2h} geometry the π- system of the HOMO and LUMO of the C_{2v} geometry conformation are completely delocalized and show high reactivity towards nucleophiles, electrophiles and radicals.

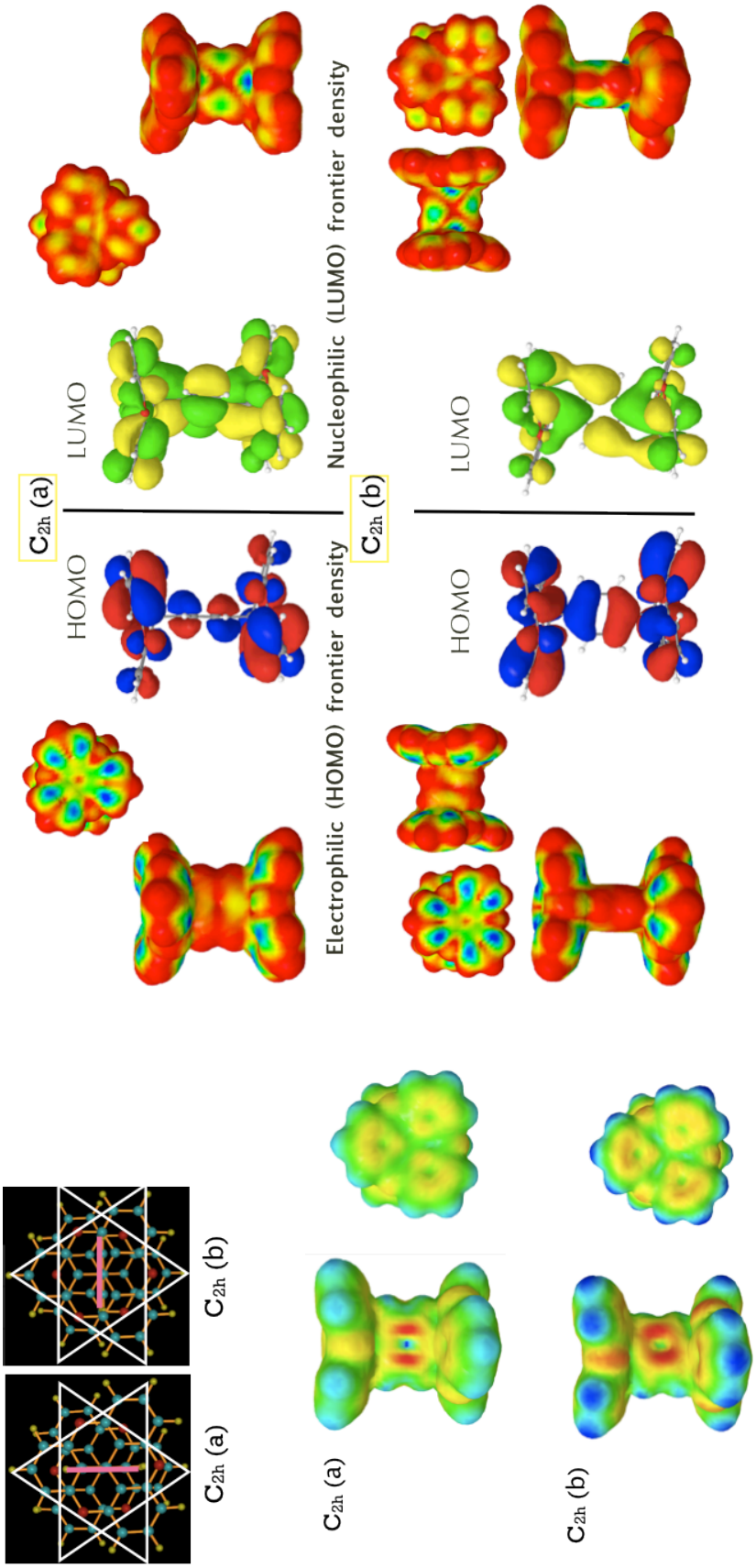

Figure 6.14: Electrophilic (HOMO) and nucleophilic (LUMO) frontier density surfaces for C_{2h} geometry of the phenyl rod rotor

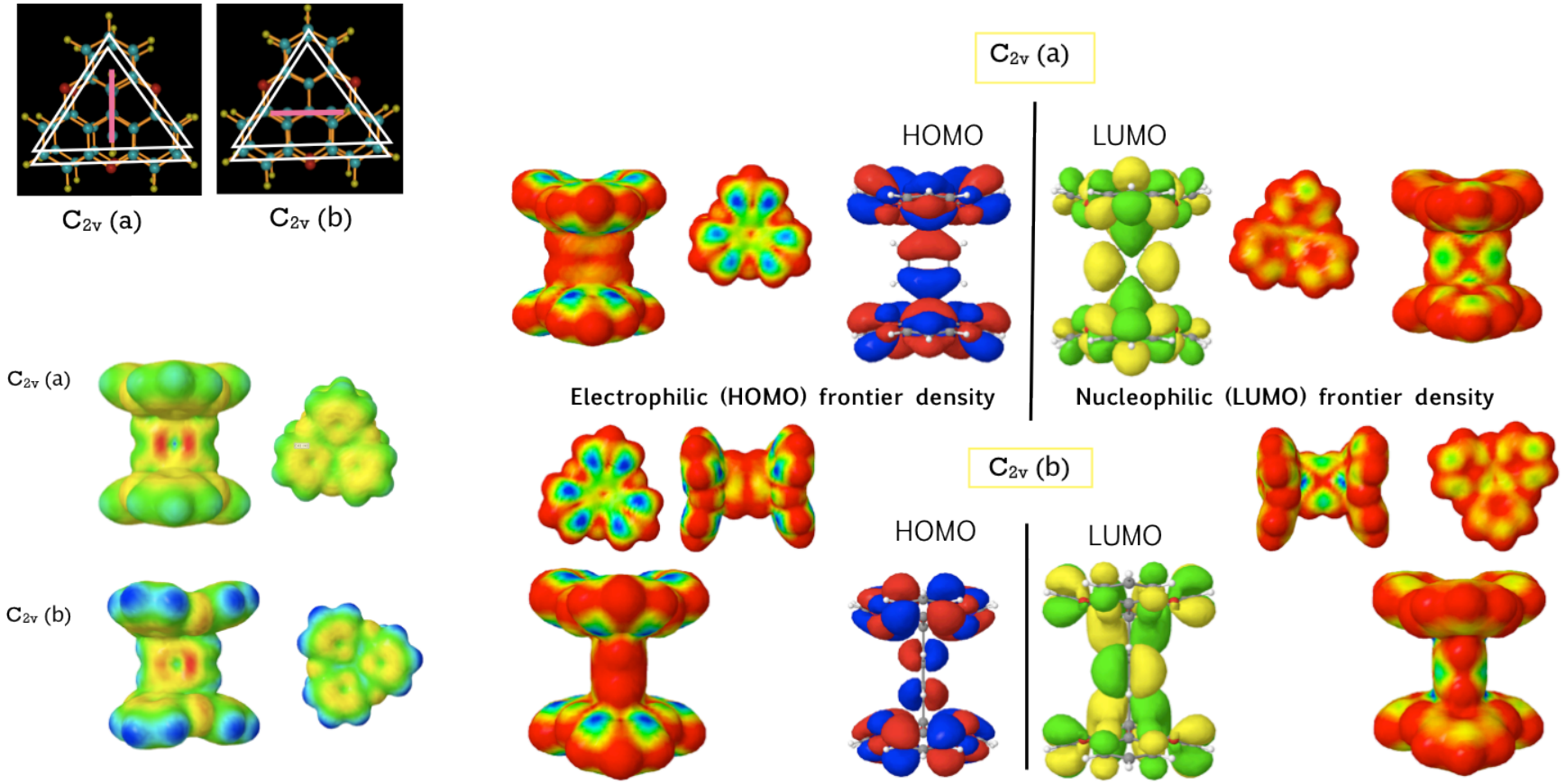

Figure 6.15: Electrophilic (HOMO) and nucleophilic (LUMO) frontier density surfaces for C_{2v} geometry of the phenyl rod rotor

6.2.2 Rotational Potential

Based on the results described in the last section, the rotational potential was calculated. In Fig. 6.16 the top view of the possible geometries is depicted and we also hypothesized possible minima and maxima for the phenylene position. The rotational potential was then calculated considering dispersion and the following rotational potentials depicted in Fig. 6.16 were obtained.

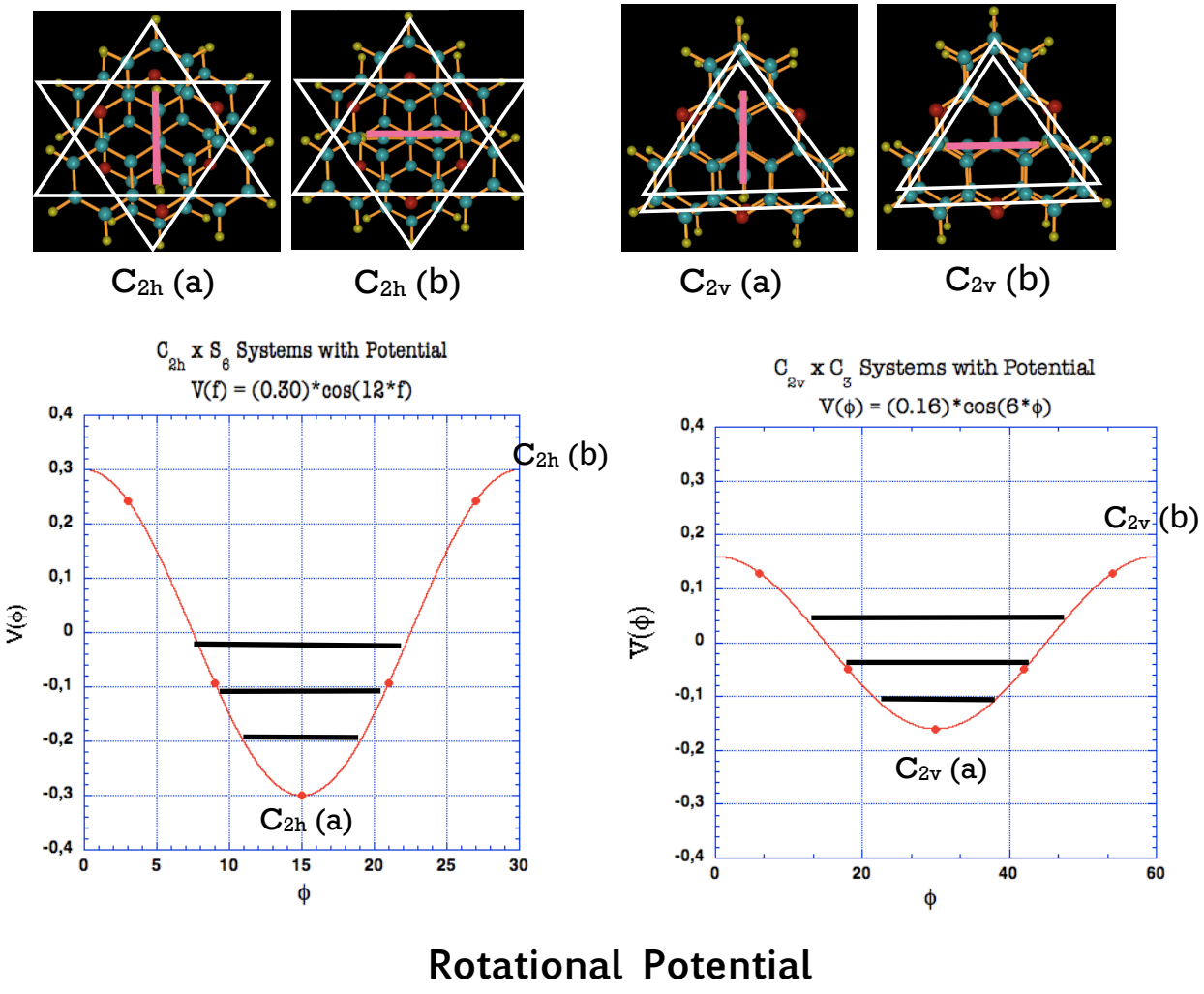

Figure 6.16: DFT calculation of the rotational potential of the phenyl rod rotor.

For the dynamic C_{2h} x S_6 system a rotation barrier of 0.60 kcal was calculated in the case of the C_{2v} x C_3 system the barrier obtained was 0.32kcal. Both barriers are extremely low and

indicate nearly free rotation of the phenylene moiety, the C_{2v} x C_3 system rotational barrier is higher but considering the very low values of the rotational barrier the difference is not significant. These results together withe the results of the VT XRay studies encouraged us to perform solid state NMR measurements on the phenyl rod rotor, in order to be able to track this postulated nearly free rotation.

6.2.3 Conclusion DFT studies

The data obtained by DFT calculations is in good agreement with the data obtained by ADP studies. The values obtained by DFT are 0.32 and 0.60 kcal/mol compared to values of 0.2-0.4 kcal/mol. These high level calculations which included dispersion made us confident of having designed a system with nearly free rotation. In order to confirm this finding a third time we went on for solid state NMR studies.

6.3 ^{2}H SSNMR Measurements

In order to be able to collect ^{2}H SSNMR data, of the phenyl rod rotor **33** (Fig. 6.17, **33b**) isotopic labeling is necessary, since the ^{2}H natural abundance is low. Furthermore a significant quantity, in the ideal case 250 mg, of the deuterated material is needed for a good signal to noise ratio. For the interpretation of the data it is necessary to be aware of the fact, that the quadrupolar coupling depends on the molecular orientation with respect to the magnetic field. A reorientation of the molecule influences the shape of a ^{2}H spectrum and can lead to a reduction of its width. The ^{2}H line shapes also provides information about the rate of the molecular motions are taking place as well as the motional mechanism for the dynamic process. This sensitivity towards molecular motion in solid state was used for this measurements.

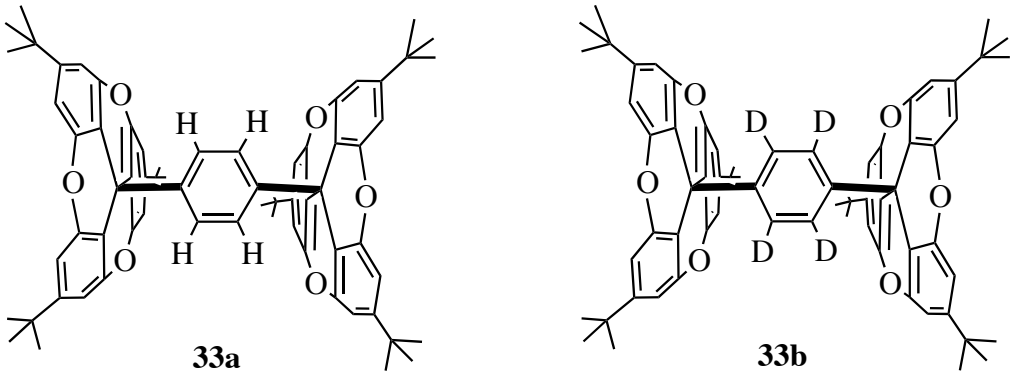

Figure 6.17: Deuterated TOTA-phenyl-*d4*-TOTA sandwich, with a rotating phenyl ring in the middle

In order to understand the mechanism of the phenyl ring rotation of (Fig. 6.17, **33b**), preliminary ^{2}H SSNMR measurements at ambient temperature were performed [¶] and compared to simulations for two-, three-, and -six-fold rotations of the phenyl ring (Fig. 6.18). From the preliminary studies, a fast 2-fold uniaxal jump of the phenyl ring was hypothesized. This assumption was based on the line width of the spectrum, a 3-fold or a 6-fold uniaxal jump would have given rise to a narrower line width in the spectrum. In a next step ^{2}H SSNMR measurements

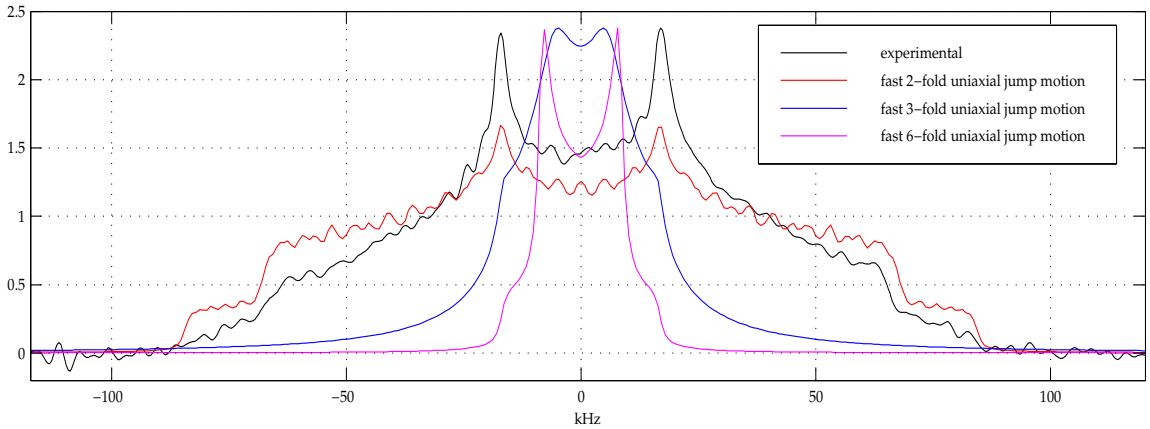

Figure 6.18: Comparison of experimental data @ RT and simulations of fast uniaxial jump motions (C_{qcc}=180 kHz,η=0.07, LLB=1.5 kHz, GLB=0.5 kHz)

[¶]All SSNMR studies were performed by Dr. Jacco Douwe van Beek at ETH Zürich, in the physical chemistry institute, in a collaboration

at 7.9 K were performed in order to see the possible lower limit of the rotation barrier. From the ADP studies and DFT calculations an extremely low rotation of about 0.3 kcalmol^{-1} was predicted. For extremely fast rotation the static SSNMR spectrum can only be achieved at low temperature and indeed at 7.9 K a static spectrum was achieved with a line width of 300 kHz. Compared to the spectrum at ambient temperature with a line width of 120 kHz there was a clear broadening of the signal (Fig. 6.19). In a next step the measured spectra was compared to

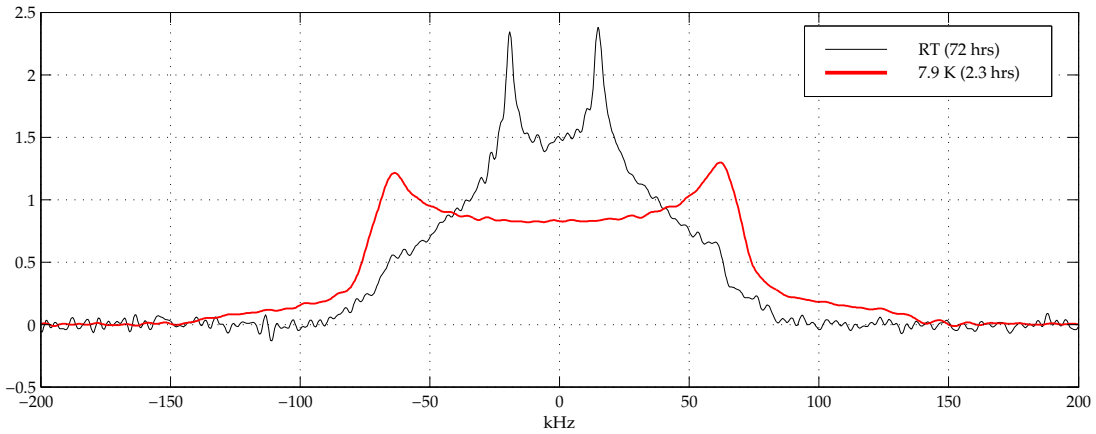

Figure 6.19: Comparison of ^{2}H spectra at two temperatures (measurement time indicated)

the simulated spectrum (Fig. 6.20), this step was performed in order to check the reliability of the simulation.

After these two preliminary experiments we had a reliable system and the VT SSNMR experiment could be undertaken. At very low T (under 80 K)the spectra (Fig. 6.21) showed a static behavior. At 80 K a new component comes in at around 25 kHz and the corresponding peak starts to increase. From 125 K on, this component begins to fit with the simulation (Fig. 6.22) for the 2-fold rotation. Although many different functions were tried, a perfectly fitting simulation was not achieved. This fact led to a confusion in the beginning and different reasons were considered:

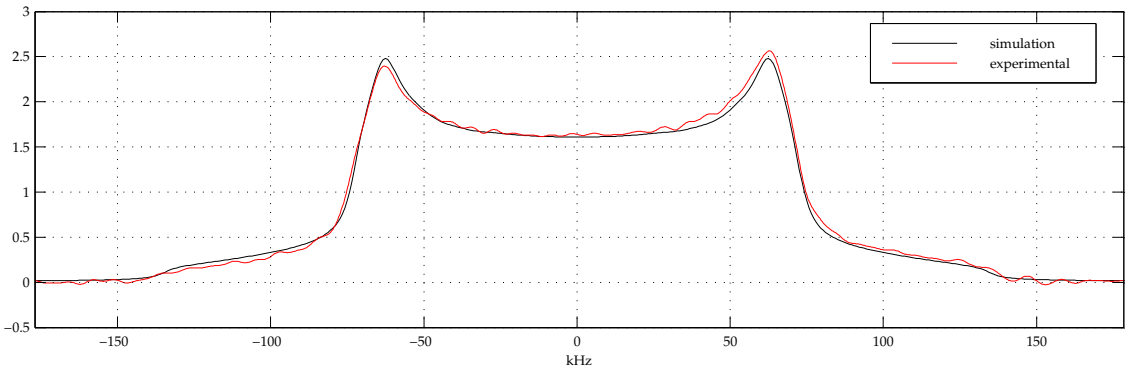

Figure 6.20: Comparison of experimental data @ 8.1 K and simulation (C_{qcc}=180 kHz, η=0.07, LLB=6.5kHz, GLB=2.5 kHz)

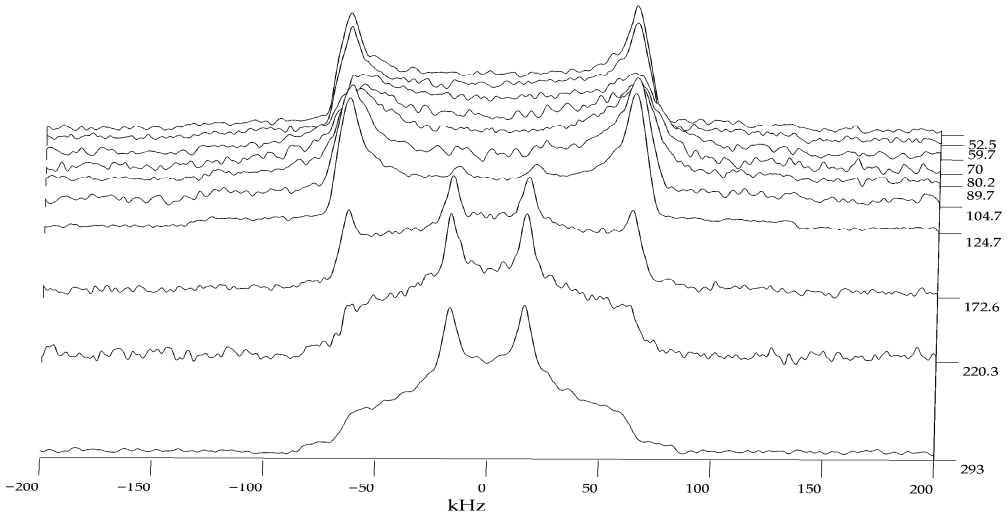

Figure 6.21: ^{2}H spectra as function of Temperature in K

- Is a mixed mechanism - between, 2-fold, 3-fold and 6-fold rotation possible?

- In which solid state is the material we are measuring?

In order to be able to answer these question we returned to the measured sample and performed Synchrotron[‖] XRD- measurements. They were showing a non homogeneous solid state of the powder we measured in the SSNMR experiments (mix of polymorphys). From the results we

[‖]at the PSI in Villigen, Switzerland

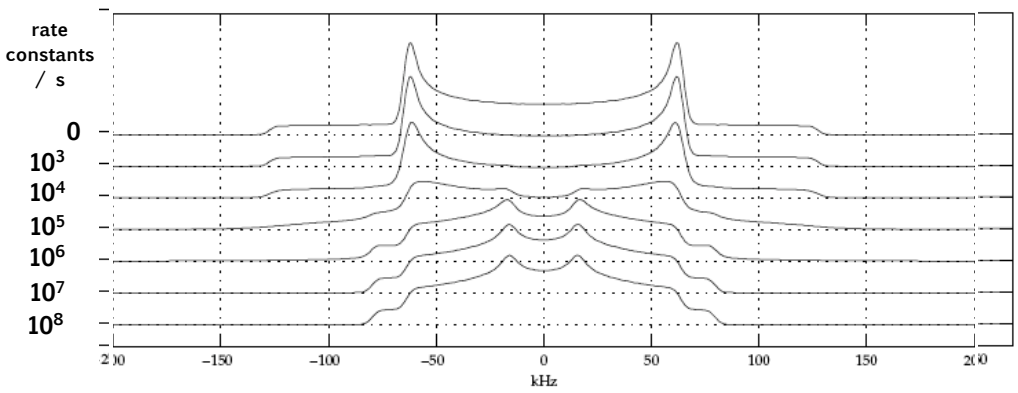

Figure 6.22: Simulated ^{2}H spectra for a 2-fold rotation at a given rate constant

obtained from these measurements we concluded, that we indeed have mixed dynamic processes- a very fast rotation part and a slower rotation part which influence the spectra such that a clear number for the rotation barrier can not be given. The fast rotation is coming from the solid material crystallized in cubic symmetry whereas the slower part comes from the material crystallized in monoclinic and orthorhombic geometry. This mix of polymorphs made the interpretation more difficult and therefore attempts to crystallize the sample in a controlled fashion were undertaken. First of all seeding of the crystallization was tried and also only crystallization in CH_2Cl_2 and this successfully led to cubic powder, which will be measured in the near future.

6.3.1 Conclusion ^{2}H SSNMR studies

The measured dynamics was in good agreement with the ADP studies and DFT studies for the fast rotation part. But, the obtained spectra revealed also a slower rotation part. Which is a problem of polymorphs. The XRD difracogram of the sample was only measured after the ^{2}H SSNMR experiments and therefore the presence of different polymorphs was only realized after the measurements. To be more precise, the single crystal with monoclinic point group symmetry was obtained during these measurements and until then, the presence of different polymorphs

with different dynamic behaviors was not considered. Nonetheless, the ^{2}H SSNMR studies show a fast dynamic behavior and confirmed the previous dynamic results.

6.4 XRD Diffractograms

In order to understand the solid state structure of the measured sample XRD.[153] diffractograms were recorded on the synchrotron at the PSI clearly showed a mix of solid state structures as summarized in Table. 6.10). For clarity only the peak positions as a function of unit cell dimensions of the three found point group symmetries are indicated.

In Fig. 6.23 the measured XRD diffractogram recorded in November 2009, August 2010, and November 2010 are depicted. The diffractograms simulated from the obtained single crystal X-Ray measurements are shown in Fig. 6.24, 6.25, and 6.26.

Table 6.10: The 7 crystal systems.[154]

Entry	Symmetry	reference system	Peak position as a function of unit cell dimensions
1	cubic	a=b=c, α=β=γ=90°	$\frac{1}{d^2} = \frac{h^2+k^2+l^2}{a^2}$
2	tetragonal	a=b≠c, α=β=γ=90°	
3	orthorombic	a≠b≠c, α=β=γ=90°	$\frac{1}{d^2} = \frac{h^2}{a^2} + \frac{k^2}{b^2} + \frac{l^2}{c^2}$
4	hexagonal	a=b≠c, α=β=90°, γ=120°	
5	rhombohedral	a=b=c, α=β=γ≠90°	
6	monoclinic	a≠b≠c, α=β= 90°≠γ	$\frac{1}{d^2} = \frac{h^2}{a^2\sin^2\beta} + \frac{k^2}{b^2} + \frac{l^2}{c^2\sin^2\beta} + \frac{2hl\cos\beta}{ac\sin^2\beta}$
7	triclinic	a≠b≠c, $\alpha \neq \beta \neq \gamma$	

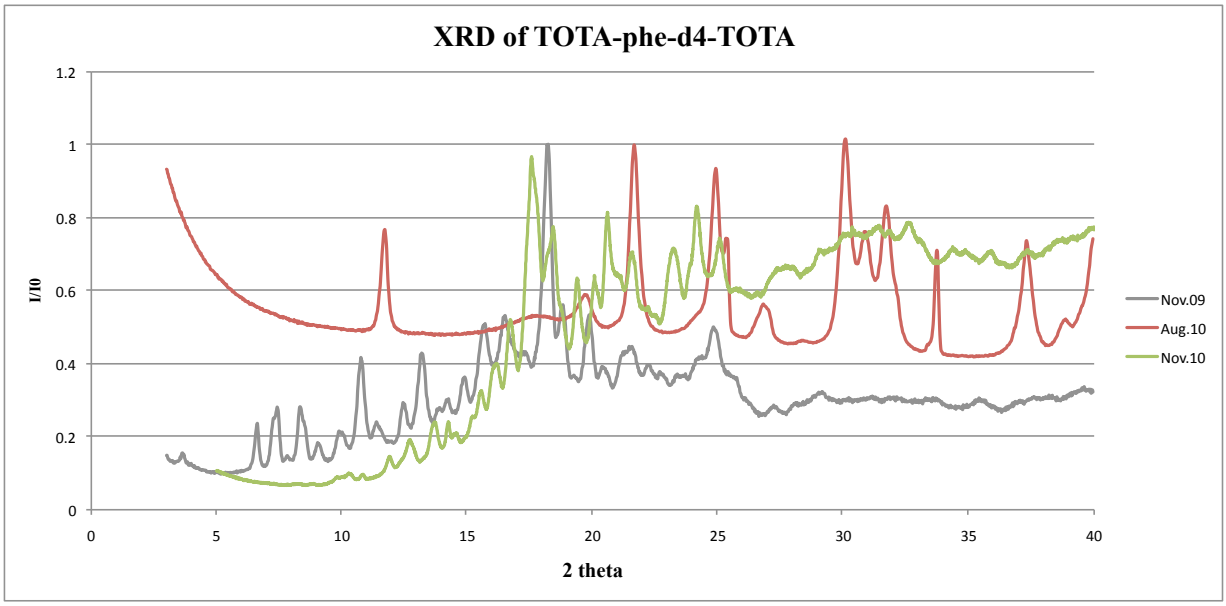

Figure 6.23: XRD diffractogram of the samples measured by SSNMR. The sample in Nov. 09 was measured after SSNMR experiments, whereas the sample in Aug. 2010 was measured before SSNMR studies and the sample in Nov. 2010 after.

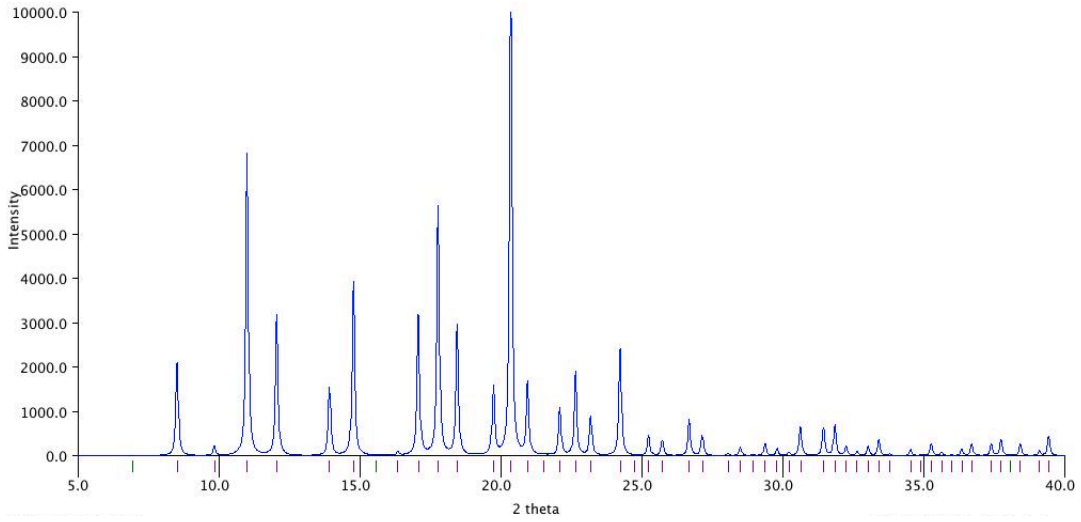

Figure 6.24: Simulated XRD from X-Ray data of a cubic crystal at 298 K, λ (Cu K_a=1.5418)

The diffractogram recorded in November 2009 looks completely different from the one recorded in August 2010, it showed a mixture of three polymorphs. Most of the powder was monoclinic, some of it cubic and traces of the orthorhombic polymorph were found as well. In

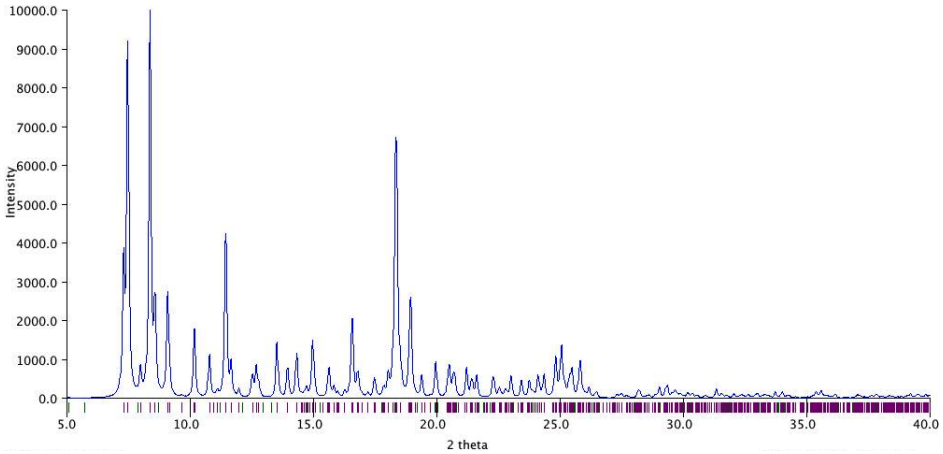

Figure 6.25: Simulated XRD from X-Ray data of a monoclinic crystal at 300 K, λ (Cu K_a=1.5418)

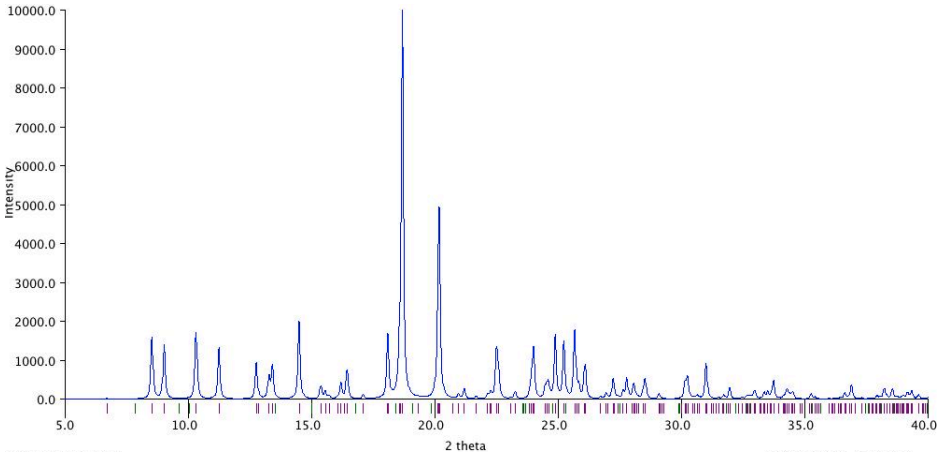

Figure 6.26: Simulated XRD from X-Ray data of a cubic crystal at 298 K, λ (Cu K_a=1.5418)

the sample recorded in August 2010 most the diffractogram is no conclusive, a preferred orientation effect might be the reason for the pattern found or a forth polymorph might cause the unknown pattern in the diffractogram. The diffractogram of the sample recorded in November 2010, which is the same sample as the one recorded in August 2010 but after SSNMR experiment, shows a change in the solid structure. This observation indicates a possibility of a change in the solid state structure during the SSNMR experiment and might be caused by our SSNMR

experiment design. In the two SSNMR experiments undertaken the first experiment was taken at 8 K and this might lead to a polymorph transition.

6.5 Conclusion XRD studies

The finings of the XRD studies supported the findings in the ^{2}H SSNMR studies, the mixed dynamic process of very fast and slower rotation can be explained by different packing in the polymorphs. In the monoclinic structure it was observed that the disorder of the phenyl ring is small and that the ellipsoids do not change as much as in the cubic structure. Therefore a ADP treatment was not achievable, the same hold for the orthorhombic structure. Furthermore the ^{2}H SSNMR experiments design seems to have been unlucky chosen. The sample measured 2010 shows that there is a polymorph change during the experiment. The XRD diffractogram before the SSNMR experiments looks different than after (Fig. 6.23). Furthermore the XRD diffractograms measured after the SSNME experiments (Nov. 2009 and Nov. 2010) look similar, which might be a indication for the same process happening.

Chapter 7

Conclusion & Outlook

The presented thesis was based on a design principle, which is based on the transmission of the molecular structure to other fundamental properties; in this case, the dynamic properties which are derived from a combination of combined building blocks with different momentum of inertia. Furthermore, this investigation of the dynamics has relied on a range of techniques that include current organic synthetic methodology, variable tempertaure X-Ray crystallography, DFT calculations and solid state NMR spectroscopy. This thesis reports on an extensive investigation on the synthesis of a set of different rod rotors with trioxatricornan or *tert*-butyltrioxatricornan caps. The experimental realization of a corresponding compounds required to explore suitable routes of synthesis including crystallization and optimizations. A series of unique trioxatricornan rod rotors have been prepared and in the case of the above described phenyl linked molecular rod rotor extensive molecular dynamics studies were undertaken: ADP studies of three single crystal VT data sets, leading to the same result, a phenyl rotation barrier of 0.2-0.4 kcal/mol, then DFT studies were performed confirming the low rotation barrier with values of 0.32 and 0.6 kcal/mol depending on the geometry of the trioxatricornan ring, and last but not least solid state NMR studies confirming the very fast rotation, but also showing that in some polymorphs rotation

might be hindered. The presence of different crystal packings was a draw back and prevented an optimal conclusion. Ongoing studies are the growing of a cubic powder for re-measurements of the solid state NMR studies. A first try on the cubic powder was not successful, the measurements were started at 8K and this led to a change in the polymorphs and therefor another batch of cubic sample has to be prepared before another experiment is performed. Nonetheless, in this project we could present a system with a nearly free rotation and a closer look in the other synthesized systems might be promising, especially since the technology is now established. The multiplicity of the barrier and the difference in momentum in inertia seem to be in favor of having a nearly free rotation of the rotator part in our molecular rod rotor design.

Chapter 8

Experimental

8.1 Materials and Methods

Martin's salt was prepared by using the reported protocol. Unless otherwise noted, all reactions were carried out under nitrogen and pro analysi grade solvents were used. Anhydrous THF was supplied from an Mbraun solvent purification system. For work-up and purification, distilled solvents of technical grade were used. Glassware were dried at 150 $^{\circ}C$ for at least 24 hours and allowed to cool under high vacuum. Deuterated solvents were purchased from Cambridge Isotope Laboratory (Andover, MA). NMR spectra were recorded on a Bruker 400 and 500MHz spectrometers. The ^{1}H NMR and ^{13}C NMR chemical shifts are reported relative to residual solvent signals. X-Ray diffraction experiments using synchrotron radiation were performed at the Paul Scherrer Institute in Villigen, Switzerland. X-Ray structure analyses were carried out by the X-Ray Crystallography Facility. Infrared spectra were recorded on a JASCO FT/IR-4100 spectrophotometer. Mass spectra were performed by the MS Laboratory of the Organic Chemistry Institute of the University of Zurich (HR-ESI). Analytical thin-layer chromatography was performed with Macherey-NagelPOLYGRAM SIL N-HR/UV254 or ALOX N/UV254. Flash

silica gel column chromatography was performed with Merck silica gel 60 (particle size 0.040-0.063 mm). Melting points were recorded on a Tecon Series 150 melting point apparatus.

8.1.1 Single Crystal X-ray Diffraction Methods

All single crystal X-ray measurements and variable temperature measurements were made by the X-Ray Crystallography Facility, Institute of Organic Chemistry, University of Zurich, on a Nonius KappaCCD area-detector diffractometer[155] using graphite-monochromated Mo Kα radiation (λ= 0.71073 Å) and an Oxford Cryosystems Cryostream 700 cooler. Data reduction was performed with HKL Denzo and Scalepack.[156] The intensities were corrected for Lorentz and polarization effects, but not for absorption. The structures were solved by direct methods using SIR92,[157] which revealed the positions of all non-hydrogen atoms. The non-hydrogen atoms were refined anisotropically. All of the H-atoms were placed in geometrically calculated positions and refined using a riding model where each H-atom was assigned a fixed isotropic displacement parameter with a value equal to 1.2U_{eq} of its parent atom (1.5U_{eq} for the methyl groups). Refinement of the structure was carried out on F^2 by using full-matrix least-squares procedures, which minimized the function $\sum w(F_0^2 - F_c^2)^2$. The weighting scheme was based on counting statistics and included a factor to down weight the intense reflections. Neutral atom scattering factors for non-hydrogen atoms were taken from Maslen, Fox and O'Keefe[158] and the scattering factors for H-atoms were taken from Stewart, Davidson and Simpson.[161] Anomalous dispersion effects were included in F_c;[162] the values for f ' and f " were those of Creagh and McAuley.The values of the mass attenuation coefficients are those of Creagh and Hubbel.[163, 164] All calculations were performed using the SHELXL97 program67 and figures were produced with ORTEPII.[164]

8.1.2 ^{2}H Solid-State NMR

Solid-state NMR experiments were performed on a Varian InfinityPlus! spectrometer, operating at a 1H frequency of 220 MHz, using a home-built static probehead. A standard quadrupolar echo sequence was used for all measurements with 90 degree pulses applied with typical rf amplitudes of 150 kHz. All data were processed with matNMR[165] .

8.1.3 Powder Diffraction Measurements

Powder diffraction measurements were carried out at the Paul Scherrer Institute/Swiss Light Source in Villigen, Switzerland. Samples were measured at the Materials Science X04SA beamline. The powder diffractometer was equipped with the second generation Mythen 2 microstrip detector covering an angular range of 120°.[166, 167] Samples were prepared, mounted and sealed in glass capillary tubes. Temperatures were maintained with Oxford Instruments LN2 Cryojet.

The PSI/SLS results of the refinement with silicon (NIST 640c) from measurements made in November 2010:

λ = 0.9999± 0.000025 Å

E = 12.385714 ± 0.000309 KeV

2θ-Offset = + 0.007458 ± 0.000017 degree

The PSI/SLS results of the refinement with silicon (NIST 640c) from measurements made in Augsut 2010:

λ = 0.886276± 0.000025 Å

E = 12.385714 ± 0.000309 KeV

2θ-Offset = + 0.007458 ± 0.000017 degree

8.2 Syntheses

8.2.1 Tris(2,6-dimethoxyphenyl)methanol[168]

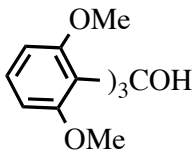

2

To a dry two necked 250mL round-bottom flask, equipped with N_2 inlet, stir bar, and septum, dry THF (75mL) and 1,3-dimethoxybenzen (13.1 mL, 0.1 mol) were added. The solution was cooled in an aceton/dry ice bath. Then, 2.5 M *n*-BuLi (40 mL, 0.1 mol) was transferred ,under an inert atmosphere, over 20min by a addition funnel. Stirring was continued for another 60min before the aceton/dry ice bath was removed. Afterwards the THF was distilled under inert atmosphere at 250 mbar at ambient temperature. To the residual lithium salt, 50 mL of dry toluene was added. The suspension was cooled to 0 °C before ethylchloroformate (3.25 mL, 0.033 mol) in 50 mL dry toluene was added slowly by a addition funnel. Upon addition of the first few drops of ethylchlorofromate the solution turns pale blue, then the color deepens until the addition is complete. The reaction mixture was then stirred overnight at ambient temperature and than quenched with 100 mL of water. The mixture was extracted with toluene (3 x 50 mL), the organic layers were washed with H_2O (30 mL) and brine (30 mL). The combined organic layers were dried over $MgSO_4$, filtered and evaporated. The desired compound was purified by

recrystallization in hexane to yield 6.14 g (71 %) of a white solid.

^{1}H NMR (500 MHz, $(CD_3)_2CO$), δ ($(CD_3)_2CO$) = 2.09): 7.32 (3H, t, J = 8 Hz, ArH), 6.49 (6H, d, J = 8 Hz, ArH), 3.41 (18H, s, OCH_3)

^{13}C {^{1}H} NMR (125.8 MHz, $(CD_3)_2CO$, δ $(CD_3)_2CO$) = 205.87 (C=O)): 159.69, 128.46, 106.92, 79.51, 56.61.

MS(ESI): m/z: M^+ 440.20($C_{25}H_{28}O_7$).

M.p.: 298-300 °*C*

M.p.: 158-161 °*C*

8.2.2 12c-ethoxy- 4,8,12- trioxa -4,8,12,12c- tetrahydrodibenzo [*cd,mn*] pyrenium tetrafluoroborate[123]

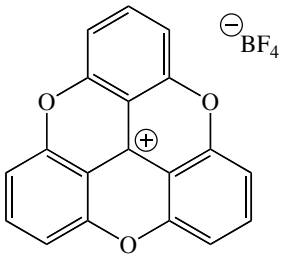

4

To a dry three necked 600 mL round-bottom flask, equipped with an over-head stirrer and two glass stoppers tris(2,6-dimethoxyphenyl)methanol (0.015 mol) and pyridinium hydrobromide (0.2 mol) were added. The glass stoppers were equipped with teflon sleeves before moundting them to the necks. All joints were sealed with teflon band. Then the round bottom flask containing the solid mixture was entered in a preheated silca oil bath (200°C) and the oil bath temperature was raised to 205 °C. The solid mixture melted and gave a deep purple suspension which tuned deep red after 5 hours stirring at 205°C. After further 2 hours of stirring the oil

bath was removed and the reaction was quenched with 100 mL water. The red solution was then left to cool to rambient temperature before it was filtered through a glass filter (pore size 4). The residue was suspended again in 100 mL water and filtered again. This procedure was repeated until the suspension was not turning orange anymore (6 times). The filtrate was then combined and 1 M NaOH was added until a basic pH was reached. At a basic pH the red solution tuned clear and a participate was was visible. This participate was filtered thought a glass filter (pore size 4) and dried over vacuum at 40 °C for 12 hours. Then a recrystallization in EtOH was performed to yield a beige powder (3.72 g, 0.011 mol, 75 %) which was dried over vacuum for 4 hours before it was dissolved in THF and $Et_2O \cdot HBF_4$ (0.012 M) was added and a bright yellow participate was yielded and filtered through a glass filter (pore size 4) to give bright yellow participant (3.73 g, 0.1 mol) in 100 % yield.

^{1}H NMR (400 MHz, $(CD_3)_2CO$), δ ($(CD_3)_2CO$) = 2.09): 8.65 (3H, t, J = 8.5 Hz, ArH), 7.99(6H, d, J = 8.5 Hz, ArH).

^{13}C {^{1}H} NMR (125.8 MHz, $(CD_3)_2CO$, δ $(CD_3)_2CO$): 153.77, 143.76, 112.66, 106.53, 68.46

MS (LC/MS (ESI)): m/z: M^+ 285.10 ($C_{19}H_{18}O_3$)

8.2.3 4-*tert*-butyl-2,6-dimethoxyphenol

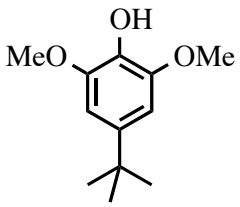

6

A solution of 2,6-dimethoxyphenol (77 g, 0.53 mol) in CH_3SO_3H (115 mL) was warmed under reflux conditions to 40 °C. *t*-BuOH (155 mL, 1.59 mol) was added slowly, keeping the temperature between 50-55 °C. After the addition, the temperature was kept at 50 °C for approximately 2 hours, then allowed to come to room temperature overnight. The reaction mixture was poured onto ca. 500 g ice, and then extracted with diethyl ether (3 x 100 mL). The organic phases were combined and washed with water (3 x 100 mL), saturated aqueous $NaHCO_3$ (2 x 250 mL), and again water (2 x 50 mL), dried with $MgSO_4$, and concentrated on the rotary evaporator to yield a yellow oil (ca. 200 ml) that was used directly in the next reaction.

^{1}H NMR (300 MHz, $CDCl_3$, δ ($CDCl_3$) = 7.26): 6.61 (2H, s, ArH), 5.37 (1H, s, OH), 3.89 (6H, s, OCH_3), 1.31 (9H, s, $C(CH_3)_3$).

MS (GC/MS): m/z: M^+ 210 ($C_{12}H_{18}O_3$)

8.2.4 Diethyl-4-*tert*-butyl-2,6-dimethoxyphenyl phosphate

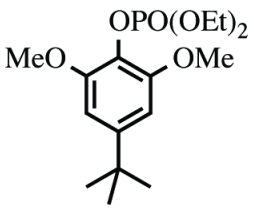

7

4-*tert*-butyl-2,6-dimethoxyphenol (0.53 mol) was dissolved in diethyl phosphite (82 mL, 0.64 mol) and CCl_4 (75 mL) at 0 °C under nitrogen atmosphere. After about 10 minutes of stirring, triethylamine (96 mL, 0.69 mol) was added gradually, maintaining the temperature below 10 °C. This addition was done over a period of 4 hours, and then the reaction mixture was allowed to come to room temperature and stirred overnight. The reaction mixture was concentrated, and

dissolved in a mixture of diethyl ether (400 mL) and water (400 mL). The aqueous and organic phases were separated, and the aqueous phase was washed again with diethyl ether (20 mL). The combined organic phases were washed with water (100 mL), 1M HCl (2 x 75 mL), water (100 mL), 4M NaOH (2 x 75 mL), and water (100 mL), dried with $MgSO_4$, and evaporated to dryness to give a yellow solid. Recrystallization from hexane yielded 133.8 g (72.6%) of off-white flakes.

^{1}H NMR (300 MHz, $CDCl_3$, δ ($CDCl_3$) = 7.26):6.59 (2H, s, ArH), 4.31 (4H, q, J = 7.10 Hz, $POCH_2CH_3$), 3.86 (6H, s, OCH_3), 1.38 (6H, td, J = 7.10 Hz, $POCH_2CH_3$), 1.30[9H, s, $C(CH_3)_3$].

^{13}C {^{1}H} NMR (75.5 MHz, CDCl3, δ ($CDCl_3$) = 77.0): 151.6, 148.8, 127.9, 103.0, 64.6, 56.5, 35.4, 31.8, 16.5.

MS (GC-MS): m/z: M+ 346 ($C_{16}H_{27}O_6P$).

M.p.: 73-76 °C

8.2.5 1-*tert*-butyl-2,5-dimethoxybenzen

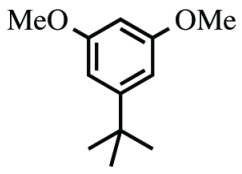

8

Diethyl-4-*tert*-butyl-2,6-dimethoxyphenyl phosphate (133.8 g, 0.4 mol) was dissolved in a 1:5 mixture of dry THF (50 mL) and dry diethyl ether (250 mL). Ammonia (ca. 500 mL) was condensed using a dry ice / ethanol bath, and lithium metal (4 g, 0.57 mol) was added slowly to prepare the dark blue solution. Diethyl-4-*tert*-butyl-2,6-dimethoxyphenyl phosphate in THF/Et_2O was then added drop wise over 2 hours. During this addition, additional lithium metal (2.4 g, 0.35 mol)

was added to the solution to maintain its dark blue colour. After the completion of the addition, the reaction mixture was stirred for one hour, followed by slow quenching with saturated aqueous NH_4Cl (ca. 100 mL). The cooling bath was removed, and the reaction mixture was allowed to stir overnight at room temperature, allowing for the evaporation of the ammonia through the appropriate outflow apparatus. The reaction mixture was washed with diethyl ether (2 x 400 mL). The organic phase was then washed with water (100 mL), 2M NaOH (2 x 200 mL), and water (2 x 100 mL), followed by drying over K_2CO_3 and concentrated by rotary evaporation. The product was recrystallized from hexane yielding 67.3 g (88.9 %) of white crystals.

^{1}H NMR (300 MHz, $CDCl_3$, δ ($CDCl_3$) = 7.26): 6.54 (2H, d, J = 2.2 Hz), 6.31 (1H, t, J = 2.2 Hz), 3.80 (6H, s, OCH_3), 1.30 (9H, s,$C(CH_3)_3$)).

^{13}C {^{1}H} NMR (75.5 MHz, CDCl3, δ ($CDCl_3$) = 77.0): 160.5, 153.9, 104.1, 96.8, 55.2, 35.0, 31.3

MS (GC/MS): m/z: M^+ 194 ($C_{12}H_{18}O_2$)

M.p.: 49-51 °C

8.2.6 2-bromo-5-*tert*-butyl-1,3-dimethoxybenzene

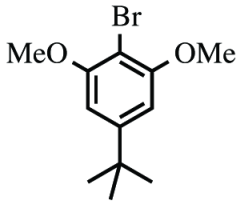

10

1-*tert*-butyl-2,5-dimethoxybenzen (67.3 g, 0.35 mol) was dissolved in 500 mL CCl_4 at 0 °C, and Br_2 (21 mL, 0.4 mol) in 110 mL CCl_4 was added drop wise over 2 hours to give a cloudy red solution. After addition, the reaction mixture was stirred for 1.5 hours at 0 °C. The product was

concentrated and recrystallized from hexane to yield 83.4 g (76%) of a crystalline white product.

^{1}H NMR (400 MHz, $CDCl_3$, δ ($CDCl_3$) = 7.26): 6.60 (2H, s, ArH), 3.91 (6H, s, OCH3), 1.33 (9H, s, $CH_3)_3$).

^{13}C {^{1}H} NMR (75.5 MHz, CDCl3, δ ($CDCl_3$) = 77.0): 154.9, 150.5, 100.7, 96.3, 54.7, 33.5, 29.6.

MS (GC/MS):m/z: M^+ 272 ($C_{12}H_{17}BrO_2$)

M.p.: 118-120 °*C*

8.2.7 tris(4-*tert*-butyl-2,6-dimethoxyphenyl)methanol[170]

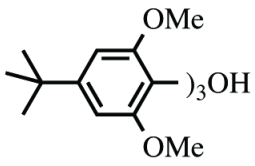

11

2-bromo-5-*tert*-butyl-1,3-dimethoxybenzene (8.33 g, 30.6 mmol) was added to a mixture of 50 mL dry toluene and 60 mL dry THF. ^{t}BuLi (36 mL, 61.2 mmol) was added slowly, maintaining the temperature below - 60 °C. After the addition, the reaction mixture was stirred for 1 hour at - 78 °C, followed by the drop wise addition of diethyl carbonate (1.25 mL, 10.2 mmol) in 15 mL of dry THF. The reaction mixture was then allowed to come to room temperature, generating a bright green solution, followed by reflux for 2 days. The transparent brown reaction mixture was then cooled to RT and quenched with 30 mL of technical grade ethanol. The reaction mixture was washed with 100 mL diethyl ether and then the organic phase was washed with water (100 mL). The aqueous layers were washed with diethyl ether (30 mL), and then the combined organic phases were washed once again with water, followed by drying over $MgSO_4$ and removal of the

solvent by rotary evaporation. Recrystallization from hexane gave a fine, white solid (4.49 g, 76 %).

^{1}H NMR (300 MHz, $CDCl_3$, δ ($CDCl_3$) = 7.26): 6.72 (1H, s, OH), 6.49 (6H, s, ArH), 3.39 (18H, s, OCH3), 1.27 (27H, s, $C(CH_3)_3$).

^{13}C {^{1}H} NMR (75.5 MHz, CDCl3, δ ($CDCl_3$) = 77.0): 158.2, 149.2, 125.9, 124.9, 104.2, 56.6, 34.6, 31.3.

M.p.: 176-178 °C

8.2.8 2,6,10-tri-*tert*-butyl-12c-ethoxy-4,8,12-trioxa-4,8,12,12c- tetrahydro dibenzo [cd,mn] pyrene

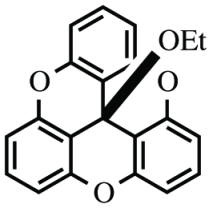

13

tris(4-*tert*-butyl-2,6-dimethoxyphenyl)methanol (4.49 g, 7.38 mmol) in water (300 mL) was treated with concentrated HCl (12 mL) and the blue solution was refluxed for 4 hours. The reaction mixture was filtered and the filter cake was washed several times with water until the crude off-white xanthon was obtained. After drying, the crude material (3.84 g, 7.02 mmol) was mixed with excess pyridine hydrochloride (12 g, 106 mol) and the round boittom flask was equipped with an overhead stirrer then the melt was stirred at 150 ąC for 4 hours. The reaction mixture changed colour from dark purple to deep red. The hot reaction mixture was quenched with water (50 mL). This solution was filtered (pore 4 glass filter), and the filter cake washed with water and water again. This procedure was repeated 5 times. The filtrates were combined

and treated with 2M NaOH until the solution was basic to litmus paper and a white precipitate appeared. The pasty precipitate was collected by filtration (pore 4 glass filter) and dissolved in technical grade ethanol under reflux. Upon cooling, the final product precipitated and was collected by filtration as a white powder (2.3 g, 66% yield).

^{1}H NMR (300 MHz, $CDCl_3$, δ ($CDCl_3$) = 7.26): 7.06 (6H, s, ArH), 3.13 (2H, q, OCH_2CH_3), 1.35 (27H, s, $C(CH_3)_3$), 0.92 (3H, q, OCH_2CH_3)

^{13}C {^{1}H} NMR (75.5 MHz, CDCl3, δ ($CDCl_3$) = 77.0): 154.0, 153.0, 125.9, 108.4, 106.9, 56.9, 35.3, 31.4, 15.3.

8.2.9 2,6,10-tri-*tert*-butyl-12c-ethoxy-4,8,12-trioxa-4,8,12,12c-tetrahydrodibenzo[cd,mn]pyrenium hexafluorophosphate

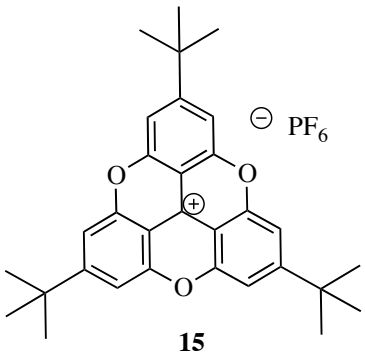

15

2,6,10-tri-tert-butyl-12c-ethoxy-4,8,12-trioxa-4,8,12,12c- tetrahydrodibenzo[cd,mn]pyrene (3.39) Aqueous 65% HPF6 (0.89 mL, 7.05 mmol) was added drop wise to a solution of 3.39 (3.51 g, 7.05 mmol) in diethyl ether (400 mL) at 0 ąC. The formation of a bright yellow precipitate was seen immediately. The reaction mixture was stirred at 0 ąC for 1 hour, filtered, washed with

cold diethyl ether, and dried under vacuum to give 4.0 g (95%) of the yellow product as a fine yellow powder.

^{1}H NMR (300 MHz, $CDCl_3$, δ ($CDCl_3$) = 7.26): 7.67 (6H, s, ArH), 1.50 (27H, s, $C(CH_3)_3$)

^{13}C {^{1}H} NMR (75.5 MHz, CDCl3, δ ($CDCl_3$) = 77.0): 169.7, 153.5, 142.3, 110.1, 103.8, 37.8, 31.5.

MS (ESI): M^+ 453.3 ($C_{31}H_{33}O_3$)

8.2.10 12c-((trimethylsilyl)ethynyl)-4,8,12-trioxa-4,8,12,12c- tetrahydro dibenzo [cd,mn] pyrene

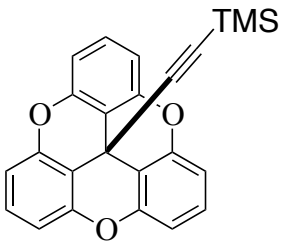

16a

An oven-dried 100 mL flask containing a Teflon stir bar and nitrogen atmosphere was charged with ethynyltrimethylsilane (1.2 mL, 8.75 mmol) and 20 mL dry THF. The solution was subsequently cooled to Ð 78 °C with a dry ice/acetone bath and ^{n}BuLi (3.6 mL, 9 mmol) was added drop wise with a disposable syringe. The solution was stirred for 45 minutes. Then, 12c-ethoxy-4,8,12-trioxa-4,8,12,12c-tetrahydrodibenzo[*cd*,*mn*]pyrene (1g, 2.7 mmol) were added slowly with a spatula. The resulting yellow suspension was allowed to stir for further 4 hours at -78 °C. Then the dry/ice acetone bath was removed and the reaction was quenched with 10 mL saturated aqueous NH_4Cl. The layers were separated and the aqueous layer washed three times with Et_2O. The organic layers were combined, dried over $MgSO_4$ and the solvent removed

by rotary evaporation. The desired product was purified by chromatography on silica gel (R_f = 0.3), with hexane as the eluent, to yield 875 mg (85%) of white powder.

^{1}H NMR (500 MHz, $CDCl_3$, δ (CD_2Cl_2) = 5.32): 7.32 (3H, t, J = 7.25 Hz, ArH), 6.99 (6H, d, J = 7.25 Hz, ArH, 0.01 [9H, s, $Si(CH_3)_3$]

^{13}C {^{1}H} NMR (125.8 MHz, CDCl3, δ (CD_2Cl_2) = 53.8): 152.6, 146.2, 132.3, 128.9, 122.2, 113.6, 111.6, 104.2, 94.5, 0.00.

MS (CG/MS): M^+ 378 ($C_{24}H_{18}O_3Si$)

M.p.: 298-300 °*C*

8.2.11 12c-(ethynyl)-4,8,12-trioxa-4,8,12,12c-tetrahydro dibenzo [cd,mn] pyrene

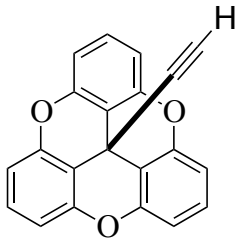

16b

To a solution of 12c-((trimethylsilyl)ethynyl)-4,8,12-trioxa-4,8,12,12c- tetrahydro dibenzo [cd,mn] pyrene (875 mg, 2.2 mmol) in 20 mL methanol / 20 mL CH_2Cl_2 was added potassium carbonate (1.5 g, 11.0 mmol) and the mixture was stirred at room temperature for 6 hours. Diethyl ether was added to the reaction mixture, which was then transferred to a separatory funnel. The organic phase was washed twice with water, and then dried over magnesium sulfate. The solvent was evaporated under reduced pressure to obtain a white powder which was used without further purification with a yield of 650 mg (95%)

^{1}H NMR (400 MHz, $CDCl_3$, δ ($CDCl_3$) = 7.26): δ= 7.32 (3H, t, J = 8.25 Hz, ArH), 7.01 (6H,

d, J = 8.5 Hz, ArH), 2.46 [1H, s, sp^1(H)]

^{13}C {^{1}H} NMR (100.6 MHz, CDCl3, δ ($CDCl_3$) = 77.0): δ= 153.1, 147.2, 133.2, 129.4, 126.2, 121.6, 114.1, 112.2, 83.4, 77.9.

MS (GC/MS): M^+ 310 ($C_{24}H_{10}O_3$)

M.p.: $>$ 300 °*C*

8.2.12 12c-(4-iodophenyl)-4,8,12-trioxa-4,8,12,12c- tetrahydro dibenzo [cd,mn] pyrene

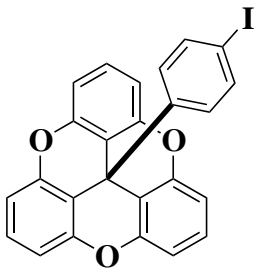

17a

An oven-dried 100 mL flask containing a Teflon stir bar and nitrogen atmosphere was charged with 1, 4 diiodobenzen (355 mg, 1.08 mmol) and 20 mL dry THF. The solution was subsequently cooled to Ð 78 °C with a dry ice/acetone bath and ^{n}BuLi (0.45 mL, 0.72 mmol) was added drop wise with a disposable syringe. The solution was stirred for 45 minutes. Then, 12c-ethoxy-4,8,12-trioxa-4,8,12,12c-tetrahydrodibenzo[*cd,mn*]pyrene (162 mg, 0.44 mmol) were added slowly with a spatula. After 2 hours of stirring at -78 °*C*, the solution was allowed to warm to 0 °*C* with an ice bath and the reaction was quenched with 10 mL saturated aqueous NH_4Cl and diethyl ether (10 mL) was added. The aqueous layer was collected and then washed again with diethyl ether (10 mL). The organic layers were then collected, dried over $MgSO_4$, and concentrated to give a white powder. The desired product was purified by column chromatography on silica gel (R_f = 0.2) with hexane as the eluent, and it was collected and concentrated (203 mg) in 94% yield

^{1}H NMR (400 MHz, CD_2Cl_2, δ (CD_2Cl_2) = 5.36): 7.54 (2H, d, J = 8 Hz, ArH), 7.41 (3H, t, J = 8 Hz, ArH), 7.05 (6H, d, J = 8.5 Hz, ArH), 6.83 (2H, d, J = 8 Hz, ArH)

^{13}C {^{1}H} NMR (100.6 MHz, CDCl3, δ ($CDCl_3$) = 77.0): 152.5, 145.9, 137.9, 128.9, 125.3, 113.5, 111.7

MS (ESI): : $(M+Na)^+$ = 488.277 ($C_{25}H_{12}D_4INaO_3^+$)

M.p.: 287-288 °*C*

8.2.13 12c-(4-bromophenyl)-4,8,12-trioxa-4,8,12,12c- tetrahydro dibenzo [cd,mn] pyrene

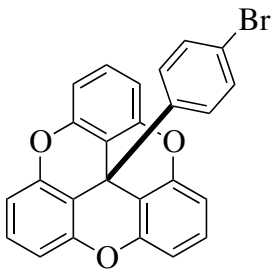

18 a

An oven-dried 100 mL flask containing a Teflon stir bar and nitrogen atmosphere was charged with 1, 4 bromoidobenzene (1.22 g, 4.32 mmol) and 20 mL dry THF. The solution was subsequently cooled to Ð 78 °C with a dry ice/acetone bath and ^{n}BuLi (2.1 mL, 5.2 mmol) was added drop wise with a disposable syringe. The solution was stirred for 45 minutes. Then, 12c-ethoxy-4,8,12-trioxa-4,8,12,12c-tetrahydrodibenzo[*cd*,*mn*]pyrene (1g, 2.7 mmol) were added slowly with a spatula. After 2 hours of stirring at -78 °*C*, the solution was allowed to warm to 0 °*C* with an ice bath and the reaction was quenched with 10 mL saturated aqueous NH_4Cl and diethyl ether (10 mL) was added. The aqueous layer was collected and then washed again with diethyl ether (10 mL). The organic layers were then collected, dried over $MgSO_4$, and concentrated to give a white powder. The desired product was purified by column chromatography on silica gel (R_f =

0.2) with hexane as the eluent, and it was collected and concentrated (1.13 g) in 95% yield

^{1}H NMR (300 MHz, $CDCl_3$, δ ($CDCl_3$) = 7.26): δ= 7.42 (2H, d, J = 6.6 Hz, ArH), 7.41 (3H, t, J = 8.1 Hz, ArH), 7.01 (6H, d, J = 8.1 Hz, ArH), 6.96 (2H, d, J = 6.9 Hz, ArH)

^{13}C {^{1}H} NMR (100.6 MHz, CDCl3, δ ($CDCl_3$) = 77.0): 153.1, 145.8, 130.2, 126.2, 128.2, 114.2, 112.6

MS (ESI): : $(M+Na)^+$ = 462.993 ($C_{25}H_{12}D_4BrNaO_3^+$)

M.p.: 289-291 °*C*

8.2.14 2,6,10-tri-*tert*-butyl-12c-(4-iodophenyl)-4,8,12-trioxa-4,8,12,12c-tetrahydrodibenzo[cd,mn]pyrene

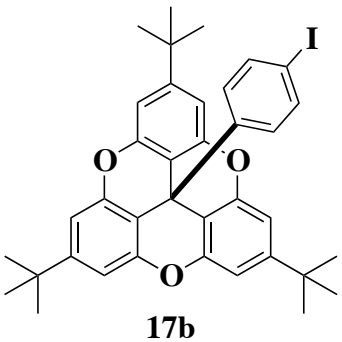

17b

An oven-dried 100 mL flask containing a Teflon stir bar and nitrogen atmosphere was charged with 1, 4 diiodobenzene (993 mg, 3 mmol) and 20 mL dry THF. The solution was subsequently cooled to -78 °C with a dry ice/acetone bath and ^{n}BuLi (7.75 mL, 3.1 mmol) was added drop wise with a disposable syringe. The solution was stirred for 45 minutes. Then, 2,6,10-tri-*tert*-butyl-12c-ethoxy-4,8,12-trioxa-4,8,12,12c-tetrahydrodibenzo[*cd,mn*]pyrene (600 mg, 1 mmol) were added slowly with a spatula. After 2 hours of stirring at -78 °*C*, the solution was allowed to warm to 0 °*C* with an ice bath and the reaction was quenched with 10 mL saturated aqueous

NH_4Cl and diethyl ether (10 mL) was added. The aqueous layer was collected and then washed again with diethyl ether (10 mL). The organic layers were then collected, dried over $MgSO_4$, and concentrated to give a white powder. The desired product was purified by column chromatography on silica gel (R_f = 0.4) with hexane as the eluent, and it was collected and concentrated (578 mg) in 94% yield.

^{1}H NMR (400 MHz, $CDCl_3$, δ ($CDCl_3$) = 7.26): 7.49 (2H, t, ArH, J = 8.0 Hz), 7.00 (6H, s, ArH), 6.82 (2H, d, ArH, J = 8.0 Hz), 1.33 (27H, s, $C(CH._3)_3$).

^{13}C {^{1}H} NMR (100.6 MHz, CDCl3, δ ($CDCl_3$) = 77.0): 152.5, 152.1, 146.2, 137.8, 128.0, 120.9, 111.3, 108.9, 35.2, 31.4, 22.6.

MS (ESI): $(M+Na)^+$ 679.2 ($C_{37}H_{37}IO_3Na^+$).

M.p.: 275-277 °*C*

8.2.15 2,6,10-tri-*tert*-butyl-12c-(4-bromophenyl)-4,8,12-trioxa-4,8,12,12c-tetrahydrodibenzo[cd,mn]pyrene

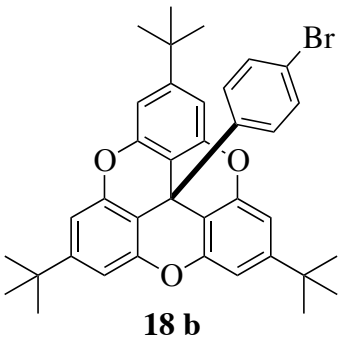

18 b

An oven-dried 100 mL flask containing a Teflon stir bar and nitrogen atmosphere was charged with 1, 4 dibromobenzene (290 mg, 1.23 mmol) and 20 mL dry THF. The solution was subsequently cooled to -78 °C with a dry ice/acetone bath and ^{n}BuLi (3.20 mL, 1.28 mmol) was added

drop wise with a disposable syringe. The solution was stirred for 45 minutes. Then, 2,6,10-tri-*tert*-butyl-12c-ethoxy-4,8,12-trioxa-4,8,12,12c-tetrahydrodibenzo[*cd*,*mn*]pyrene (240 mg, 0.4 mmol) were added slowly with a spatula. After 2 hours of stirring at -78 °*C*, the solution was allowed to warm to 0 °*C* with an ice bath and the reaction was quenched with 10 mL saturated aqueous NH_4Cl and diethyl ether (10 mL) was added. The aqueous layer was collected and then washed again with diethyl ether (10 mL). The organic layers were then collected, dried over $MgSO_4$, and concentrated to give a white powder. The desired product was purified by column chromatography on silica gel ($R_f = 0.4$) with hexane as the eluent, and it was collected and concentrated (220 mg) in 88% yield.

^{1}H NMR (300 MHz, $CDCl_3$, δ ($CDCl_3$) = 7.26): 7.28 (2H, t, ArH, J = 8.0 Hz), 6.95 (2H, d, ArH, J = 8.0 Hz), 7.00 (6H, s, ArH), 1.33 [27H, s, $C(CH_3)_3$)];.

^{13}C {^{1}H} NMR (100.6 MHz, CDCl3, δ ($CDCl_3$) = 77.0): 153.1, 152.5, 145.4, 131.8, 127.7, 120.9, 111.4, 108.9, 35.2, 31.4, 15.3.

MS (ESI): $(M+H)^+$ 609.4 ($C_{37}H_{37}BrO_3^+$).

M.p.: 275-277 °*C*

8.2.16 2,6,10-tri-*tert*-butyl-12c-(4-bromophenyl-d_4)-4,8,12-trioxa-4,8,12,12c- tetrahydrodibenzo [cd,mn] pyrene

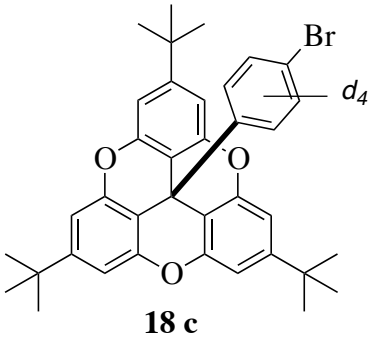

18 c

To a dry two necked 50mL round-bottom flask, equipped with N_2 inlet, stir bar, and septum, dry THF (20mL) and 1,4-dibromobenzen-d_4 (974 mg, 4.07mmol) were added. The solution was cooled in an aceton/dry ice bath. *n*-BuLi (1.64 mL, 4.10 mmol) was added drop wise with a disposable syringe. The solution was stirred for 45 minutes. Then, 2,6,10-tri-*tert*-butyl-12c-ethoxy-4,8,12-trioxa-4,8,12,12c-tetrahydrodibenzo[*cd*,*mn*]pyrene (1.16 g, 1.94 mmol) was than added slowly by spatula, and stirring was continued for another hour at -78°*C*, then the cooling bath was removed and the stirring continued another 4 hours at ambient temperature. H_2O (5mL) and NH_4Cl (sat. solution, 5 mL) were then added, and the THF was removed under reduced pressure. The mixture was extracted with Et_2O (3 x 20mL), the organic layers were washed with H_2O (30mL) and brine (30mL). The combined organic layers were dried over $MgSO_4$, filtered and evaporated. The desired compound was purified by column chromatography on silica gel (R_f=0.38) with 9:1 hexanes: methylenchloride as the eluent to yield 699 mg (59 %) of a white solid.

^{1}H NMR (400 MHz, $CDCl_3$, δ ($CDCl_3$) = 7.26): 7.00 (6H, s, ArH), 1.33 (27H, s, $C(CH_3)_3$).

^{13}C {^{1}H} NMR (100.6 MHz, CDCl3, δ ($CDCl_3$) = 77.0): 153.4, 153.2, 132.0 (2D, t, J (13C,D)= 25 Hz), 127.8 (2D, t, J (13C,D)= 25 Hz), 112.1, 111.4, 108.9, 35.1, 31.9, 22.6, 14.1.

MS (HR-ESI): : $(M+Na)^+$ = 637.20567 ($C_{37}H_{33}D_4BrNaO_3^+$)

M.p.: 275-277 °*C*

8.2.17 12c-(4-trimethylsilylethynylphenyl)-4,8,12-trioxa-4,8,12,12c- tetrahydrodibenzo[cd,mn]pyrene

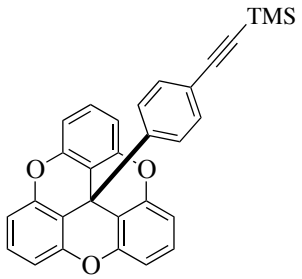

30a

A degassed solution of 12c-(4-bromophenyl)-4,8,12-trioxa-4,8,12,12c- tetrahydro dibenzo [cd,mn] pyrene (70 mg, 0.16 mmol), ethynyltrimethylsilane (0.03 mL, 0.20 mmol), copper iodide (2 mg, 0.01 mmol), and palladium tetrakis(triphenylphosphine) (9 mg, 0.008 mmol) in 10 mL triethylamine was heated in a sealed flask to 75 $^{\circ}C$ and stirred at this temperature for 30 hours. The reaction mixture was allowed to cool to room temperature, and then diluted with methylene chloride and filtered thought a silica plug. Then, the reaction mixture was transferred to a separatory funnel, washed twice with water, and dried over magnesium sulfate. The solvent was evaporated under reduced pressure. The desired product was purified by column chromatography on silica gel (R_f = 0.2) with hexane as the eluent to yield 68 mg (93%) of a white powder.

^{1}H NMR (400 MHz, CD_2Cl_2, δ (CD_2Cl_2) = 5.36): 7.31 (3H, t, ArH, J = 8.0 Hz), 7.24 (2H, t, ArH, J = 8.0 Hz), 7.01 (6H, t, ArH, J = 8.0 Hz), 6.89 (2H, t, ArH, J = 8.0 Hz), 0.18 (9H, s, $Si(CH_3)_3$).

^{13}C {^{1}H} NMR (100.6 MHz, CDCl3, δ (CD_2Cl_2) = 53.8): 153.0, 147.7, 133.5, 129.4, 126.2, 120.9, 112.2, 81.6, 74.3, 63.4, 30.2, 0.00

MS (ESI): : $(M+Na)^+ = 481.571$ ($C_{30}H_{22}NaO_3Si^+$)

8.2.18 12c-(4-ethynylphenyl)-4,8,12-trioxa-4,8,12,12c- tetrahydrodibenzo[cd,mn]pyrene

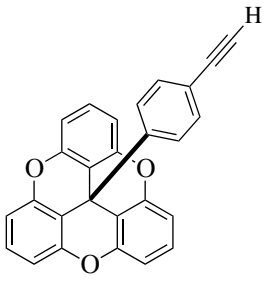

30b

To a solution of 12c- (4-trimethylsilylethynylphenyl) -4,8,12 -trioxa-4,8,12,12c- tetrahydrodibenzo [cd,mn] pyrene (68 mg, 0.15 mmol) in 5 mL methanol / 5 mL THF was added potassium carbonate (260 mg, 1.5 mmol) and the mixture was stirred at room temperature for 6 hours. Diethyl ether was added to the reaction mixture, which was then transferred to a separatory funnel. The organic phase was washed twice with water, and then dried over magnesium sulfate. The solvent was evaporated under reduced pressure. The solvent was evaporated under reduced pressure to obtain a baige powder which was used without further purification with a yield of 54 mg (95%).

^{1}H NMR (400 MHz, CD_2Cl_2, δ (CD_2Cl_2) = 5.36): 7.32 (3H, t, ArH, J = 8.0 Hz), 7.22 (2H, t, ArH, J = 8.0 Hz), 7.01 (6H, t, ArH, J = 8.0 Hz), 6.89 (2H, t, ArH, J = 8.0 Hz), 2.48 ([1H, s, sp^1(H)]).

^{13}C {^{1}H} NMR (100.6 MHz, CD_2Cl_2, δ (CD_2Cl_2) = 53.8): 153.1, 153.0, 147.7, 133.5, 126.3, 121.3, 114.2, 112.2, 82.0, 65.5, 33.4, 30.0.

MS (ESI): : $(M+Na)^+ = 409.2$($C_{30}H_{22}NaO_3Si^+$)

M.p.: $> 300\ ^{\circ}C$

8.2.19 Bis [4,8,12-trioxa-4,8,12,12c- tetrahydrodibenzo [cd,mn] pyrene] ethynylene

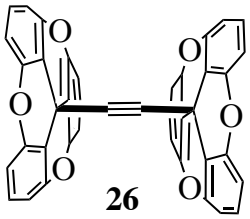

26

An oven-dried 100 mL flask containing a Teflon stir bar and nitrogen atmosphere was charged with 12c-(ethynyl)-4,8,12-trioxa-4,8,12,12c-tetrahydrodibenzo [cd,mn] pyrene (100 mg, 0.33 mmol) and 10 mL dry THF. The solution was subsequently cooled to -78 °C with a dry ice/acetone bath and ^{n}BuLi (0.16 mL, 0.39 mmol) was added drop wise with a disposable syringe. The solution was stirred for 45 minutes. Then,12c-ethoxy-4,8,12-trioxa-4,8,12,12c-tetrahydrodibenzo[*cd,mn*]pyrene (116 mg, 0.37 mmol) were added slowly with a spatula. After 2 hours of stirring at -78 $^{\circ}C$, the solution was allowed to warm to 0 $^{\circ}C$ with an ice bath and the reaction was quenched with 10 mL saturated aqueous NH_4Cl and diethyl ether (10 mL) was added. The aqueous layer was collected and then washed again with diethyl ether (10 mL). The organic layers were then collected, dried over $MgSO_4$, and concentrated to give a white powder. The desired product was purified by column chromatography on silica gel (R_f = 0.2) with hexane/ CH_2Cl_2 as the eluent, and it was collected and concentrated (111mg) in 58% yield.

^{1}H NMR (400 MHz, CD_2Cl_2, δ (CD_2Cl_2) = 5.36) = 7.26): δ= 7.35 (6H, t, J = 8 Hz, ArH), 6.92 (12H, d, J = 8Hz, ArH).

^{13}C {^{1}H} NMR (100.6 MHz, CD_2Cl_2, δ (CD_2Cl_2) = 53.8): δ= 153.8, 152.2, 110.8, 110.0, 85.4, 33.9.

MS (ESI): $(M+Na)^+ = 617.1$ ($C_{40}H_{18}NaO_6^+$)

M.p.: > 300 °*C*

8.2.20 Bis [4,8,12-trioxa-4,8,12,12c- tetrahydrodibenzo [cd,mn] pyrene] phenylene

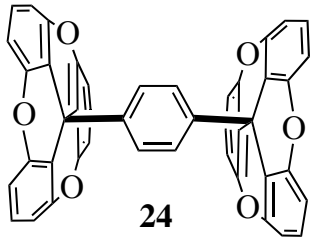

24

An oven-dried 100 mL flask containing a Teflon stir bar and nitrogen atmosphere was charged with 12c-(bromophenylene)-4,8,12-trioxa-4,8,12,12c-tetrahydrodibenzo [cd,mn] pyrene (150 mg, 0.34 mmol) and 10 mL dry THF. The solution was subsequently cooled to -78 °C with a dry ice/acetone bath and ^{t}BuLi (0.43 mL, 0.68 mmol) was added drop wise with a disposable syringe. The solution was stirred for 45 minutes. Then, 12c-ethoxy-4,8,12-trioxa-4,8,12,12c-tetrahydrodibenzo[*cd*,*mn*]pyrene (146 mg, 0.34 mmol) were added slowly with a spatula. After 2 hours of stirring at -78 °*C*, the solution was allowed to warm to 0 °*C* with an ice bath and the reaction was quenched with 10 mL saturated aqueous NH_4Cl and diethyl ether (10 mL) was added. The aqueous layer was collected and then washed again with diethyl ether (10 mL). The organic layers were then collected, dried over $MgSO_4$, and concentrated to give a white powder. The desired product was purified by column chromatography on silica gel ($R_f = 0.2$) with hexane/ CH_2Cl_2/toluene as the eluent, and it was collected and concentrated (111mg) in 58% yield.

^{1}H NMR (400 MHz, $CDCl_3$, δ ($CDCl_3$) = 7.26): 7.19 (6H, t, J = 8 Hz, ArH), 6.81 (4H, s), 6.88 (12H, d, J = 8Hz, ArH).

^{13}C {^{1}H} NMR (100.6 MHz, CDCl3, δ ($CDCl_3$) = 77.0): 153.7, 152.5, 129.6, 128.7, 110.4,

108.7, 29.7

MS (ESI): $(M+Na)^+ = 669.6$ ($C_{44}H_{22}NaO_6{}^+$)

M.p.: > 300 °*C*

8.2.21 Bis [2,6,10-tri-*tert*-butyl-4,8,12-trioxa-4,8,12,12c- tetrahydrodibenzo [cd,mn] pyrene] phenylene-d_4

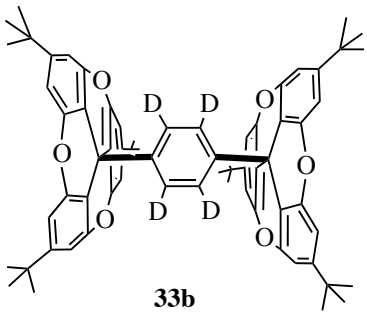

33b

An oven-dried 100 mL flask containing a Teflon stir bar and nitrogen atmosphere was charged with 2,6,10-tri-*tert*-butyl-12c-(bromophenylene-d_4)-4,8,12-trioxa-4,8,12,12c-tetrahydrodibenzo [cd,mn] pyrene (657 mg, 1.07 mmol) and 10 mL dry THF. The solution was subsequently cooled to -78 °C with a dry ice/acetone bath and ^{t}BuLi (1.34 mL, 2.14 mmol) was added drop wise with a disposable syringe. The solution was stirred for 45 minutes. Then, 2,6,10-tri-*tert*-butyl-12c-ethoxy-4,8,12-trioxa-4,8,12,12c-tetrahydrodibenzo[*cd*,*mn*]pyrene (704 mg, 1.17 mmol) were added slowly with a spatula. After 2 hours of stirring at -78 °*C*, the solution was allowed to warm to 0 °*C* with an ice bath and the reaction was quenched with 10 mL saturated aqueous NH_4Cl and diethyl ether (10 mL) was added. The aqueous layer was collected and then washed again with diethyl ether (10 mL). The organic layers were then collected, dried over $MgSO_4$, and concentrated to give a white powder. The desired product was purified by column chromatography on silica gel ($R_f = 0.2$) with hexane/ CH_2Cl_2/toluene as the eluent, and it was collected and concentrated (829mg) in 78% yield.

^{1}H NMR (500 MHz, $CDCl_3$, δ ($CDCl_3$) = 7.26): 7.01 (6H, s), 1.3 (27H, s).

^{13}C {^{1}H} NMR (125.75 MHz, CDCl3, δ ($CDCl_3$, d_1= 8 s) = 77.0): 153.2, 152.0, 145.0, 126.4 (2D, t, J (13C,D)= 25 Hz), 112.3, 109.4, 61.0, 53,9, 35.6, 32.8.

MS (ESI): $(M+Na)^+$ =1009.53157 ($C_{68}H_{66}D_4NaO_6^+$)

IR: 2960.2, 2905.24, 2868.59, 2364.3, 2277.52, 2163.74, 2050.92, 1981.5, 1715.37, 1650.77, 1620.88, 1602.56, 1482.99, 1460.81, 1447.31, 1426.1, 1395.25, 1363.43, 1293.04, 1234.22, 1202.4, 1099.23, 1038.48, 1024.98, 958.448, 921.807, 907.344, 851.418, 835.99, 792.6, 733.78, 719.318, 673.035, 660.5, 650.858.

M.p.: $> 300\ ^\circ C$

8.2.22 Bis [4,8,12-trioxa-4,8,12,12c- tetrahydrodibenzo [cd,mn] pyrene] diethynylene

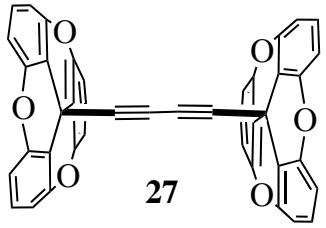

27

A solution of 12c-(ethynyl)-4,8,12-trioxa-4,8,12,12c-tetrahydro dibenzo [cd,mn] pyrene (84 mg, 0.27 mmol) and copper acetate monohydrate (1100 mg, 5.4 mmol) in THF(10 mL) and ethanol (10 mL) was heated to reflux. The reaction mixture was stirred at this temperature for 72 hours, then allowed to cool and diluted with methylene chloride. The mixture was transferred into a separatory funnel and washed twice with water, then dried over magnesium sulfate. Solvent was evaporated under reduced pressure. The desired product was purified by column chromatography on silica gel (Rf = 0.5) with 9:1 methylene chloride: hexanes as the eluent to yield 74 mg (44%) of a white solid.

^{1}H NMR (500 MHz, CD_2Cl_2, δ (CD_2Cl_2) = 5.36): δ= 7.24 (6H, t, J = 8.5 Hz, ArH), 7.06 (2H,

d, J = 8Hz, ArH), 6.84 (12H, d, J = 8Hz, ArH).6.76 (2H, d, J = 8Hz, ArH)

^{13}C {^{1}H} NMR (100.6 MHz, 100.6 MHz, CD_2Cl_2, δ (CD_2Cl_2) = 53.8): 152.1, 129.2, 111.8, 109.3. 80.5, 69.0, 53.4, 22.6.

MS (ESI): 641.3 ($C_{42}H_{18}NaO_6^+$)

M.p.: <300 °*C*

8.2.23 Bis [4,8,12-trioxa-4,8,12,12c- tetrahydrodibenzo [cd,mn] pyrene] diphenylene

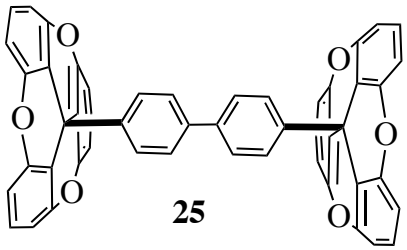

25

An oven dried 100 mL flask with a tefon stir bar and under nitrogen was charged with 4,4Õ-diiodobiphenyl (200 mg, 0.493 mmol) and dissolved in 20 mL dry THF. After cooling to -78 °*C*, *n*BuLi (0.4 mL, 0.99 mmol) was added drop wise. The solution was allowed to stir for 1 hours. Then, 12c-ethoxy-4,8,12-trioxa-4,8,12,12c-tetrahydrodibenzo[*cd*,*mn*]pyrene (704 mg, 1.17 mmol) were added slowly with a spatula. After 2 hours of stirring at -78 °*C*, the solution was allowed to warm to 0 °*C* with an ice bath and the reaction was quenched with 10 mL saturated aqueous NH_4Cl solution. The organic and aqueous phases were separated and the aqueous phase washed three times with Et_2O. The combined organic phase was dried ($MgSO_4$) and the solvent removed by rotary evaporation. The desired product was purified by column chromatography on silica gel (R_f = 0.1) with hexane/dichlormethane/toluene (10:1:1) as the eluent to yield 135 mg (75%) of a white solid.

^{1}H NMR (400 MHz, $CDCl_3$, δ ($CDCl_3$) = 7.26): 7.19 (6H, t, J = 8 Hz, ArH), 6.81 (4H, s),

6.88 (12H, d, J = 8Hz, ArH).

^{13}C {^{1}H} NMR (100.6 MHz, CDCl3, δ ($CDCl_3$) = 77.0): 153.1, 152.4, 145.6, 140.1, 128.2, 126.0, 111.1, 108.2, 35.0.

MS (ESI): 722.2 ($C_{50}H_{26}NaO_6^+$)

M.p.: <300 °*C*

8.2.24 1,4-Bis[12c-Ethynyl-4,8,12-trioxa-4,8,12,12c-tetrahydrodibenzo[cd,mn]pyrene] pyridineylene

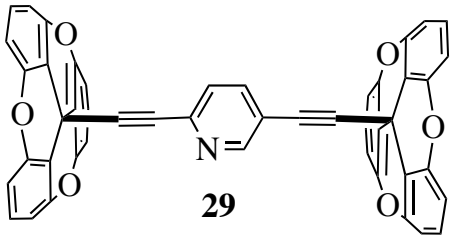

29

A degassed solution of 2,5 dibromopyridine (57 mg, 0.24 mmol), 12c-(ethynyl)-4,8,12-trioxa-4,8,12,12c-tetrahydro dibenzo [cd,mn] pyrene (156 mg 0.48 mmol), copper iodide (2 mg, 0.001 mmol), and palladium tetrakis(triphenylphosphine) (13.5 mg, 0.012 mmol) in 5 mL THF and 5 mL *i*-Pr_2NH was heated to 80°*C* and stirred at this temperature for 48 hours. The reaction mixture was allowed to cool to room temperature, and then diluted with dichloromethane and filtered thought a silica plug. The mixture was transferred to a separatory funnel, washed twice with water, and dried over magnesium sulfate. The solvent was evaporated under reduced pressure. The desired product was purified by column chromatography on silica gel (R_f = 0.2) with 8:1:1 hexane/dichloromethane /toluene as the eluent to yield 273 mg (81%) of a white solid.

^{1}H NMR (500 MHz, $CDCl_3$, δ ($CDCl_3$) = 7.26): 8.16 (1H, s, ArH), 7.23 (1H, d, J = 8 Hz, ArH), 7.20 (6H, t, J = 8.4 Hz, ArH), 6.97 (1H, d, J = 8Hz, ArH), 6.90 (12H, d, J = 8Hz, ArH).

^{13}C {^{1}H} NMR (100.6 MHz, CDCl3, δ ($CDCl_3$) = 77.0): 152.3, 152.0, 141.3, 138.6, 129.2,

126.7, 118.6, 111.9, 96.1, 83.3, 29.4.

MS (ESI): : $(M+Na)^+ = 718.1252$ ($C_{47}H_{21}NNaO_6^+$)

M.p.: $<300\ ^\circ C$

8.2.25 1,4-Bis[12c-Ethynyl-4,8,12-trioxa-4,8,12,12c-tetrahydrodibenzo[cd,mn]pyrene] phenylene

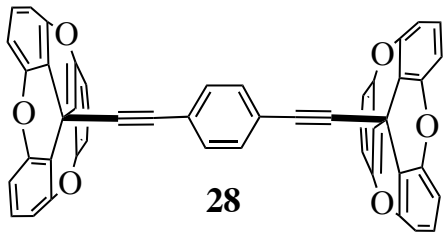

28

A degassed solution of 1,4-diiodobenzene (359 mg, 1.09 mmol), 12c-(ethynyl)-4,8,12-trioxa-4,8,12,12c-tetrahydro dibenzo [cd,mn] pyrene (200 mg 0.64 mmol), and $Pd(PPh_3)_2Cl_2$ (54 mg, 0.077 mmol) in 10 mL piperidine was heated to 80 $^\circ C$ and stirred at this temperature for 64 hours. The reaction mixture was allowed to cool to room temperature, and then diluted with dichloromethane and filtered thought a silica plug. The mixture was transferred to a separatory funnel, washed twice with water, and dried over magnesium sulfate. The solvent was evaporated under reduced pressure. The desired product was purified by column chromatography on silica gel ($R_f = 0.2$) with 8:1:1 hexane/dichloromethane /toluene as the eluent to yield 232 mg (52%) of a white solid.

^{1}H NMR (500 MHz, CD_2Cl_2, δ (CD_2Cl_2) = 5.36): 7.31 (6H, d, J = 8.5 Hz, ArH), 7.04 (1H, s, ArH), 6.99 (12H, d, J = 8 Hz, ArH),

^{13}C {^{1}H} NMR (125.5 MHz, CDCl3, δ ($CDCl_3$) = 77.0): 150.7, 131.9, 122.0, 125.6, 109.6, 86.8, 80.9, 25.4

MS (ESI): $(M+Na)^+ = 717.13086$ ($C_{48}H_{22}NaO_6^+$)

M.p.: $<300\ ^\circ C$

8.2.26 1,4-Bis[12c-phneylene-4,8,12-trioxa-4,8,12,12c-tetrahydrodibenzo[cd,mn]pyrene] ethylene

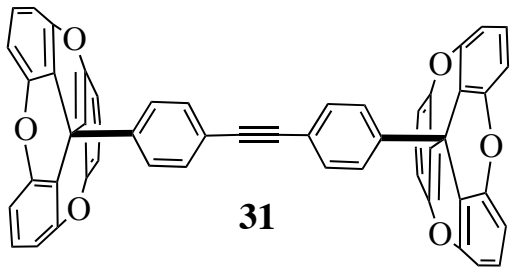

31

A degassed solution of 12c-(4-ethynylphenyl)-4,8,12-trioxa-4,8,12,12c- tetrahydrodibenzo[cd,mn]pyrene (54 mg, 0.14 mmol), copper iodide (1 mg, 0.0005 mmol), 12c-(4-bromophenyl)-4,8,12-trioxa-4,8,12,12c- tetrahydro dibenzo [cd,mn] pyrene(62 mg 0.14 mmol), and palladium tetrakis(triphenylphosphine) (8 mg, 0.007 mmol) in 10 mL triethyleamine was heated to 80 $^\circ C$ and stirred at this temperature for 48 hours. The reaction mixture was allowed to cool to room temperature, and then diluted with dichloromethane and filtered thought a silica plug. The mixture was transferred to a separatory funnel, washed twice with water, and dried over magnesium sulfate. The solvent was evaporated under reduced pressure. The desired product was purified by column chromatography on silica gel ($R_f = 0.2$) with 8:1:1 hexane/dichloromethane /toluene as the eluent to yield 48 mg (46%) of a white solid.

^{1}H NMR (400 MHz, $CDCl_3$, δ ($CDCl_3$) = 7.26): 7.31 (6H, d, J = 8.5 Hz, ArH), 7.04 (1H, s, ArH), 6.99 (12H, d, J = 8 Hz, ArH),

^{13}C {^{1}H} NMR (125.8 MHz, CDCl3, δ ($CDCl_3$) = 77.0): 152.65, 133.12, 129.09, 125.86, 113.35, 111.72, 81,02, 73.72, 29.70

MS (ESI): $(M+Na)^+ = 769.16130$ ($C_{52}H_{26}NaO_6^+$)

M.p.: <300 °*C*

8.2.27 1,4-Bis[12c-phneylene-4,8,12-trioxa-4,8,12,12c-tetrahydrodibenzo[cd,mn]pyrene] [2.2.2] -bicyclooctane

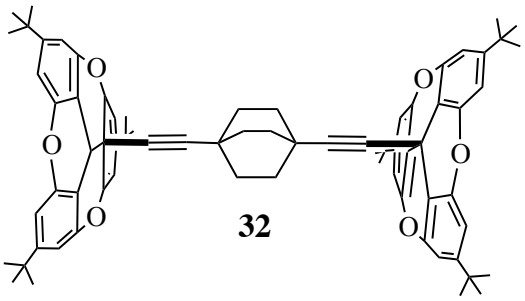

An oven dried 100 mL flask with a tefon stir bar and under nitrogen was charged with 1,4 bisethylenyl [2.2.2] -bicyclooctane[171] (30 mg, 0.191 mmol) and dissolved in 20 mL dry THF. After cooling to -78 °*C*, *n*BuLi (0.26 mL, 0.42 mmol) was added drop wise. The solution was allowed to stir for 1 hours. Then, 2,6,10-tri-*tert*-butyl-12c-ethoxy-4,8,12-trioxa-4,8,12,12c-tetrahydrodibenzo[*cd*,*mn*]pyrene (239 mg, 0.40 mmol) were added slowly with a spatula. After 2 hours of stirring at -78 °*C*, the solution was allowed to warm to 0 °*C* with an ice bath and the reaction was quenched with 10 mL saturated aqueous NH_4Cl solution. The organic and aqueous phases were separated and the aqueous phase washed three times with Et_2O. The combined organic phase was dried ($MgSO_4$) and the solvent removed by rotary evaporation. The desired product was purified by column chromatography on silica gel ($R_f = 0.1$) with hexane/dichlormethane (10:1) as the eluent to yield 116mg (58%) of a white solid.

^{1}H NMR (500 MHz, CD_2Cl_2, δ (CD_2Cl_2) = 5.36): 6.93 (6H, s, ArH),1.40 (6H, s, sp^3 C), 1.31 [27H, s, $C(CH_3)_3$)].

^{13}C {^{1}H} NMR (125.8 MHz, CDCl3, δ ($CDCl_3$) = 77.0): 153.75, 152.73, 109.71, 108.94, 90.01, 81.34, 35.13, 31.33, 26.10 **MS (ESI)**: $(M+Na)^+$ = 1085.8 ($C_{74}H_{78}NaO_6^+$)

M.p.: $<$300 °*C*

Appendix A

Appendix

A.1 X-Ray Data

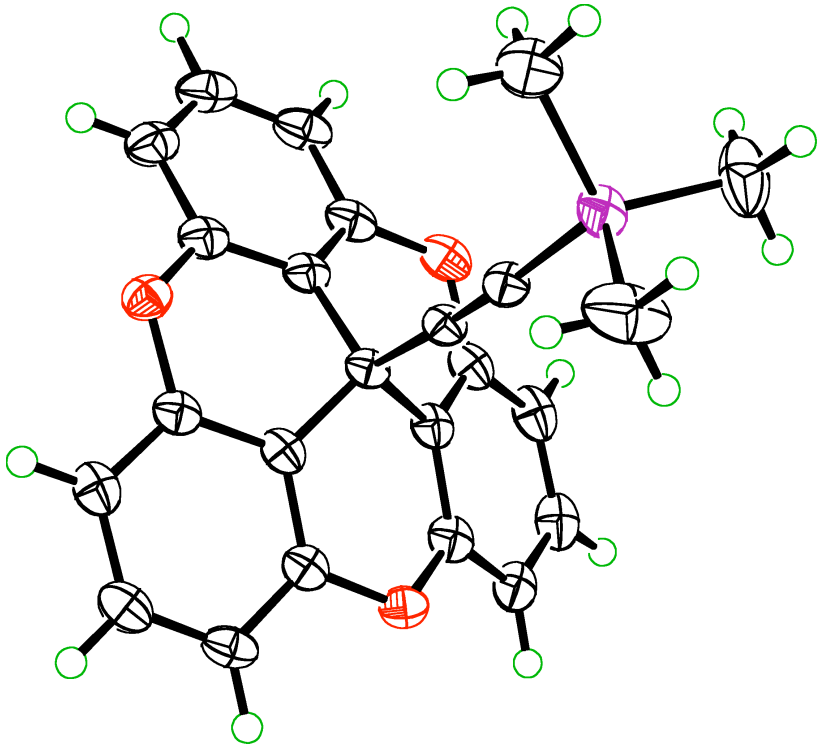

Protected Alkyne

Crystallised from	hexane / CH_2Cl_2 / toluene	
Empirical formula	$C_{24}H_{18}O_3Si$	
Formula weight [g mol^{-1}]	382.49	
Crystal colour, habit	colourless, plate	
Crystal dimensions [mm]	0.04 × 0.12 × 0.15	
Temperature [K]	160(1)	
Crystal system	triclinic	
Space group	$P\bar{1}$ (#2)	
Z	2	
Reflections for cell determination	5323	
2θ range for cell determination [°]	9–152	
Unit cell parameters	a [Å]	10.2769(7)
	b [Å]	10.3952(7)
	c [Å]	10.4758(7)
	α [°]	87.007(6)
	β [°]	66.120(6)
	γ [°]	68.804(6)

V [Å^3]	948.3(1)
F(000)	400
D_x [g cm^{-3}]	1.339
μ(Cu $K\alpha$) [mm^{-1}]	1.278
Scan type	ω
$2\theta_{(max)}$ [°]	152
Total reflections measured	16279
Symmetry independent reflections	6532
R_{int}	0.027
Reflections with $I > 2\sigma(I)$	5041
Reflections used in refinement	6532
Parameters refined	257
Final $R(F)$ [$I > 2\sigma(I)$ reflections]	0.0696
$wR(F^2)$ (all data)	0.2129
Weights:	$w = [\sigma^2(F_o^2) + (0.1376P)^2 + 0.1850P]^{-1}$ where $P = (F_o^2 + 2F_c^2)/3$
Goodness of fit	1.078
Final Δ_{max}/σ	0.001
$\Delta\rho$ (max; min) [e Å^{-3}]	0.75; -0.48
$\sigma(d_{(C-C)})$ [Å]	0.003 – 0.004

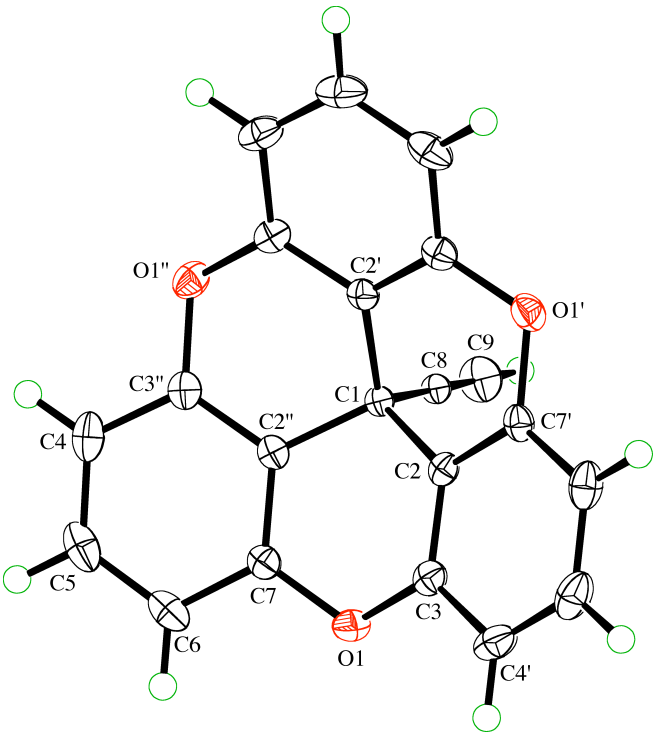

Alkyne substituted Building Block

Crystallised from		hexane
Empirical formula		$C_{21}H_{10}O_3$
Formula weight [g mol^{-1}]		310.31
Crystal colour, habit		yellow, prism
Crystal dimensions [mm]		0.25 ´ 0.25 ´ 0.32
Temperature [K]		160(1)
Crystal system		cubic
Space group		$Pa\bar{3}$ (#205)
Z		8
Reflections for cell determination		1213
2q range for cell determination [°]		4–55
Unit cell parameters	a [Å]	14.1447(4)
	b [Å]	14.1447(4)
	c [Å]	14.1447(4)
	a [°]	90

b [°]	90
g [°]	90
V [Å^3]	2830.0(1)
F(000)	1280
D_x [g cm^{-3}]	1.457
m(Mo Ka) [mm^{-1}]	0.0974
Scan type	f and w
$2q$(max) [°]	55
Total reflections measured	17835
Symmetry independent reflections	1083
R_{int}	0.110
Reflections with $I > 2s(I)$	827
Reflections used in refinement	1083
Parameters refined	75
Final $R(F)$ [$I > 2s(I)$ reflections]	0.0626
$wR(F^2)$ (all data)	0.1846
Weights:	$w = [s^2(F_o^2) + (0.1148P)^2 + 0.9481P]^{-1}$ where $P = (F_o^2 + 2F_c^2)/3$
Goodness of fit	1.028
Final D_{max}/s	0.001
Dr (max; min) [e Å^{-3}]	0.32; -0.29
$s(d_{(C-C)})$ [Å]	0.003 – 0.005

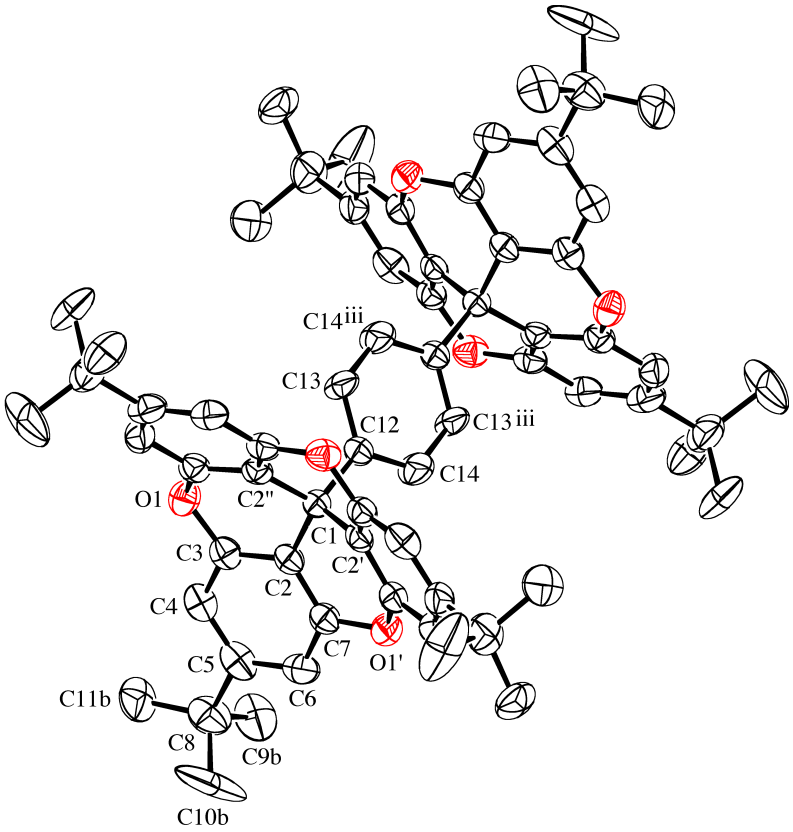

1st crystallization of the molecular rod rotor

Crystallised from	CH_2Cl_2
Empirical formula	$C_{68}H_{78}O_{10}$
Formula weight [g mol^{-1}]	1055.35
Crystal colour, habit	orange, prism
Crystal dimensions [mm]	0.15 ´ 0.17 ´ 0.25
Temperature [K]	160(1)
Crystal system	cubic
Space group	$Pa\bar{3}$ (#205)
Z	4
Reflections for cell determination	1856
2q range for cell determination [°]	4–50

Unit cell parameters	a [Å]	17.8302(9)
	b [Å]	17.8302(9)
	c [Å]	17.8302(9)
	a [°]	90
	b [°]	90
	g [°]	90
	V [Å^3]	5668.5(5)
F(000)		2264
D_x [g cm^{-3}]		1.237
m(Mo Ka) [mm^{-1}]		0.0814
Scan type		w
2q(max) [°]		50
Total reflections measured		18143
Symmetry independent reflections		1676
R_{int}		0.113
Reflections with $I > 2s(I)$		1032
Reflections used in refinement		1676
Parameters refined; restraints		176; 78
Final $R(F)$ [$I > 2s(I)$ reflections]		0.1028
$wR(F^2)$ (all data)		0.3320
Weights:	$w = [s^2(F_o^2) + (0.1638P)^2 + 9.0606P]^{-1}$ where $P = (F_o^2 + 2F_c^2)/3$	
Goodness of fit		1.098
Final D_{max}/s		0.001
Dr (max; min) [e Å^{-3}]		0.73; -0.32
$s(d_{(C-C)})$ [Å]		0.005 – 0.002

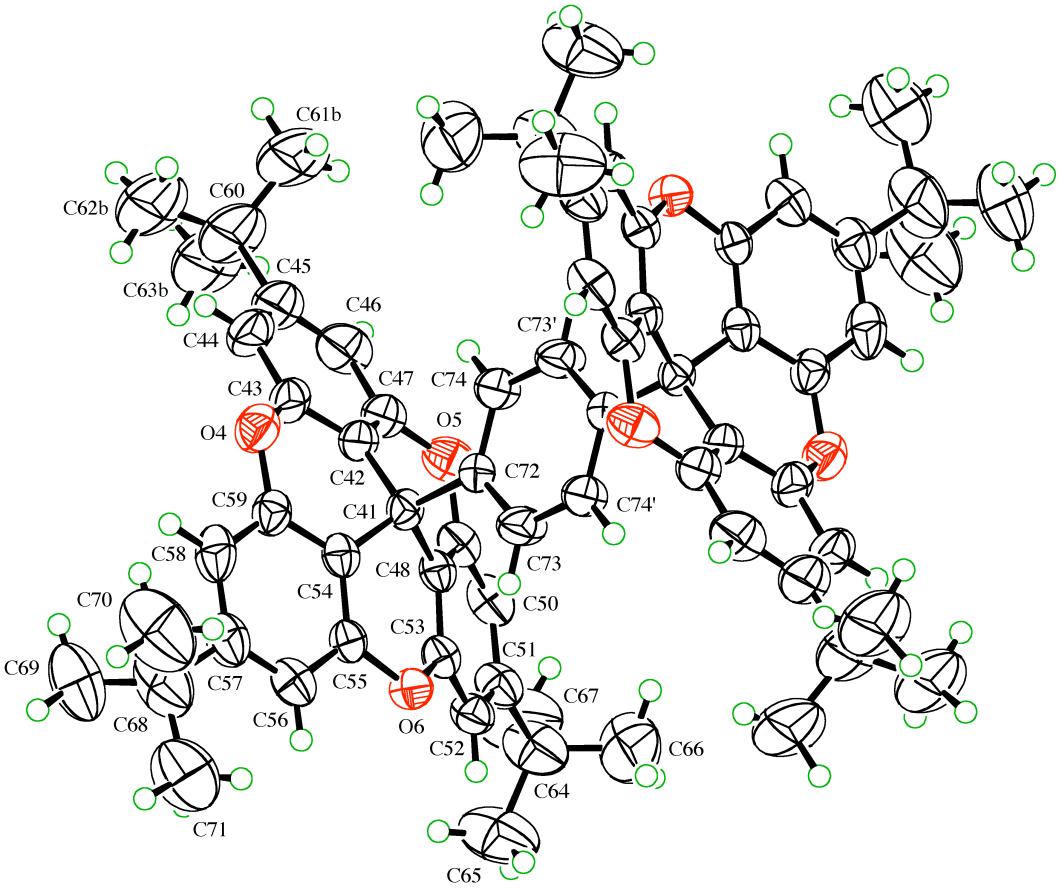

2nd crystallization of the molecular rod rotor

Crystallised from	$CDCl_3$ / hexane
Empirical formula	$C_{69.5}H_{71.5}Cl_{4.5}O_6$
Formula weight [g mol^{-1}]	1162.36
Crystal colour, habit	colourless, plate
Crystal dimensions [mm]	0.08 ´ 0.25 ´ 0.30
Temperature [K]	100(1)
Crystal system	monoclinic
Space group	*C*2/*c* (#15)
Z	8
Reflections for cell determination	376461
2*q* range for cell determination [°]	4–50

Unit cell parameters	a [Å]	47.4644(4)
	b [Å]	12.1083(1)
	c [Å]	22.2498(2)
	a [°]	90
	b [°]	96.3236(5)
	g [°]	90
	V [Å^3]	12709.5(2)
F(000)		4904
D_x [g cm^{-3}]		1.215
m(Mo Ka) [mm^{-1}]		0.257
Scan type		f and w
2q(max) [°]		50
Transmission factors (min; max)		0.833; 0.991
Total reflections measured		126459
Symmetry independent reflections		11220
R_{int}		0.096
Reflections with $I > 2s(I)$		8430
Reflections used in refinement		11220
Parameters refined; restraints		772; 76
Final $R(F)$ [$I > 2s(I)$ reflections]		0.0906
$wR(F^2)$ (all data)		0.2672
Weights:	$w = [s^2(F_o^2) + (0.1453P)^2 + 59.2772P]^{-1}$ where $P = (F_o^2 + 2F_c^2)/3$	
Goodness of fit		1.050
Secondary extinction coefficient		0.0005(2)
Final D_{max}/s		0.001
Dr (max; min) [e Å^{-3}]		1.33; -1.19
$s(d_{(C-C)})$ [Å]		0.005 – 0.01

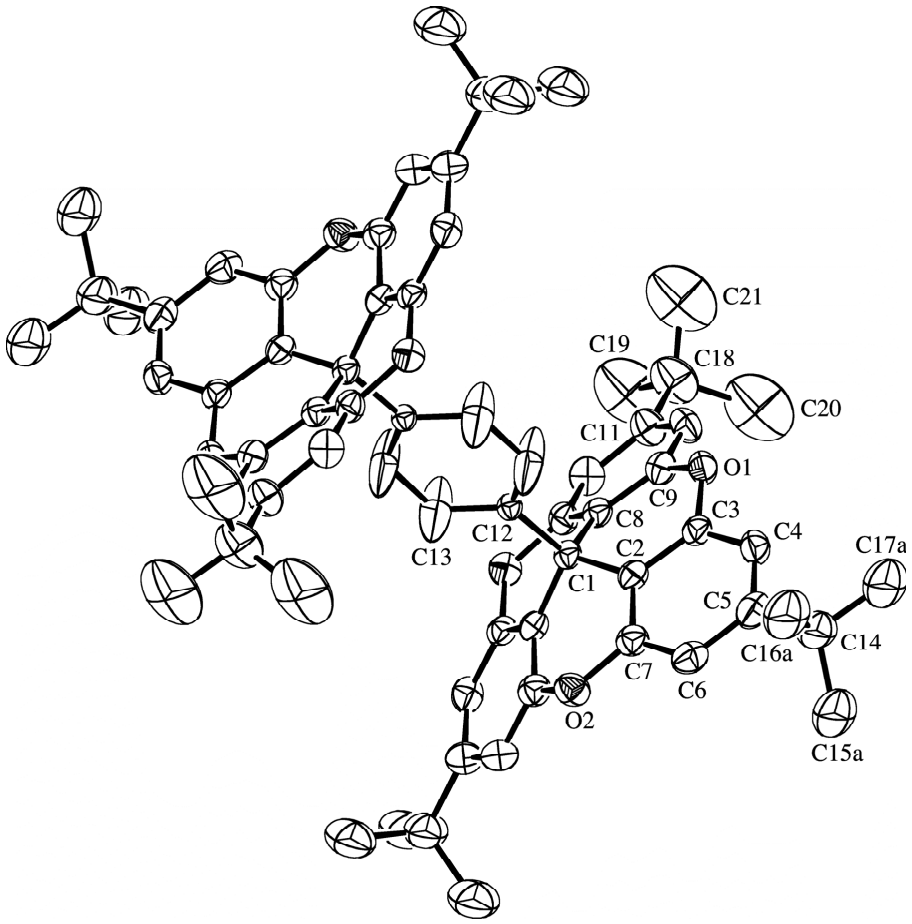

Orthorombic structure

Crystallised from		CH_2Cl_2
Empirical formula		$C_{72}H_{74}Cl_{12}O_6$
Formula weight [g mol^{-1}]		1460.81
Crystal colour, habit		orange, prism
Crystal dimensions [mm]		0.17 ´ 0.25 ´ 0.35
Temperature [K]		160(1)
Crystal system		orthorhombic
Space group		*Cmca* (#64)
Z		4
Reflections for cell determination		87928
2*q* range for cell determination [°]		4–50
Unit cell parameters	*a* [Å]	19.6150(2)
	b [Å]	13.7937(4)

	c [Å]	26.4086(5)
	a [°]	90
	b [°]	90
	g [°]	90
	V [Å^3]	7145.2(3)
F(000)		3032
D_x [g cm^{-3}]		1.358
m(Mo Ka) [mm^{-1}]		0.515
Scan type		f and w
2q(max) [°]		50
Transmission factors (min; max)		0.893; 0.978
Total reflections measured		32202
Symmetry independent reflections		3254
R_{int}		0.097
Reflections with $I > 2s(I)$		2616
Reflections used in refinement		3254
Parameters refined; restraints		272; 168
Final $R(F)$ [$I > 2s(I)$ reflections]		0.1357
$wR(F^2)$ (all data)		0.3781
Weights:	$w = [s^2(F_o^2) + (0.1881P)^2 + 64.1552P]^{-1}$ where $P = (F_o^2 + 2F_c^2)/3$	
Goodness of fit		1.069
Secondary extinction coefficient		0.005(1)
Final D_{max}/s		0.002
Dr (max; min) [e Å^{-3}]		1.09; -0.66
$s(d_{(C-C)})$ [Å]		0.006 – 0.02

Bibliography

1. "machine noun" The Oxford Dictionary of English (revised edition). Ed. Soanes, C.; Stevenson, A. Oxford University Press, 2005. Oxford, Reference Online. Oxford University Press. Universitat Zurich. 16 August 2010 *http://www.oxfordreference.com/views/ENTRY.html?subview=Mainentry=t140.e45657*

2. Mislow, K. *Chemtracts-Organic Chemistry*, **1989**, *2*, 151.

3. Einstein, A. *Annalen der Physik*, **1905**, *322 (8)*, 549.

4. Smoluchowski, v. M. *Bulletin International de l'Academie des Sciences de Cracovie*, **1906**, 202.

5. Brown, R. *Pogg. Annalen*, **1828**, *14*, 294.

6. Smoluchowski, v. M. *Phys. Z.13*, **1912**, *13*, 1069.

7. Reinman, P. *Phys. Rep.*, **2002**, *361* , 57.

8. Feynman, R. P.; Leighton, R. L.; Sands, M. *The Feynman lectures on physics*; Addison-Wesley: Reading, MA,963; p 46-1.

9. Kelly, T. R.; Tellitu, I.; Sestelo J. P. *Angew. Chem. Int. Ed. Engl.*, **1997**, *36* , 1866.

10. Kelly, T. R.; Tellitu, I.; Sestelo J. P. *J. Org. Chem.*, **1998**, *63* , 3655.

11. Davis, A. P. . *Angew. Chem. Int. Ed. Engl.*, **1998**, *37* , 909.

12. Cross, R. L. *Nature*, **2004**, *427*, 407.

13. Abraham, R. T. , Tibbetts, R. S. *Science*, **2005**, *308* , 510.

14. Kaim, G.; Dimroth, P. *The EMBO Journal* **1999**, *18* , 4118.

15. Asbury, C. L.; Fehr, A. N.; Block, S. M. *Science*, **2003**, *302*, 2130.

16. Asbury C.; Wordeman, L., PBIO 558, Spring 2007, University of Washington,

17. Kottas, G. S.; Clarke, L. I.; Horinek, D. ; Michl, J. *Chem. Rev.* ,**2005**, *105*, 1281.

18. An Overview of NSF Research, Nanoscience. *http://www.nsf.gov/news/overviews/nano/index.jsp* (accessed August 05, 2010).

19. *Molecular Catenanes, Rotaxanes and Knots*; Sauvage, J.-P., Dietrich-Buchecker, C., Eds.; Wiley-VCH: Weinheim, 1999.

20. Schill, G. *Catenanes, Rotaxanes, and Knots*; Academic Press:New York, 1971

21. Balzani, V.; Venturi, M.; Credi, A. *Molecular Devices and Machines*; Wiley-VCH: Weinheim, 2003.

22. Ebert, L. *Leibziger Vortraege*, **1924**, *S. Hirzel Verlag, Stuttgart*, 74.

23. Wagner, Z. *Z. Phys. Chem. Abt. B*, **1931**, *14*, 166.

24. Eucken, A.; Weigert, K. *Z. Phys. Chem. Abt. B*, **1933**, *23*, 265.

25. Teller, E.; Weigert, K. *Nachr. Ges. Wiss. Goettingen, Geschaeftliche Mitt.*,**1933**, 218.

26. Kemp, J. D.; Pitzer, K. S. *J. Chem. Phys.*, **1936**, *4*, 749.

27. Kemp, J. D.; Pitzer, K. S. *J. Am. Chem. Soc.*, **1937**, *59*, 276.

28. March, J. *Advanced Organic Chemistry: Reactions, Mechanisms, and Structure*, John Wiley & sons, 4th edition.

29. Clayden, J.; Greeves , N; Warren, S. ; Wothers, P. *Organic Chemistry*, Oxford University Press, USA; 1 edition (August 31, 2000)

30. Smith, L. G. *J. Chem. Phys.*, **1949**, *17*, 139.

31. Pople, J. A.; Santry *Mol. Phys.*, **1965**, *9*, 301.

32. Pople, J. A. *Tetrahedron*, **1974**, *30*, 1605.

33. Lowe, J. P. *Science*, **1973**, *179*, 527.

34. Schreiner, P. R. *Angew. Chem., Int. Ed.*, **2002**, *41*, 3579.

35. Pophristic,V.; Goodman,L. *Nature*, **2001**, *411*, 565

36. Goodman, L.; Gu, H. *J. Chem. Phys.* , **1999**, *110*, 4268.

37. Goodman,L. ; Pophristic,V.;Weinhold,F. *Acc. Chem. Res.*, **1999**, *32*, 983-993.

38. Yirong M.; Jiali G. *Acc. Chem. Res.*, **2007**, *40*, 113.

39. Kuhn, R. Molekulare Asymmetrie in Stereochemie; Freuberg, H., Ed.; Franz, Deutike: Leipzig-Wien, 1933, 803.

40. Christie, G. H.; Kenner, J. *J. Chem. Soc., Trans.*, **1922**, *121*, 614.

41. Christie, G. H.; Kenner, J. *J. Chem. Soc., Trans.*, **1922**, *121*, 594.

42. *Dynamic Stereochemistry of Chiral Compounds - Principles and Applications* . Edited by Christian Wolf . RSC Publishing : Cambridge, U.K., 2008, p. 85-108

43. Oki, M. *Acc.Chem. Res.*, **1990**, *23*, 351.

44. *Dynamic Stereochemistry of Chiral Compounds - Principles and Applications* . Edited by Christian Wolf . RSC Publishing : Cambridge, U.K., 2008, p. 17.

45. *Dynamic Stereochemistry of Chiral Compounds - Principles and Applications* . Edited by Christian Wolf . RSC Publishing : Cambridge, U.K., 2008, p. 105.

46. Charbonneau, G.-P.; Delugeard, Y. *Acta Cryst.*, **1976**, *B32*, 1420.

47. Roberts, R.M.G. *Magn. Reson. chem.*, **1985**, *23*, 52.

48. Dyanes, J.J,; Baudais, F. L.; Boyd, R.K. *Can. J. Chem.*, **1985**, *63*, 259.

49. Cailleau, H.; Girard, A.; Moussa, F.; Zeyen, C. M. E. *Solid State Commun.*, **1979**, *29*, 1292.

50. Grein, F. *J. Phys. Chem. A*, **2002**, *106*, 38323.

51. Liberles, A.; Matlosz, B. J. *J. Org. Chem.*, **1971**, *36*, 2710.

52. Okuyama, K.; Hasegawa, T.; Ito, M.; Mikami, N. *J. Phys Chem.*, **1984**, *88*, 1711.

53. Xu, D.; Cooksy, A.L *J. Mol. Struct.-THEOCHEM*, **2007**, *815*, 119.

54. Karim, A. R.; Linden, A.; Baldridge, K. K.; Siegel, J. S. *Chem. Sci.*, **2010**, *1*, 102.

55. Mavridis A.; Moustakali-Mavridis, I. *Acta Crystallogr., Sect. B: Struct. Crystallogr. Cryst. Chem.*, **1977**, *33*, 362.

56. Espiritu, A. A.; White, J. G. . Kristallogr., Kristallgeom., Kristallphys., Kristallchem., **1978**, *147*, 177.

57. Abramenkov, A. V.; Almenningen, A.; Cyvin, B. N.; Cyvin, S. J.; Jonvik, T.; Khaikin, L. S.;Roemming C.; Vilkov, L. V. *Acta Chem. Scand., Ser. A,*, **1988**, *42a*, 674.

58. Thomas, R.; Lakshmi, S.; Pati, S. K.; Kulkarni, G. U. *J. Phys. Chem. B*, **2006**, *110*, 24674.

59. Inoue,K.; Takeuchi, H.; Konaka, S. *J. Phys. Chem. A* , **2001**, *105*, 6711.

60. Toyota, S.; Yamamori, T.; Asakura, M.; Oki, M. *Bull. Chem. Soc. Jpn.*, **2000**, *73*, 205.

61. Toyota, S.; Yamamori, T.; Makino, T.; Oki, M. *Bull. Chem. Soc. Jpn.*, **2000**, *73*, 2591.

62. Toyota, S.; Yamamori, T.; Makino, T. *Tetrahedron*, **2001**, *57*, 3521.

63. Toyota, S.; Iida, T.; Kunizane, C.; Tanifuji, N.; Yoshida, Y. *Org. Biomol. Chem.*, **2003**, *1*, 2298.

64. Toyota, S.; Yanagihara, T.; Yoshida, Y.; Goichi, M. *Bull. Chem. Soc. Jpn* ., **2005**, *78*, 1351.

65. Bedard, T.C.; Moore, J.S. *J. Am. Chem. Soc.*, **1995**, *117*, 10662.

66. For an overview of molecular structures that emulate certain aspects of macroscopic gyroscopes, see: : K. Skopek, M. C. Hershberger and J. A. Gladysz, *Coord. Chem. Rev.* ,**2007**, *251*, 1723.

67. Garcia-Garibay, M.A. *Proc. Natl. Acad. of Sci.*, **2005**, *102*, 10793.

68. Khuong, T.-A.V.; NuŰez, J.E.; Godinez, C.E.; Garcia-Garibay, M.A. *Acc. Chem. Res.*, **2006**, *39*, 413.

69. Mortko, C. J.; Garcia-Garibay, M.A. *Topics Curr. Chem.*, **2006**, *262*, 179.

70. Dominguez, Z.; Dang, H.; Strouse, M.J.; Garcia-Garibay, M.A. *J. Am. Chem. Soc.*, **2002**, *124*, 2398.

71. Godinez, C.E.; Zepeda, G.; Garcia-Garibay, M.A. *J. Am. Chem. Soc.*, **2002**, *124*, 4701.

72. Dominguez, Z.; Dang, H.; Strouse, J.M.; Garcia-Garibay, M.A. *J. Am. Chem. Soc.*, **2002**, *124*, 7719.

73. Dominguez, Z.; Khuong, T.A.V.; Sanrame, C.N.; Dang, H.; NuŰez, J.E.; Garcia-Garibay, M.A. *J. Am. Chem. Soc.*, **2003**, *125*, 8827.

74. Khuong, T.A.V.; Zepeda, G.; Ruiz, R.; Kahn, S.I.; Garcia-Garibay, M.A. *Cryst. Growth & Design*, **2004**, *4*, 15.

75. Godinez, C.E.; Zepeda, G.; Garcia-Garibay, M.A. *J. Org. Chem.*, **2004**, *69*, 1652.

76. Karlen, S.D.; Kahn, S.I.; Garcia-Garibay, M.A *Cryst. Growth & Design*, **2005**, *5*, 53.

77. Karlen, S.D.; Garcia-Garibay, M.A. *Chem. Commun.*, **2005**, 189.

78. Karlen, S.D.; Ortiz, R.; Chapman, O.L.; Garcia-Garibay, M.A. *J. Am. Chem. Soc.*, **2005**, *127*, 6554.

79. Nunez, J. E.; Khuong, T.-A.V.; Campos, L. M.; Farfan, N.; Dang, H.; Karlen, S. D.; Garcia-Garibay, M.A. *Cryst. Growth & Design*, **2006**, *25*, 205.

80. Karlen, S.D.; Godinez, C.E.; Garcia-Garibay, M.A *Org. Lett.*, **2006**, *8*, 1615.

81. Horansky, R.D.; Clarke, L.I.; Winston, E.B.; Price, J.C.; Karlen, S.D.; Jarowski, P.D.; Santillan, R.; Garcia-Garibay, M.A. *Phys. Rev. B*, **2006**, *74*, 054306.

82. Godinez, C.E.; Garcia-Garibay, M.A. *Cryst. Growth & Design*, **2009**, *9*, 3124.

83. Rodriguez-Molina, B.; Ochoa, M.E.; FarfĞn, N.; Santillan, R.; Garcia-Garibay, M.A.*J. Org. Chem.*, **2009**, *74*, 8554.

84. Jarowski, P.D.; Houk, K.N.; Garcia-Garibay, M.A. *J. Am. Chem. Soc.*, **2007**, *129*, 3110.

85. Nunez, J.E.; Natarajan, A.; Khan, S.I.; Garcia-Garibay, M.A *Org. Lett.*, **2007**, *9*, 3559.

86. Gould, S.L.; Tranchemontagne, D.; Yaghi, O.M.; Garcia-Garibay, M.A. *J. Am. Chem. Soc.*, **2008**, *130*, 3246.

87. Santillan, R.; Karlen, S.D.; Dang, H.; Garcia-Garibay, M.A. *J. Mex. Chem. Soc.*, **2008**, *52*, 125.

88. Garcia-Garibay, M.A. *Nature Materials*, **2008**, *7*, 431.

89. Karlen, S.D.; Reyes, H.; Taylor, R.E.; Khan, S.I.; Hawthorne, M.F.; Garcia-Garibay, M.A. *Proc. Nat. Acad. Sci. USA*, **2010**, *107*, 14973.

90. Rodriguez-Molina, B.; Pozos, A.; Cruz, R.; Romero, M.; Flores, B.; Farfan, N.; Santillan, R.; Garcia-Garibay, M.A. *Org. Biomol. Chem.*, **2010**, *8* , 2993.

91. (a) L. Nedelec, J. C. Gasc, V. Delaroff, R. Bucourt and G. Nomine, *Tetrahedron*, **1978**, *34*, 2729; (b) M. M. Bhadbhade and V. Venkatesan, *Acta Crystallogr., Sect. C: Cryst. Struct. Commun.*, **1984**, *40*, 1905.

92. Horinek, D. ; Michl, J. *PNAS*, **2005**, *102*, 14175.

93. Tinkertoy is a toy set of wooden dowels, joints, wheels, etc., used by children to assemble structures.

94. Kaszynski, P.; Michl, J. *J. Am. Chem. Soc.*, **1988**, *110*, 5225.

95. Kaszynski, P., Friedli, A. C.; Michl, J. *J. Am. Chem. Soc.*, **1992**, *114*, 601.

96. Zheng, X.; Mulcahy, M.E.; Horinek, D.; Galeotti, F.; Magnera, T.F.; Michl, J. *J. Am. Chem. Soc.*, **2004**, *126*, 4550.

97. Debije, P. *Verh. Dtsch. Phys. Ges.*, **1913**, *15*, 678.

98. Debije, P. *Verh. Dtsch. Phys. Ges.*, **1913**, *15*, 738.

99. Debije, P. *Verh. Dtsch. Phys. Ges.*, **1913**, *15*, 857.

100. Cruickshank, D. W. J. *Acta Crystallogr.*, **1956**, *9*, 754.

101. Cruickshank, D. W. J. *Acta Crystallogr.*, **1956**, *9*, 1005.

102. Maverik, E.; Dunitz, J. D. *Mol. Phys.*, **1987**, *62*, 451.

103. Dunitz, J. D.; Schomaker, V.; Trueblood, K. N. J. *J. Phys. Chem.*, **1988**, *92*, 856.

104. Schomaker, V.; Trueblood, K. N. *Acta Crystallogr.*, **1998**, *B54*, 507.

105. Dunitz, J. D.; Maverick, E. F.; Trueblood, K. N. *Angew. Chem., Int. Ed. Engl.*, **1988**, *27*, 880.

106. Maverick, E. F.; Knobler, C. B.; Khan, S. I.; Canary, J. W.; Dicker, I. B.; Trueblood, K. N. *Helv. Chim. Acta*, **2003**, *86*, 1309.

107. Bürgi, H.-B.; Capelli, *Helv. Chim. Acta*, **2003**, *86*, 1625.

108. Mehring, M. *Principles of High Resolution NMR in Solids*, Springer, Berlin, 1983.

109. Schmidt-Rohr, K.; Spiess, H. W. *Multidimensional Solid-State NMR and Polymers*, Academic Press, New York, 1994.

110. *Handbook of Spectroscopy*, Vo-Dinh, Gauglitz (eds.), Wiley In Volume: Methods 2: NMR Spectroscopy.

111. Bakhmutov, V. I. *Dynamic Stereochemistry of Chiral Compounds - Principles and Applications* John Wiley Sons, Ltd: Chichester, U.K. 2004, p.13.

112. Azevedo, E. R.; Bonagamba, T. J. *Braz. J. Phys.*, **2006**, *36*, 61.

113. *Solid State NMR Spectroscopy: Principles and Applications* . Edited by Melinda J. Duer. Wiley-Blackwell; 1 edition (December 31, 2001)

114. Brown, S. P.; Spiess, H. W. *Chem. Rev.*, **2001**, *101*, 4125.

115. M. Oki: *Practical NMR Relaxation for Chemists*, Vol. 4 aus der Reihe: Methods in Stereochemical Analysis, VCH Verlagsgesellschaft Weinheim, Deerfield Beach-Florida 1985.

116. Jackman, L.M.; Cotton, F. A., Eds.; "*Dynamic Nuclear Magnetic Resonance*", Academic Press: New York, 1975.

117. J. Sandström *Dynamic NMR Spectroscopy* Academic Press: London 1982.

118. Gutowsky , H. S.; Holm, C.H. *J. Chem. Phys.*, **1956**, *25*, 1228.

119. Clar, E.; Steward, D. G. *J. Am. Chem. Soc.*, **1953**, *75*, 2667.

120. Clar, E.; Steward, D. G. *J. Am. Chem. Soc.*, **1954**, *76*, 3504.

121. Allison, G.; Bushby, R.; Paillaud J.-L.; Thornton-Patt, M. *J. Chem. Soc. Perkin Trans. 1*, **1995**, 385.

122. Inoue, J.; Fukui, K.; Kubo, T.; Nakazawa, S.; Sato, K.; Shiomi, D.; Morita, Y.; Yamamoto, K.; Takui T.; Nakasuji, K. *J. Am. Chem. Soc.*, **2001**, *123*, 12702.

123. Martin, J. C.; Smith, R.G, *J. Am. Chem. Soc.*, **1964**, *86*, 2252.

124. Sabacky, M. J.; Johnson, C. S.; Smith, R. G.; Gutowsky, H. S.; Martin, J. C. *J. Am. Chem. Soc.*, **1967**, *89*, 2054.

125. Theilacker, W.; Schulz, H.; Baumgarte, U.; Droessler, H.-G.; Rohde, W.; Thater, F.; Uffmann, H. *Angew. Chem.*, **1957**, *69*, 322.

126. Johnson, C.E.; Bovey, F. A. *J. Chem. Phys.*, **1958**, 1012.

127. Lankamp, H.; Nauta, W. Th.: MacLean, C. *Tetrahedron Letters*, **1968**, 249.

128. Carey, F.A..; Tremper, H. S.: MacLean, C. *J. Am. Chem. Soc.*, **1968**, *90*, 2578.

129. Nemcova, I.; Nemec, I. *J. Electroanal. Chem.*, **1971**, *30,*, 506.

130. Nemcova, I.; Nemec, I. *Chem. zvesti.*, **1972**, *26*, 115.

131. Sabacky, M.J.; Johnson, C.S.; Smith, R.G.; Gutowsky, H.S.; Martin, J.C. *J. Am. Chem. Soc.*, **1967**, *89*, 2054.

132. Müller, E.; Moosmayer, A.; Rieker, A.; Scheffler, K. *Tetrahedron*, **1967**, *39*, 3877.

133. Bowie, W.T.; Feldman, M. . *J. Am. Chem. Soc.*, **1977**, *99*, 4721.

134. Feldman, M.; Flythe, W.C. *J. Am. Chem. Soc.*, **1978**, *43*, 2596.

135. Kessler, H.; Moosmayer, A.; Rieker, A. *Tetrahedron*, **1969**, *25*, 287.

136. Nemcova, I.; Malat, M.; Zahradnik, R. *Collect. Czech. Chem. Commun.* , **1969**, *39*, 2880.

137. Goldacre, R.J..; Phillips, J.N. *J. Chem. Soc.* , **1949**, 1724.

138. Diffenbach, R. A.; Sano, K.; Taft, R. W. *J. Am. Chem. Soc.* , **1966**, *88*, 4747.

139. Komatsu, K.; Akamatsu, H.; Jinbu, Y.; Okamoto, K. *J. Am. Chem. Soc.* , **1988**, *110*, 633.

140. *a.)* Ito, S.; Morita, N.; Asao, T. *Tetrahedron Lett.* , **1994**, *35*, 751. *b.)* Ito, S.; Kikuchi, S.; Morita, N.; Asao, T. *Chem. Lett.*, **1996**, 175.

141. Krebs, F. C.; Laursen, B. W.; Johannsen, I.; Faldt, A.; Bechgaard, K.; Jacobsen C. S.; Thorup, N.; Boubekeurd, K. *Acta Cryst.* , **1999**, *B55*, 410.

142. Lofthagen, M.; VernonClark. R.; Baldridge, K.K.; Siegel, J.S. *J. Org. Chem.*, **1992**, *57*, 61.

143. Müller, E.; Moosmayer, A.; Rieker, A.; Scheffler, K. *Tetrahedron Letters* , **1967**, *39*, 3877.

144. Moosmayer, A.; Rieker, A.; Scheffler, K. *Tetrahedron*, **1969**, *25*, 287.

145. Lofthagen, M. Synthesis of Polycyclic Macrocages from molecular Keystones. Structure and Dynamics, **1992**, PhD Thesis, University of California, San Diego, USA.

146. Lofthagen, M.; Siegel, J.S *J. Org. Chem.*, **1995**, *60*, 2885.

147. Lofthagen, M.; Chadha. R.; Siegel, J.S. *J. Am. Chem. Soc.*, **1991**, *113*, 8785.

148. Lofthagen, M.; VernonClark. R.; Baldridge, K.K.; Siegel, J.S. *J. Org. Chem.*, **1992**, *57*, 61.

149. VernonClark, R.N. Synthesis, Analysis, and Calculational Comparison, using Semiempirical and Molecular Mechanical Methods, of Centrally Substituted Trioxatricornan Structures. Investigations of Thtough-Bond Interactions. **1992**, PhD Thesis, University of California, San Diego, USA.

150. Kottas, G. S.; Clarke, L. I.; Horinek,D.; Michl, J. *J. Chem. Rev.*, **2005**, *1281*.

151. Faldt, A.; Krebs, C. F.; Thorup, N. *J. Chem. Soc., Perkin Trans. 2*, **1997**, 2219.

152. Polik, W.F.; Schmidt, WebMO User's Guide, WebMO/Manual Version: 3.3, 2003, Michigan USA.

153. Pecharsky, V. K.; Zavalij, P. *Origin of the power diffraction pattern, Fundamentals of Powder Diffraction and Structural Characterization of Materials*, Springer Science + Business Media, LLC (Paperback edition 2005).

154. Pecharsky, V. K.; Zavalij, P. *Origin of the power diffraction pattern, Fundamentals of Powder Diffraction and Structural Characterization of Materials*, Springer Science + Business Media, LLC (Paperback edition 2005), Chapter 2.7 to 2.10 p.153- 185.

155. Hooft, R. *KappaCCD Collect Software*, Nonius BV, Delft, The Netherlands, 1999.

156. Otwinowski, Z.; Minor, W. *Methods in Enzymology*, Vol. 276 , *Macromolecular Crystallography*, Part A, Eds. C.W. Carter Jr., R.M. Sweet, Academic Press, New York, 1997, pp. 307-326.

157. Altomare, A.; Cascarano, G.; Giacovazzo, C.; Guagliardi, A.; Burla, M.C.; Polidori, G.; Camalli, M. *SIR92, J. Appl. Crystallogr.* , **1994**, *27*, 435.

158. Maslen, E.N.; Fox, A.G.; O'Keefe, M.A., *International Tables for Crystallography,* Ed. A.J.C. Wilson, Kluwer Academic Publishers, Dordrecht, 1992, Vol. C, Table 6.1.1.1, pp. 477-486.

159. Stewart, R.F.; Davidson, E.R.; Simpson, W.T. *J. Chem. Phys* , **1965**, *42*, 3175.

160. Ibers, J.A.; Hamilton, W.C. *Acta Crystallogr.* , **1964**, *17*, 781.

161. Creagh, D.C.; McAuley, W.J. *International Tables for Crystallography,* Ed. A.J.C. Wilson, Kluwer Academic Publishers, Dordrecht, 1992, Vol. C, Table 4.2.6.8, pp. 219-222.

162. Creagh, D.C.; Hubbel, *International Tables for Crystallography,* Ed. A.J.C. Wilson, Kluwer Academic Publishers, Dordrecht, 1992, Vol. C, Table 4.2.4.3, pp. 200-206.

163. Sheldrick, G.M. *SHELXL97*, Program for the Refinement of Crystal Structures, University of G öttingen, Germany, 1997.

164. Johnson, C.K. *ORTEPII*, Report ORNL-5138, Oak Ridge National Laboratory, Oak Ridge, Tennessee, 1976.

165. van Beek, J. D. *J. Magn. Res.* , **2007**, *187*, 19.

166. Schmitt, B.; Br önnimann, Ch.; Eikenberry, E.F.; Gozzo, F.; H örmann, C.; Horisberger, R.; Patterson, B. *Nucl. Instrum. Meth. A* , **2003**, *501*, 267.

167. Gozzo, F.; Schmitt, B.; Bortolamedi, Th.; Giannini, C.; Guagliardi, A.; Lange, M.; Meister, D.; Maden, D.; Willmott, P.; Patterson, B.D. *J. Alloy Compd.* , **2004**, *362*, 206.

168. These reaction conditions were investigated by Michael Lofthagen and Russell VernonClark under the direction of Prof. J. Siegel at the University of California at San Diego, 04.06.1990.

169. Faldt, A.; Krebs, F. C.; Thorup, N.. *J. Chem. Soc., Perkin Trans. 2* , **1997**, 2219.

170. Synthesis of *tert*-butylated Martin's salt was done according to literature[169]

171. many thanks to Cortnie Vogelsberg, University of California, Los Angeles, CA USA, which made 1,4 dicarboxylate [2.2.2] -bicyclooctane which was then converted to the 1,4 dibromo [2.2.2] -bicyclooctane by a hunsdieker reaction[172] and by a subsequent sonogaschira reaction the diacetylene was achieved.

172. Hunsdiecker, H.; Hunsdiecker, C. *Berichte der deutschen chemischen Gesellschaft (A and B Series)* , **1942**, *75*, 291.